ABSTRACT

GALLEN, SEAN FRANCIS. The Development of Topography in Ancient and Active Orogens: Case Studies of Landscape Evolution in the Southern Appalachians, USA and Crete, Greece. (Under the direction of Karl Wegmann).

Understanding the development of topography is fundamental to the geosciences. Topography represents the sum of all tectonic and geodynamic processes that force the earth's surface upward paired with those that act to bring it down. Spatial and temporal changes in topographic relief can modulate the various feedbacks between atmospheric, earth surface and rock exhumation processes, sediment flux, and the magnitude and style of gravity driven natural hazards. Plate tectonics provides the first-order framework necessary to understand how topography is built through the interaction of lithospheric plates. However, density contrasts in the mantle can also influence the elevation of the earth's surface through dynamic topography, while poorly understood nuances of mountain building at convergent margins complicate drawing direct connections between tectonics and topography. Such linkages are further confounded by non-linearity between rock uplift and erosion, variations in rates of deformation, changes in climate and the properties of bedrock. Great advances in our understanding of the evolution of topography have been achieved, yet numerous questions remain regarding the evolution of topography in ancient and active orogens.

This research addresses knowledge gaps in the development of topography through case-studies of landscape evolution in the southern Appalachians Mountains, USA and the forearc overlying the Hellenic subduction zone. Chapter 1 explores the origins of modern topographic relief in the southern Appalachians, where tectonic activity ceased prior to 200 Ma. Conventional theories invoked to explain modern relief in the region are challenged. Quantitative analyses of digital elevation models and numerical modeling are coupled to provide the magnitudes and timing of changes in topographic relief. The results suggest that the southern Appalachians experienced a phase of topographic rejuvenation during the Miocene that increased the distance between the

valley bottoms and mountain peaks > 160%. The most parsimonious driving mechanism to explain all evidence presented is uplift by dynamic topography.

Chapter 2 confronts a long-standing debate over the style of orogenesis above the Hellenic subduction zone where two competing hypotheses are used to explain the rise of topography. Distinguishing between these hypotheses hinges on the kinematics of large faults associated with a series to topographic escarpments, known as the Hellenic troughs. Late Pleistocene marine terraces, optically stimulated luminescence geochronology, and structural mapping in South-central Crete and the Late Quaternary eustatic curve provide the dataset to test the kinematics of the Ptolemy fault, one of the Hellenic trough faults. Long term (10^4 – 10^5 yr) rock uplift rates are synthesized and active faults identified. Fault-scaling properties demonstrate that active onshore extensional faulting is geometrically inconsistent with contractional shortening along the Ptolemy fault. This finding indicates that the Ptolemy, and probably all of the Hellenic trough faults, accommodates extension-to-transtension. The regional uplift of South-central Crete is interpreted as the result of underplating along the plate interface, as demonstrated by uplift of both the foot-and-hanging walls of active extensional faults with respect to sea level. The Hellenic troughs are grabens rising over an inflating subduction wedge.

Chapter 3 exploits fortuitous geologic circumstances in South-central Crete to document the landscape response to changes in the rate of rock uplift and the impact that lithology has on geomorphic sensitivity to tectonic signals. Suites of topographic and drainage basin metrics responsive to rock uplift are used to evaluate how changing conditions are manifested in the landscape. Findings indicate that the landscape is insensitive to changes in rock uplift rate that initiated > 400 Ka, suggesting geomorphic response times here are long. Carbonates reduce ability of the landscape to record tectonic signals, likely due to the development of karst hydrology. These findings demonstrate that landscapes may not represent the active tectonic displacement field.

The Development of Topography in Ancient and Active Orogens: Case Studies of Landscape Evolution in the Southern Appalachians, USA and Crete, Greece

by
Sean Francis Gallen

A dissertation submitted to the Graduate Faculty of
North Carolina State University
in partial fulfillment of the
requirements for the degree of
Doctor of Philosophy

Marine, Earth and Atmospheric Sciences

Raleigh, North Carolina

2013

APPROVED BY:

_____	_____
Dr. Karl W. Wegmann Committee Chair	Dr. DelWayne R. Bohnenstiehl
_____	_____
Dr. James P. Hibbard	Dr. Elana L. Leithold

_____
Dr. Frank J. Pazzaglia

DEDICATION

This is dedicated to my grandparents, Frank and Patricia Sullivan. Their love and dedication to one another and their family has served as an important and positive example throughout my entire life.

BIOGRAPHY

I was born in a small town just east of Philadelphia, PA in November of 1981. I grew up in Manlius, NY and graduated from Fayetteville-Manlius high school in 2000. My love for the mountains encouraged me to enroll at the University of Vermont, where I discovered my passion for the geosciences. I graduated in 2004 and took some time off from academics, trading in the Green Mountains of Vermont for the Rockies of Wyoming and Utah. While out west I suffered a serious snowboarding injury that forced me to refocus and motivated me to pursue a Master of Science in geology at Western Washington University. My experiences at Western furthered my zeal for the geosciences, specifically tectonics, where my thesis research focused on tectonics and rock magnetism. During my Master's I became intrigued by active tectonics and interactions between earth surface and tectonic processes. After graduating in 2008, I once again decided to take some time off from academics. This hiatus lasted only about a month before I knew I wanted to go back to school to pursue a Ph.D. focused on active tectonics. I was fortunate enough to have recently read a paper about some interesting work in the Yellowstone area and look up the lead author, Karl Wegmann. I learned that he studied active tectonics, was an Assistant Professor at North Carolina State University and was looking for students. I enrolled at North Carolina State University in 2009 where Karl has allowed me to work on numerous wonderful projects. Much of the research that I have carried out over the four years of my Ph.D. is presented in this dissertation.

Curriculum Vita - Sean F. Gallen

Dept. of Marine, Earth and Atmospheric Sciences, North Carolina State University, Raleigh, NC 27695

1. Professional Preparation:

University of Vermont	Geology & Political Science	B.A.	2004
Western Washington University	Geology	M.Sc.	2008
North Carolina State University	Earth Sciences	Ph.D.	2013

2. Appointments:

2009 – 2013 Research Assistant/Teaching Assistant, North Carolina State University, Dept. of Marine, Earth and Atm. Sciences, Raleigh, NC

2008 Research Assistant, Western Washington University, Department of Geology, Pacific Northwest Paleomagnetism Laboratory, Bellingham, WA

2006 – 2007 Teaching Assistant, Western Washington University, Department of Geology, Bellingham, WA

3. Publications:

In preparation:

Gallen, S.F., Wegmann, K.W., Bohnenstiehl, D., Pazzaglia, F.J., Brandon, M.T., Fassoulas, C., *in prep.* Coastal Uplift, Activity and the Kinematics of the Hellenic Trough Faults: Tectonic Geomorphology of an Extending Forearc above a Retreating Subduction Zone, Crete, Greece: *For submission to Geophysical Journal International*.

Gallen, S.F., Wegmann, K.W., *in prep.* Evaluating Landscape Response Times and Sensitivity to Temporal Gradients in Rock Uplift and Lithology in the Hellenic forearc, Crete, Greece: *For submission to Geomorphology*.

Gallen, S.F., Wegmann, K.W., *in prep.* Rise of the Messara Graben: uplift rates and sediment flux from an actively extending forearc basin, Crete, Greece: *For submission to Basin Research*.

*Published***:**

Gallen, S.F., Wegmann, K., Bohnenstiehl, D., 2013, Miocene rejuvenation of topographic relief in the southern Appalachians: GSA Today, v. 23, no. 2 p. 4-10.

Gallen, S.F., Wegmann, K., Frankel, K., Hughes, S., Lewis, R., Lyons, N., Paris, P., Ross, K., Bauer, J., Witt, A., 2011. Hillslope response to knickpoint migration in the southern Appalachians:

Implications for the evolution of post-orogenic landscapes: Earth Surface Processes and Landforms, v. 36, no. 9, p. 1254-1267.

4. Synergistic Activities:

1. Mentored two undergraduate students during NSF sponsored summer research exchange program between NCSU and Wake Technical Community College
2. Reviewer manuscripts submitted to Asian Journal of Earth Science
3. Invited research seminar at the geology department of Appalachian State University

5. Awards and Honors

Sigma Xi Gants-in-Aid of Research ($500) - Did the Minoans do it? Testing Natural verses Anthropogenic Controls on Holocene Valley-Bottom Aggradation in the Messara Plain, Crete, Greece, 2012.

People's Choice Award, Best Talk – North Carolina State University, Department of Marine, Earth, and Atmospheric Science and Department of Forestry and Environment Resources Graduate Research Symposium, 2012.

Outstanding Paper Award – Geological Society of America Southeastern Sectional Meeting, 2012.

First Place, Best Poster – North Carolina State University, Graduate Research Symposium, 2012.

Best Talk – North Carolina State University, Department of Marine, Earth, and Atmospheric Science Graduate Research Symposium, 2011.

Runner up, Best Poster – North Carolina State University, Graduate Research Symposium, 2011.

Inducted into Phi Kappa Phi Honor Society, 2011.

Nominated for Outstanding Graduate Teaching Assistant award, NCSU, 2011.

GSA Graduate student research grant ($2,485) – Using Pleistocene Marine Terraces to Constrain Vertical Tectonics of South-central Crete, 2010.

WWU Research and Sponsored Programs Grants ($2,000) – Testing Tectonic Models for the Position of Paleocene Trench-Ridge-Trench Triple Junctions with Paleomagnitism, 2007.

Dean's List, University of Vermont, 2004.

Professional Affiliations:

Geological Society of America, American Geophysical Union, Phi Kappa Phi

ACKNOWLEDGMENTS

I first must thank my loving girlfriend, Amanda DiLorenzo. Without her support, sacrifice and humor it would not have been possible to complete this degree. The love and support of my entire family has made this accomplishment and all of my successes, academic or otherwise, possible. I am indebted to numerous fellow graduate students for discussions and support throughout my time at NCSU, particularly Robert Lewis, Mark Voli, Nathan Lyons, Steve Smith, Stephen Hughes, and Katherine Ryker.

The research in the southern Appalachians was inspired by a trip to the mountains of western North Carolina in the Fall of 2009. This was a field outing between the NCSU Advance Geomorphology Seminar, the Georgia Tech Geomorphology class and folks from the North Carolina State Geological Survey aimed at exploring landscape evolution and natural hazards of the southeastern United States. Dr. Kurt Frankel, who passed away untimely before the completion of this work, is largely responsible for organizing that trip, which ignited my curiosity and passion for understanding the processes that maintain mountainous topography in the southern Appalachians.

I have long been interested in tectonics along convergent margins. I am thankful to have been given the opportunity to conduct research on Crete aimed at better understanding the development of topography above the Hellenic subduction zone. Many of the ideas put forth in this research are based on discussions with others including Karl W. Wegmann, DelWayne R. Bohnenstiehl, Frank J. Pazzaglia, Mark T. Brandon, and Charalampos (Babbis) Fassoulas. I am grateful for the hospitality and friendship of Nikos and Morro Somarakis, proprietors of the San Georgio Hotel. The primary funding for this research comes from Donors to the American Chemical

Society. Additional support for this research comes from a 2011 Geological Society of America Graduate Student Research Grant and a 2013 Sigma Xi grant in aid of research.

My committee members, DelWayne Bohnenstiehl, James Hibbard, Elana (Lonnie) Leithhold, and Frank Pazzaglia are thanked for their time, knowledge, and advice throughout this process. I must give a special thanks to Del for being so generous with his time and patient with me when I dropped by his office, mostly unannounced, to discuss a variety of topics from statistics to faulting to knickpoints. Last and certainly not least, I would like to acknowledge my advisor, Karl Wegmann. Karl has been central to my development as a graduate student and scientist, providing me with a balance of freedom and guidance that has made my Ph.D. successful and productive. His approachability and transparency has been fundamental in building my confidence as a researcher and provided me the foundation from which to model my career. I am extremely thankful to have had a mentor who invested the time, energy and resources to improve all aspects of my development as geologist. Karl has not only been a great role model academically, but also as positive example of dedication to one's family. I could not have asked for a better advisor or friend to have helped me throughout the entirety of my Ph.D.

TABLE OF CONTENTS

LIST OF TABLES

Chapter 1:

Chapter 2:

Chapter 3:

LIST OF FIGURES

Chapter 1:

Chapter 2:

Chapter 3:

Chapter 1

Miocene Rejuvenation of Topographic Relief in the Southern Appalachians

(Reprinted with permission from the Geological Society of America)

Published in *GSA Today* in February 2013 with the following coauthors:

Wegmann, K.W.[1]; Bohnenstiehl, D.R.[1]

[1] Department of Marine, Earth and Atmospheric Sciences, North Carolina State University, Raleigh, NC, USA.

Miocene rejuvenation of topographic relief in the southern Appalachians

Sean F. Gallen*, Karl W. Wegmann, *and* ***DelWayne R. Bohnenstiehl,*** *Dept. of Marine, Earth, and Atmospheric Sciences, North Carolina State University, 2800 Faucette Drive, Raleigh, North Carolina 27695, USA*

ABSTRACT

Conventional wisdom holds that the southern Appalachian Mountains have not experienced a significant phase of tectonic forcing for >200 myr; yet, they share many characteristics with tectonically active settings, including locally high topographic relief, steep slopes, incised river gorges, and frequent mass-wasting events. Two competing hypotheses are commonly used to explain their modern topographic expression. One suggests that relief is largely controlled by variable lithologic resistance to weathering and that their modern form has long persisted in a dynamic equilibrium. The second postulates that their relief is a product of recent rejuvenation, driven either by climate change or the epeirogenic uplift of the land surface driven by mantle forcing. Within portions of the Cullasaja River basin of the southern Appalachians, we show that relief has increased by >150% since the Miocene. Evident within the basin are a set of retreating knickpoints that delineate a rugged, actively incising landscape from lower-relief relict topography. Constraints on the timing of knickpoint entry into the basin suggest that the process of landscape rejuvenation began well prior to the late Cenozoic (<4 myr) transition to a more oscillatory (glacial-interglacial) climate regime. Furthermore, the geomorphology of the Cullasaja River basin is difficult to reconcile in the context of a transition to a more erosive climatic regime but is consistent with an epeirogenically uplifted landscape. Consequently, these observations lend new support to the idea that the rugged topography of the southern Appalachians has developed in response to post-orogenic regional uplift in the Miocene.

INTRODUCTION

Topographic relief exerts an essential control on the rates and processes involved in landscape denudation (Ahnert, 1970; Montgomery and Brandon, 2002), influencing feedbacks between atmospheric, earth-surface and rock exhumation processes, variations in sediment flux, and the magnitude and style of gravity-driven natural hazards. A long-standing debate in the geosciences is centered upon the nature of topographic decay in post-orogenic mountain ranges (Davis, 1889; Hack, 1960; Bishop, 2007). Central to this debate are the still-rugged terrains within the modern Appalachians Mountains of eastern North America, where the last significant phase of tectonic activity presumably ceased shortly after Late Triassic rifting of the Atlantic margin (Hatcher, 1989).

Two hypotheses have been put forth to explain the occurrence of locally high topographic relief, steep slopes, incised river gorges, and frequent mass-wasting events along the passive margin of the southern Appalachians (e.g., Gallen et al., 2011; Wooten et al., 2008). One suggests that topography has persisted though time in a dynamic equilibrium, with relief largely controlled by the variable erodibility of rock units (Hack, 1960; Matmon et al., 2003). The second posits that modern relief is a product of recent rejuvenation (Hack, 1982); however, whether the process governing this resurgence is climate change (Molnar, 2004; Hancock and Kirwan, 2007) or dynamic mantle processes forcing epeirogenic uplift (Pazzaglia and Brandon, 1996) is debated. Recent results obtained from the application of thermochronology (Boettcher and Milliken, 1994) and terrestrial cosmogenic radionuclides (CRNs; Matmon et al., 2003; Hancock and Kirwan, 2007) have not led to a consensus regarding the processes governing the evolution of relief within this landscape—a result of contrasting interpretations drawn from different datasets.

We test the competing hypotheses of dynamic equilibrium and topographic rejuvenation with a study of the geomorphology of the ~300 km^2 Cullasaja River basin of the southern Appalachian Mountains in western North Carolina (Figs. 1A and 1B). The Cullasaja is a tributary to the Little Tennessee River, its waters traveling >1500 river kilometers before discharging into the Gulf of Mexico (Fig. 1A). The timing and magnitude of changes in relief within the basin are quantified through the analysis of a 6-m horizontal resolution LiDAR elevation dataset. Results indicate that the Cullasaja basin landscape has undergone a period of rejuvenation, with relief increasing >150% since the Miocene. The timing of this rejuvenation and the geomorphic expression of the Cullasaja basin landscape, however, suggest that climate change is not the fundamental driving process (cf. Molnar, 2004). Rather, observational evidence favors a model where relief develops as the landscape is epeirogenically uplifted.

STUDY AREA

The Cullasaja River basin contains the geomorphic features required to reconstruct its paleo-relief, including numerous active river knickpoints—sharp convexities in an otherwise concave-up longitudinal river profile—and a preserved relict landscape "surface." The study area lacks evidence of late Pleistocene glaciation and because of its distance from the maximum extent of late Quaternary ice sheets (Thelin and Pike, 1991), the Cullasaja basin experienced little, if any, glacial isostatic response (Fig. 1A). This is supported by studies using decade-long continuous GPS

GSA Today, v. 23, no. 2, doi: 10.1130/GSATG163A.1.

*E-mail: sfgallen@ncsu.edu

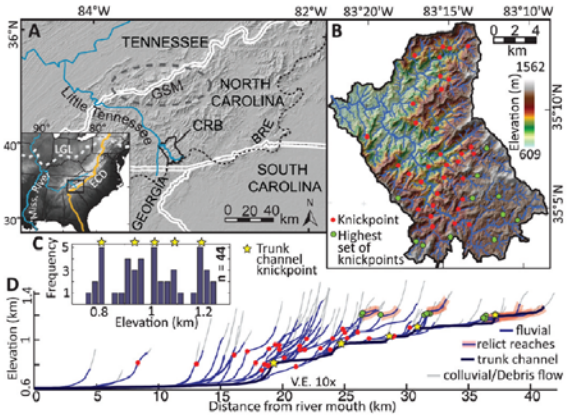

Figure 1 (A) Shaded relief map of the southern Appalachians of western North Carolina and eastern Tennessee, USA. BRE (black dashed line)—Blue Ridge Escarpment; GSM (gray dashed oval)—Great Smoky Mountains. Inset map shows the location of this region in the context of the eastern continental divide (ECD) and the southern limit of glaciation during the last glacial maximum (LGL) (Thelin and Pike, 1991). The headwaters of the Cullasaja River basin (CRB) are >1500 km from the outlet of the Mississippi River. (B) Shaded relief image of the Cullasaja basin with the position of the 44 knickpoints identified in this study. (C) Histogram of knickpoint elevations in 25 m bins. Yellow stars denote the elevations of the trunk channel knickpoints identified in D. (D) Longitudinal river profiles of 52 streams showing the location of 44 knickpoints, relict reaches, and the approximate transition between fluvial and colluvial/debris flow–dominated channels that occurs at drainage areas ≥1.25×10^5 m^2. Red dots—knickpoints; green dots—highest knickpoints.

and satellite gravity surveys to estimate vertical motions due to glacial isostatic adjustments and marine flooding of the North American continental shelf. These datasets demonstrate that the southern Appalachians are either a null region or are slowly subsiding at rates <0.3 mm yr^{-1} (Sella et al., 2007; Wu et al., 2010).

The Cullasaja basin is a detachment-limited geomorphic system with bedrock channels flowing across mostly high-grade gneisses (Gallen et al., 2011) (Fig. DR1, GSA supplemental data repository[1]). A distinct break in log-log channel slope versus upstream drainage area scaling is interpreted to represent the transition between debris flow and fluvial-dominated channels (cf. Montgomery and Foufoula-Georgiou, 1993; Wobus et al., 2006). The maximum drainage area where this scaling break was observed in the Cullasaja basin is ~1.25×10^5 m^2. We choose this as the minimum contributing area in defining the fluvial network. Three observations suggest that lithologic control on hillslope erosion and river incision is relatively uniform throughout the basin: (1) most river channels do not follow lithologic contacts; (2) channel steepness shows no obvious correlation to rock-type; and (3) the observed location of fluvial knickpoints is generally discordant with lithologic contacts (Gallen et al., 2011) (Fig. DR1B [see footnote 1]).

Tributary knickpoints cluster within five altitudinal bands that are coincident with the elevations of five prominent main-stem knickpoints (Figs. 1C and 1D). We appeal to a kinematic model of active knickpoint retreat (e.g., Niemann et al., 2001), which predicts uniformity in vertical velocity for knickpoints resulting from a common base level fall. We interpret the knickpoint clusters as independent waves of bedrock incision actively propagating though the drainage network. The process(es) responsible for knickpoint initiation is unknown; however, eustatic fluctuations are an unlikely mechanism, as it has been shown that such signals do not propagate beyond the lower alluvial reaches of the Mississippi River (Schumm, 1993). Furthermore, the size of knickpoints identified (gradients ≥0.1, dropping >20 m), the total amount of knickpoint relief in the Cullasaja basin (>400 m), and the absence of localities for large-magnitude stream capture events or deep-seated rockslides preclude autogenic knickpoint formation (cf. Wooten et al., 2008; Korup et al., 2006; Prince et al., 2011). With no obvious mechanism for generating the knickpoints, we assess the paleo-topographic conditions in the basin to test the hypothesis that the knickpoints represent a change in geomorphic boundary conditions external to the Cullasaja basin and attempt to determine when this transition began. In doing so we aim to clarify the process(es) driving landscape evolution in the southern Appalachians through the generation of these knickpoints.

DYNAMIC EQUILIBRIUM VERSUS TOPOGRAPHIC REJUVENATION

The highest flight of 11 knickpoints demarcates an important topographic transition in the Cullasaja basin; downstream of the knickpoints, local relief, hillslope and stream channel steepness, and the frequency of landslides all increase significantly when compared to the portion of the landscape isolated above the knickpoints (>1150 m) (Gallen et al., 2011) (Figs. 2A–2D; Table DR1 [see footnote 1]). The occurrence of the knickpoints across a spread in drainage areas (1.4×10^5–7.5×10^6 m^2) implies that they are not stalled at a threshold drainage area, an assumption later tested with numerical modeling (i.e., Crosby and Whipple, 2006; Berlin and Anderson, 2007). Rather, the highest set of knickpoints defines the propagating front of river incision, representing the boundary between an upper-relict landscape and a lower-actively adjusting zone (Fig. 2D) (Clark et al., 2005). This evidence has two important implications: (1) the Cullasaja basin, and probably the entirety of the southern Appalachians, is in a transient state of adjustment, rather than a dynamic equilibrium (cf. Hack, 1960; Matmon et al., 2003), where topography is rejuvenated in the passing wake of mobile knickpoints; and (2) the highest knickpoints and the relict landscape that they isolate contain information about the onset of enhanced incision and the temporal evolution of topography in this region.

ESTIMATING RATES OF EROSION

Ahnert (1970) observed that mean local relief in temperate mid-latitude drainage basins from tectonically inactive settings scales linearly with mean denudation rate. Application of Ahnert's relationship to the Cullasaja basin suggests that erosion rates,

[1]GSA supplemental data item 2013103, extended methods, results, discussion, and figures, is online at www.geosociety.org/pubs/ft2013.htm. You can also request a copy from *GSA Today*, P.O. Box 9140, Boulder, CO 80301-9140, USA; gsatoday@geosociety.org.

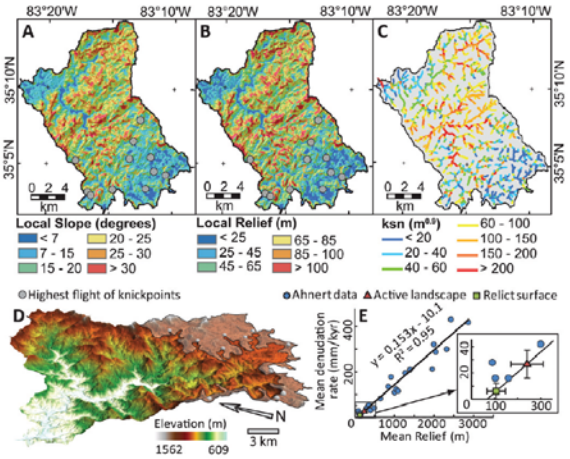

Figure 2. Topographic and fluvial metrics and characterization of relict surface. (A and B) Maps of local (A) slope and (B) relief for the Cullasaja River basin. (C) Normalized channel steepness (k_{sn}) averaged every 100 m along each stream reach. (D) Perspective view of the Cullasaja River basin highlighting the relict reach (shaded) preserved above the highest flight of knickpoints. (E) Plot showing Ahnert's (1970) global relationship between mean relief and mean denudation and the estimated mean denudation rates of the active and relict portions of the Cullasaja River basin with 1σ errors as determined in mean local relief calculations.

based on calculations of mean local relief, are 27 ± 11 and 6 ± 6 mm kyr^{-1} in the active and relict portions of the landscape, respectively (Fig. 2E; Table DR1). A slower rate of erosion for the relict landscape is supported by a reduction in landslide occurrence (Wooten et al., 2008) (Fig. DR1; Table DR1 [see footnote 1]) and an increase in mean soil thickness (Thomas, 1996) relative to the active landscape. These estimates closely align with regional ^{10}Be CRN studies; the active landscape erosion rate matches basin average rates from the Great Smokey Mountains of 27 ± 4 mm kyr^{-1} (Matmon et al., 2003), and the relict landscape prediction is consistent with West Virginia bedrock summit lowering rates (6 ± 3 mm kyr^{-1}) (Hancock and Kirwan, 2007), indicating that they are reasonable values.

PALEO-RELIEF RECONSTRUCTIONS

To estimate the magnitude of paleo-relief in the Cullasaja basin, we first determined the paleo–base level of the relict surface using the channel segments above the highest flight of knickpoints. Equilibrium longitudinal river profiles of the relict channel reaches are reconstructed using the empirically derived scaling law that relates local channel slope (S) to drainage area (A) through the channel parameters of steepness (k_s) and concavity (θ) (e.g., Flint, 1974):

$$S = k_s A^{-\theta}. \quad (1)$$

Of the 11 reaches analyzed, eight had sufficient data to determine estimates of channel steepness and concavity (Fig. DR2; Tables DR2 and DR3 [see footnote 1]). To avoid geomorphic and hydrologic complications introduced at a smaller drainage area, channel steepness indices (k_{sn}) were normalized using the mean concavity (θ_{ref}) of the eight reaches (Table DR3) (Clark et al., 2005; Wobus et al., 2006).

The elevations of the reconstructed tributary and trunk channel profiles fall within error at their confluences and are therefore graded to the same paleo–base level that is ~480 m higher than the present-day river mouth (Figs. 3 and DR2). Assuming that the ridge line erosion rates determined in West Virginia (Hancock and Kirwan, 2007) are regionally applicable to the southern Appalachians implies that the vertical distance between the ridge lines and the relict landscape of the Cullasaja basin has remained approximately the same through time. Paleo-relief in the relict landscape is thus determined to be ~300 ± 25 m by differencing the elevations of the reconstructed river profile from the modern-day drainage divide (Fig. 3). This estimation suggests that relief in the Cullasaja basin has increased 163% ± 24% since the highest knickpoints entered the mouth of the Cullasaja River (Fig. 3).

TIMING OF TOPOGRAPHIC RESURGENCE

The time that the highest trunk channel knickpoint, Highland Falls, passed the mouth of the Cullasaja basin represents a minimum age for the relict landscape and hence the initiation of newly imposed geomorphic boundary conditions. To our knowledge, there are no preserved fluvial terraces related to the upper-most knickpoints in the Cullasaja basin, eliminating more conventional methods for determining their age and propagation rates. Instead, a simple yet novel approach is used to constrain the timing of knickpoint entry into the basin. Assuming that knickpoint propagation proceeded as a kinematic wave, the travel time of the highest knickpoints from the river mouth to their current position is the same as the time required to erode the rock

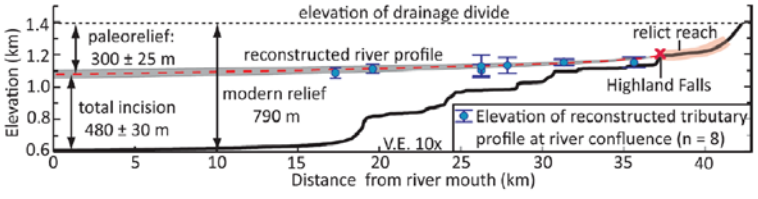

Figure 3. Modern and reconstructed paleo-river profiles with the modeled elevations of tributary-trunk channel junctions projected to the paleo profile. The 2σ elevation errors are from the normalized steepness indices and are based on linear regressions through log-log channel slope-drainage area data (Fig. DR2 [see text footnote 1]). The amount of paleo-relief in the Cullasaja River basin is based on the assumption that the ridge lines have eroded at a rate commensurate with the mean denudation rate of the relict surface (6 ± 6 mm kyr^{-1}).

volume "missing" from the active landscape (Fig. 4A) (Norton et al., 2008). The knickpoint travel time (t_k) is estimated by:

$$t_k = \left(\frac{V}{A_c}\right)\dot{E}^{-1}, \quad (2)$$

where A_c and V are the area below the knickpoint elevation contour and volume, respectively, and $\dot{E}$ is the average erosion rate within the active landscape (Fig. 4A). A minimum estimate of the volume of rock eroded from beneath the highest knickpoints is found by differencing the basin topography with a sloping surface fit to the modern drainage divide, and a maximum estimate is determined by differencing the basin topography with a horizontal surface defined by the elevation contour at the top of Highland Falls (Fig. 4B).

Using estimates of the basin average erosion rate for the active landscape between 16 and 38 mm kyr^{-1} (Figs. 2E and 4C), Highland Falls would have entered the mouth of the river between 17.6 and 4.6 Ma. Applying the mean denudation rate and average volume of eroded rock, the entry time becomes ca. 8.5 Ma (Fig. 4C). It is, however, unlikely that these knickpoints were formed at the mouth of the Cullasaja basin. Even if the Cullasaja River was not incising (0 mm kyr^{-1}), while the Little Tennessee River cut down at 600 mm kyr^{-1} (estimated from the fastest rates of river incision measured in Appalachian draining rivers by Reusser et al., 2004), such conditions would need to be sustained >150 kyr to form the largest Cullasaja basin knickpoints (>100 m). The long-term persistence of such conditions is unrealistic; rather, the knickpoints likely formed some distance down the Little Tennessee River by some other mechanism. This 17.6–4.6 Ma time range therefore provides an extreme minimum value for the age of the relict surface, and thus the onset of modern relief production in the southern Appalachians almost certainly pre-dates the transition to significant orbitally driven climate unsteadiness beginning 4 to 3 Ma (Peizhen et al., 2001; Molnar, 2004).

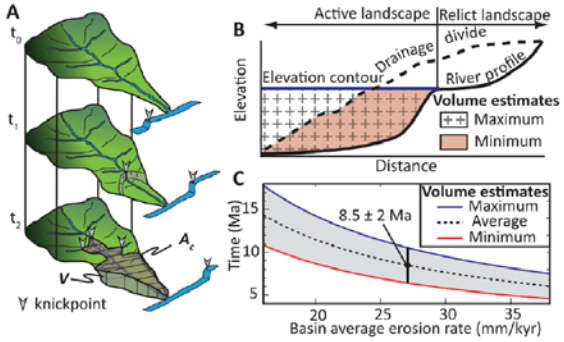

Figure 4. Conceptual model and results of volume-for-time substitutions. (A) Cartoon illustrating the idealized evolution of a drainage basin experiencing base-level lowering brought on by the propagation of a knickpoint as a kinematic wave. The final time step (t_2) identifies the volume of eroded material (V) and area of the active landscape (A_c), which are the parameters used to calculate the time since a knickpoint entered the mouth of a drainage basin using equation 2. (B) Schematic cross section illustrating the two methods used to estimate "missing" volume below the elevation of the highest trunk channel knickpoint. (C) Plot of the estimated time since the Highland Falls knickpoint entered the mouth of the Cullasaja River basin. The vertical black line is the mean basin average erosion rate determined for the active portion of the Cullasaja River basin predicted by the Ahnert (1970) trend (27 ± 11 mm kyr^{-1}) and matches that of the nearby Great Smokey Mountains (Matmon et al., 2003; 27 ± 4 mm kyr^{-1}).

Moreover, it is difficult to explain the geomorphology of the Cullasaja basin in the framework of climate change. A transition to a cooler, wetter, and rapidly fluctuating climate should enhance regional erosional efficiency (Molnar, 2004), but it would need to be locally absent in order to preserve a relict surface, which is highly unlikely in the Appalachians. A change to a more erosive environment also is predicted to reduce channel steepness (Whipple and Tucker, 1999; Wobus et al., 2010), not increase it as is observed in the Cullasaja basin. Collectively, the timing of topographic rejuvenation and geomorphology of the Cullasaja basin eliminates late Cenozoic (<4 myr) climate change as the fundamental driver of the enhancement of relief in the southern Appalachians.

TESTING KEY ASSUMPTIONS

We numerically model the spatial distribution of the 11 highest knickpoints in the Cullasaja basin to test the assumptions that the knickpoints are: (1) genetically related and (2) verify that they are still actively propagating and not stalled. Testing these assumptions is important because it will show that the uppermost knickpoints originated from a single source and are currently moving through and dissecting the relict landscape. Further, modeling will support the age constraints from above if knickpoint velocity is determined to be reasonable (e.g., within measured values). To this end, a generic knickpoint celerity model is used (Crosby and Whipple, 2006):

$$\frac{dx}{dt} = CA^p, \quad (3)$$

where dx/dt is the upstream knickpoint migration rate in m yr^{-1}, C is a dimensional coefficient of erodability in units m$^{(1-2p)}$ yr^{-1}, A is contributing drainage area, and p is a non-dimensional constant reflecting knickpoint celerity dependence on drainage area, a proxy for discharge. A brute-force two-parameter search is used to find the best-fitting C and p parameters that minimize the misfit between the observed and modeled knickpoint positions (Crosby and Whipple, 2006; Berlin and Anderson, 2007).

Using the results from the volume-for-time substitutions (eq. 2), we consider a suite of 28 model runs with knickpoints entering the Cullasaja basin between 4.5 to 18 Ma (0.5 myr intervals). Each model run worked equally well, with <2% difference in the sum of the least squares residual between the observed and modeled knickpoint positions for any given travel time (Figs. DR3 and DR4 [see footnote 1]). These models predict the position of the 11 highest knickpoints remarkably well (Figs. 5A and 5B), implying that the knickpoints do behave as a kinematic wave. Present-day minimum knickpoint velocity varies between 0.13 and 2.25 mm yr^{-1} for the set of modeled travel times, confirming that the knickpoints are mobile and dissecting the relict landscape. Best fitting p parameters ranging from 0.51 to 0.54 are consistent with a square root of area scaling (Berlin and Anderson, 2007) (Fig. DR3). The erosional

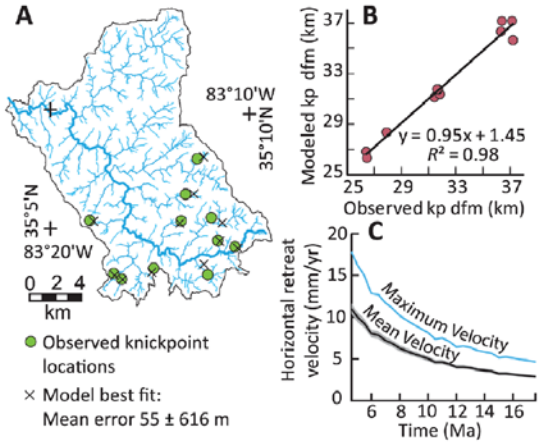

Figure 5. Knickpoint celerity model results. Example of results from the best-fitting C and p parameters for a knickpoint travel time of 8.5 myr, which is the mean time prediction based upon the estimated basin average erosion rate from the Ahnert (1970) relationship as well as the average of the two volume-for-time estimates (see Fig. 4). (A) Observed and modeled knickpoint distribution. Mean error refers to the mean of the differences between the observed knickpoint and the modeled knickpoint distance from the mouth of the Cullasaja River. (B) Relationship between observed and modeled knickpoint (kp) positions, expressed with respect to their distance from the mouth (dfm) of the Cullasaja River. (C) Maximum and mean (gray is ±1σ error) velocity of the best fitting model result associated with each run.

coefficient C, however, adjusts over nearly an order of magnitude to accommodate the modeled knickpoint travel time (Figs. DR3 and DR4). Nonetheless, the maximum and mean knickpoint velocity predicted by the numerical modeling are within the range of measured knickpoint propagation rates (Loget and Van Den Driessche, 2009) (Fig. 5C), suggesting that calculated knickpoint travel times are reasonable. Independent support for reasonable knickpoint travel times comes from estimates of river incision that are within the range of measured long-term (10^4–10^6 yr) valley incision for Appalachian-draining rivers (Mills, 2000; Reusser et al., 2006) that, based on our longitudinal profile reconstructions (Fig. 3), fall between 24 and 140 mm kyr^{-1}.

DRIVING MECHANISM FOR TOPOGRAPHIC REJUVENATION

The proposed timing of the topographic resurgence reported here is roughly concurrent with previous studies that demonstrate increased sedimentation rates and grain sizes delivered from the Appalachians eastward to off-shore basins along the Atlantic margin (Poag and Sevon, 1989; Pazzaglia and Brandon, 1996) and westward to the Mississippi embayment (Potter, 1955) and Gulf of Mexico (Galloway et al., 2011) ca. 16 to 12 Ma. This coincidence suggests a causative link between the process responsible for relief rejuvenation in the Appalachians and the flux of sediment to adjacent depocenters and implies a regional disturbance to the Appalachians in the Miocene. With no obvious surficial process driving the Miocene topographic resurgence, what mechanism can be called upon to explain the results reported in this paper? The formation of large knickpoints, the steepening of river gradients, the ongoing dissection of a relict landscape, and the pulse of sediment to offshore basins are broadly consistent with a region that has undergone uplift; however, the Appalachians generally lack evidence of late Cenozoic deformation (Hatcher, 1989).

Epeirogenic uplift of the southern Rocky Mountains and Colorado Plateau (Karlstrom et al., 2012) and the southern Sierra Nevada range (Clark et al., 2005) has produced a similar geomorphic response to what is reported here. In these settings, the uplifted regions also exhibit strong spatial correlations with geophysical anomalies in the crust and lithospheric mantle, providing insight into the driving mechanism(s). Although large-scale geophysical imaging of the tectonically passive eastern United States has received relatively little attention compared to the western United States, Grand et al. (1997) and Ren et al. (2007) have documented fragments of the relict Farallon oceanic slab within the mantle beneath the modern Appalachians. More recently, Wagner et al. (2012) produced receiver function profiles crossing the southern Appalachians of North Carolina. They document Moho holes, double Moho arrivals, and localized seismic scatters in the lithospheric mantle. One interpretation of these results is that portions of the over-thickened crust have delaminated (cf. Zandt et al., 2004), perhaps driving the uplift and rejuvenation of the southern Appalachian landscape. Further testing of this hypothesis is possible by continued collaborations between the geomorphic and geophysical communities and the arrival of the EarthScope USArray seismic observatory experiment to the eastern United States in 2013.

CONCLUSIONS

Our results show that topography in the Cullasaja River basin, and likely much of the west-draining southern Appalachians, is in a transient state of adjustment to a newly imposed regional base level (Gallen et al., 2011), and thus it is not in a dynamic equilibrium. Relief has increased here >150% since the Miocene, predating the amplification of glacial-interglacial cycles that initiated in the Pliocene and continue today. Our results favor the hypothesis that some form of dynamic mantle forcing has caused epeirogenic uplift of the Appalachians that began in the Miocene, because it can explain the generation of knickpoints and the preservation of a relict landscape in the Cullasaja basin that are difficult to account for in the context of climate change alone. Importantly, it appears that this event may be related to the increase in grain size and rate of sediments delivered to basins both east (Poag and Sevon, 1989; Pazzaglia and Brandon, 1996) and west (Potter, 1955; Galloway et al., 2011) of the Appalachian mountains, implying that the surface response to relief generation in the Cullasaja basin is likely related to a broad, regional phenomenon. This research sheds light on a long-standing enigma in the geosciences; yet, the results presented here also bring up new questions and testable hypotheses about the geomorphology and late Cenozoic geodynamic evolution of the southern Appalachians.

ACKNOWLEDGMENTS

We are forever indebted to K.L. Frankel, who passed untimely before the completion of this study. The conception of this project would not have been possible without his interest and enthusiasm about the evolution of the Appalachians. We would like to thank Marin Clark and an anonymous reviewer for excellent reviews that helped improve and refine this manuscript.

Chuck Harrington helped clarify an earlier version of this manuscript. Bernie Housen is credited with encouraging us to submit this work to *GSA Today*.

REFERENCES CITED

Ahnert, F., 1970, Functional relationships between denudation, relief, and uplift in large, mid-latitude drainage basins: American Journal of Science, v. 268, no. 3, p. 243–263, doi: 10.2475/ajs.268.3.243.

Berlin, M.M., and Anderson, R.S., 2007, Modeling of knickpoint retreat on the Roan Plateau, western Colorado: Journal of Geophysical Research, v. 112, F03S06, doi: 10.1029/2006jf000553.

Bishop, P., 2007, Long-term landscape evolution: Linking tectonics and surface processes: Earth Surface Processes and Landforms, v. 32, no. 3, p. 329–365, doi: 10.1002/esp.1493.

Boettcher, S.S., and Milliken, K.L., 1994, Mesozoic-Cenozoic unroofing of the southern Appalachian Basin: Apatite fission track evidence from Middle Pennsylvanian sandstones: The Journal of Geology, v. 102, no. 6, p. 655–668.

Clark, M.K., Maheo, J.S., Saleeby, J., and Farley, K.A., 2005, The non-equilibrium landscape of the southern Sierra Nevada, California: GSA Today, v. 15, no. 9, p. 4–10, doi: 10:1130/1052-5173(2005)015<4:TNELOT>2.0.CO;2.

Crosby, B.T., and Whipple, K.X., 2006, Knickpoint initiation and distribution within fluvial networks: 236 waterfalls in the Waipaoa River, North Island, New Zealand: Geomorphology, v. 82, no. 1–2, p. 16–38.

Davis, W.M., 1889, The river and valleys of Pennsylvania: National Geographic Magazine, v. 1, p. 183–253.

Flint, J.J., 1974, Stream gradient as a function of order, magnitude, and discharge: Water Resources Research, v. 10, no. 5, p. 969–973, doi: 10.1029/WR010i005p00969.

Gallen, S.F., Wegmann, K.W., Frankel, K.L., Hughes, S., Lewis, R.Q., Lyons, N., Paris, P., Ross, K., Bauer, J.B., and Witt, A.C., 2011, Hillslope response to knickpoint migration in the Southern Appalachians: Implications for the evolution of post-orogenic landscapes: Earth Surface Processes and Landforms, v. 36, no. 9, p. 1254–1267, doi: 10.1002/esp.2150.

Galloway, W.E., Whiteaker, T.L., and Ganey-Curry, P., 2011, History of Cenozoic North American drainage basin evolution, sediment yield, and accumulation in the Gulf of Mexico basin: Geosphere, v. 7, no. 4, p. 938–973, doi: 10.1130/ges00647.1.

Grand, S.P., van de Hilst, R.D., and Widiyantoro, S., 1997, Global seismic tomography: A snapshot of convection in the earth: GSA Today, v. 7, no. 4, p. 1–7.

Hack, J.T., 1960, Interpretation of erosional topography in humid temperate regions: American Journal of Science, v. 258-A, p. 80–97.

Hack, J.T., 1982, Physiographic divisions and differential uplift in the Piedmont and Blue Ridge: U.S. Geological Survey Professional Paper 1265-P, p. 1–49.

Hancock, G., and Kirwan, M., 2007, Summit erosion rates deduced from ^{10}Be: Implications for relief production in the central Appalachians: Geology, v. 35, no. 1, p. 89–92, doi: 10.1130/g23147a.1.

Hatcher, R.D., Jr., 1989, Tectonic synthesis of the U.S. Appalachians, *in* Hatcher, R.D., Jr., Thomas, W.A., and Viele, G.W., eds., The Appalachian-Ouachita Orogen in the United States: Boulder, Colorado, USA Geological Society of America Decade of North American Geology, v. F-2, p. 511–531.

Karlstrom, K.E., Coblentz, D., Dueker, K., Ouimet, W., Kirby, E., Van Wijk, J., Schmandt, B., Kelley, S., Lazear, G., Crossey, L.J., Crow, R., Aslan, A., Darling, A., Aster, R., MacCarthy, J., Hansen, S.M., Stachnik, J., Stockli, D.F., Garcia, R.V., Hoffman, M., McKeon, R., Feldman, J., Heizler, M., Donahue, M.S., and the CREST Working Group, 2012, Mantle-driven dynamic uplift of the Rocky Mountains and Colorado Plateau and its surface response: Toward a unified hypothesis: Lithosphere, v. 4, no. 1, p. 3–22, doi: 10.1130/L150.1.

Korup, O., 2006, Rock-slope failure and the river long profile: Geology, v. 34, no. 1, p. 45–48, doi: 10.1130/G21959.1.

Loget, N., and Van Den Driessche, J., 2009, Wave train model for knickpoint migration: Geomorphology, v. 106, no. 3–4, p. 376–382.

Matmon, A., Bierman, P.R., Larsen, J., Southworth, S., Pavich, M., and Caffee, M., 2003, Temporally and spatially uniform rates of erosion in the southern Appalachian Great Smoky Mountains: Geology, v. 31, no. 2, p. 155–158, doi: 10.1130/0091-7613(2003)031<0155:TASURO>2.0.co;2.

Mills, H.H., 2000, Apparent increasing rates of stream incision in the eastern United States during the late Cenozoic: Geology, v. 28, no. 10, p. 955–957, doi: 10.1130/0091-7613(2000)28<955:AIROSI>2.0.co;2.

Molnar, P., 2004, Late Cenozoic increase in accumulation rates of terrestrial sediment: How might climate change have affected erosion rates?: Annual Review of Earth and Planetary Sciences, v. 32, no. 1, p. 67–89, doi: 10.1146/annurev.earth.32.091003.143456.

Montgomery, D.R., and Brandon, M.T., 2002, Topographic controls on erosion rates in tectonically active mountain ranges: Earth and Planetary Science Letters, v. 201, no. 3–4, p. 481–489.

Montgomery, D.R., and Foufoula-Georgiou, E., 1993, Channel network source representation using digital elevation models: Water Resources Research, v. 29, no. 12, p. 3925–3934.

Niemann, J.D., Gasparini, N.M., Tucker, G.E., and Bras, R.L., 2001, A quantitative evaluation of Playfair's law and its use in testing long-term stream erosion models: Earth Surface Processes and Landforms, v. 26, no. 12, p. 1317–1332, doi: 10.1002/esp.272.

Norton, K.P., von Blanckenburg, F., Schlunegger, F., Schwab, M., and Kubik, P.W., 2008, Cosmogenic nuclide-based investigation of spatial erosion and hillslope channel coupling in the transient foreland of the Swiss Alps: Geomorphology, v. 95, no. 3–4, p. 474–486.

Pazzaglia, F.J., and Brandon, M.T., 1996, Macrogeomorphic evolution of the post-Triassic Appalachian mountains determined by deconvolution of the offshore basin sedimentary record: Basin Research, v. 8, no. 3, p. 255–278, doi: 10.1046/j.1365-2117.1996.00274.x.

Peizhen, Z., Molnar, P., and Downs, W.R., 2001, Increased sedimentation rates and grain sizes 2–4 myr ago due to the influence of climate change on erosion rates: Nature, v. 410, no. 6831, p. 891–897.

Poag, C.W., and Sevon, W.D., 1989, A record of Appalachian denudation in post-rift Mesozoic and Cenozoic sedimentary deposits of the U.S. Middle Atlantic continental margin: Geomorphology, v. 2, no. 1–3, p. 119–157.

Potter, P.E., 1955, The petrology and origin of the Lafayette gravel part 2. Geomorphic history: The Journal of Geology, v. 63, no. 2, p. 115–132.

Prince, P.S., Spotila, J.A., and Henika, W.S., 2011, Stream capture as driver of transient landscape evolution in a tectonically quiescent setting: Geology, v. 39, no. 9, p. 823–826, doi: 10.1130/G32008.1.

Ren, Y., Stutzmann, E., van der Hilst, R.D., and Besse, J., 2007, Understanding seismic heterogeneities in the lower mantle beneath the Americas from seismic tomography and plate tectonic history: Journal of Geophysical Research, v. 112, B01302, doi: 10.1029/2005jb004154.

Reusser, L.J., Bierman, P.R., Pavich, M.J., Zen, E., Larsen, J., and Finkel, R., 2004, Rapid Late Pleistocene incision of Atlantic passive-margin river gorges: Science, v. 305, 5683, p. 499–502, doi: 10.1126/science.1097780.

Reusser, L.J., Bierman, P.R., Pavich, M.J., Larsen, J., and Finkel, R., 2006, An episode of rapid bedrock channel incision during the last glacial cycle, measured with ^{10}Be: American Journal of Science, v. 306, no. 2, p. 69–102.

Schumm, S.A., 1993, River response to base-level change; implications for sequence stratigraphy: The Journal of Geology, v. 101, no. 2, p. 279–294.

Sella, G.F., Stein, S., Dixon, T.H., Craymer, M., James, T.S., Mazzotti, S., and Dokka, R.K., 2007, Observation of glacial isostatic adjustment in "stable" North America with GPS: Geophysical Research Letters, v. 34, L02306, doi: 10.1029/2006gl027081.

Thelin, G.P., and Pike, R.J., 1991, Landforms of the conterminous United States—A digital shaded-relief portrayal: USGS Map 2206, scale 1:3,500,000, 1 sheet.

Thomas, D.J., 1996, Soil survey of Macon County, North Carolina: Washington D.C., U.S. Department of Agriculture Natural Resources Conservation Service, 322 p.

Wagner, L.S., Stewart, K., and Metcalf, K., 2012, Crustal-scale shortening structures beneath the Blue Ridge Mountains, North Carolina, USA: Lithosphere, v. 4, no. 3, p. 242–256, doi: 10.1130/L184.1.

Whipple, K.X., and Tucker, G.E., 1999, Dynamics of the stream-power river incision model: Implications for height limits of mountain ranges, landscape response timescales, and research needs: Journal of

Geophysical Research, v. 104, B8, p. 17,661–17,674, doi: 10.1029/1999jb900120.
Wobus, C., Whipple, K.X., Kirby, E., Snyder, N., Johnson, J., Spyropolou, K., Crosby, B., and Sheehan, D., 2006, Tectonics from topography: Procedures, promise, and pitfalls, *in* Willett, S.D., Hovius, N., Brandon, M.T., and Fisher, D.M., eds., Tectonics, Climate and Landscape Evolution: Geological Society of America Special Papers 398, p. 55–74, doi: 10.1130/2006.2398(04).
Wobus, C.W., Tucker, G.E., and Anderson, R.S., 2010, Does climate change create distinctive patterns of landscape incision?: Journal of Geophysical Research, v. 115, F04008, doi: 10.1029/2009jf001562.
Wooten, R.M., Gillon, K.A., Witt, A.C., Latham, R.S., Douglas, T.J., Bauer, J.B., Fuemmeler, S.J., and Lee, L.G., 2008, Geologic, geomorphic, and meteorological aspects of debris flows triggered by Hurricanes Frances and Ivan during September 2004 in the Southern Appalachian Mountains of Macon County, North Carolina (southeastern USA): Landslides, v. 5, no. 1, p. 31–44, doi: 10.1007/s10346-007-0109-9.
Wu, X., Heflin, M.B., Schotman, H., Vermeersen, B.L.A., Dong, D., Gross, R.S., Ivins, E.R., Moore, A.W., and Owen, S.E., 2010, Simultaneous estimation of global present-day water transport and glacial isostatic adjustment: Nature Geoscience, v. 3, no. 9, p. 642–646.
Zandt, G., Gilbert, H., Owens, T.J., Ducea, M., Saleeby, J., and Jones, C.H., 2004, Active foundering of a continental arc root beneath the southern Sierra Nevada in California: Nature, v. 431, 7004, p. 41–46.

Manuscript received 10 Aug. 2012; accepted 30 Oct. 2012.

APPENDICES

Appendix 1.1: GSA Supplemental data repository item 2013103

Miocene rejuvenation of topographic relief in the southern Appalachians

GSA Supplemental data repository item 2013103; available online at
www.geosociety.org/pubs/ft2013.htm

Results and Discussion

The geology of the Cullasaja River basin consists primarily of biotite – to biotite-muscovite gneiss (Fig. DR1). The consistency of rock type coupled with our observations that lithologic contacts have no clear relationship to stream channel position, knickpoint location, or channel steepness (Fig. DR1) leads to the conclusion that bedrock control on hillslope erosion and river incision is uniform at the scale of the basin (Gallen et al., 2011).

The reference concavity (ϑ_{ref}) was calculated as the average of the eight relict reaches by linear regression through log slope – log drainage area data (Table DR2, DR3; Fig DR2). Three of the relict reaches were excluded because they did not have enough data points to yield statistically significant regressions of slope-drainage area data ($r^2 < 0.7$; Table DR2). All of the concavities extracted from the relict reaches fall within error of the theoretical range (0.3 to 0.6) for equilibrium stream channels (Table DR3; Whipple and Tucker, 1999). The χ_{ref} and normalized steepness index (k_{sn}) were used to reconstruct each relict reach to the mouth of the Cullasaja River (Fig. DR2).

Each of the 28 numerical model runs predicts the positions of the knickpoints very well. The least squares residuals for each model run, however, were not significantly different from one another (Fig. DR3, DR 4). This finding emphasizes the importance of having accurate and precise constraints on the age and/or travel times of knickpoints when using this approach to extract

information about the physical meaning of the *C* and *p* parameters with respect to steam channel incision (cf., Berlin and Anderson, 2007).

EXTENDED METHODOLOGY

Channel data extraction and knickpoint identification

The surface hydrographic network was defined from a 6-m horizontal resolution digital elevation model (DEM) using the *Flow Direction* and *Flow Accumulation* routines in ArcGIS. From the DEM, flow direction, and flow accumulation grids were used with the ArcGIS and MATLAB StreamProfiler tools package (http://geomorphtools.org). Stream channels were sampled every 3 m vertically. A 100 m smoothing window was applied to remove pre-processing artifacts and noise embedded in the DEM prior to analysis. Only knickpoints present in fluvially-dominated channels were identified. The cutoff between fluvial and colluvial channels followed previous workers in identifying this transport process transition as visible breaks in slope-area space (Montgomery and Foufoula-Georgiou, 1993; Wobus et al., 2006). Using 52 stream channels we selected the maximum drainage where this scaling break occurs as 1.25×10^5 m^2, well within the typical range of drainage areas (10^5 - 10^6 m^2) where this shift is observed to occur . Knickpoints are identified as pronounced longitudinal profile convexities that drop > 20 m vertically and with gradients ≥ 0.1.

Terrain analysis

A smoothed slope map was constructed by passing a 100 m radius mean filter over the slope model derived from the DEM within ArcGIS. Similarly, a relief map was generated by passing a 100 m circular radius focal range window over the DEM. Mean local relief and mean slope values were derived by calculating local relief and local slope values over ~ 3 km^2 blocks that were then averaged for the relict and active landscapes. The relict surface was delineated as those areas above the elevation of the highest knickpoints (~ 1150 m), characterized by mean slopes < 15° and maximum

local relief < 45 m. The standard errors in the mean local relief calculations for the active and relict landscapes were used to assign the 1σ errors to our estimates of the basin average erosion rates based on the Ahnert (1970) dataset (Fig. 2e).

Longitudinal river profile reconstructions

Paleo-river profiles were reconstructed by assuming that the modern surface hydrologic network is similar to its past configuration. This simplifying assumption allows us to carry out stepwise calculations with equation (3) for the theoretical elevation of the paleo-river profile using k_{sn}, ϑ_{ref}, and drainage area to determine the local slope for each distance-increment (pixel) downstream from the top of a knickpoint to the mouth of the drainage basin (e.g., Schoenbohm et al., 2004; Clark et al., 2005). Error in the determination of stream steepness and concavity indices using slope-area regressions propagate through into the normalized steepness index values allowing for 2σ errors to be assigned to each longitudinal profile reconstruction (Fig. DR2; Table DR3).

Volume and knickpoint travel time calculations

The volume of rock presumably eroded, or "missing" below the elevation of the highest flight of knickpoints was calculated in two ways. First, the volume between the 1150 m elevation contour, which is coincident with the elevation of the highest trunk channel knickpoint, and the modern surface of the drainage basin encompassed by this contour was calculated to get a maximum volume estimate. Second, a surface cap was created using the modern drainage divide below the 1150 m contour to the mouth of the basin. The volume between this cap and the modern basin surface was calculated and is considered a minimum volume estimate. Knickpoint travel times were determined by using these volume estimates in equation (1) and by assuming basin average erosion rates from 16 to 38 mm kyr^{-1} and calculations carried out at 0.1 mm kyr^{-1} intervals.

Knickpoint celerity model

The celerity model equation used to determine the distribution of knickpoints has two unknown parameters. Following previous researchers (Crosby and Whipple, 2006; Berlin and Anderson, 2007), a brute-force search was used to determine the best combination of *C* (detachment-limited erosion coefficient) and *p* (drainage area exponent) parameters for the model. This analysis was carried out for the range of knickpoint travel times determined from the volume-for-time substitutions between 4.5 to 18 Ma at 0.5 Ma intervals. The *C* and *p* combination resulting in the minimum sum of squared residuals for the 11 modeled knickpoints was assigned as the best fit result for a specified time (e.g., 8.5 Ma) of knickpoint entry into the mouth of the drainage basin (Crosby and Whipple, 2006; Berlin and Anderson, 2007). The *p*-value was allowed to vary from 0.2 to 1.3 over 40 evenly-space increments, while *C* varied logarithmically between 10^{-10} to 10^{-4} over 500 increments. The resulting best fit *C* and *p* combination for each modeled travel time was used to determine the maximum, mean, and minimum velocity of vertical retreat for the 11 highest knickpoints.

Data Repository Figure Captions

Additional References for Data Repository Text

Berlin, M. M., and Anderson, R. S., 2007, Modeling of knickpoint retreat on the Roan Plateau, western Colorado: Journal of Geophysical Research, v. 112, no. F3, p. F03S06, doi: 10.1029/2006jf000553.

Clark, M. K., Maheo, J. S., Saleeby, J., and Farley, K. A., 2005, The non-equilibrium landscape of the southern Sierra Nevada, California: GSA Today, v. 15, no. 9, p. 4 – 10, doi: 10:1130/1052-5173(2005)015<4:TNELOT>2.0.CO;2.

Crosby, B. T., and Whipple, K. X., 2006, Knickpoint initiation and distribution within fluvial networks: 236 waterfalls in the Waipaoa River, North Island, New Zealand: Geomorphology, v. 82, no. 1-2, p. 16-38.

Gallen, S. F., Wegmann, K. W., Frankel, K. L., Hughes, S., Lewis, R. Q., Lyons, N., Paris, P., Ross, K., Bauer, J. B., and Witt, A. C., 2011, Hillslope response to knickpoint migration in the Southern Appalachians: implications for the evolution of post-orogenic landscapes: Earth Surface Processes and Landforms, v. 36, no. 9, p. 1254-1267, doi: 10.1002/esp.2150.

Montgomery, D. R., and Foufoula-Georgiou, E., 1993, Channel network source representation using digital elevation models: Water Resources Research, v. 29, no. 12, p. 3925-3934.

North Carolina Geological Survey. 1985. Geologic map of North Carolina, scale 1:500,000: [accessed at http://www.nconemap.com; 02/01/2010].

Schoenbohm, L. M., Whipple, K. X., Burchfiel, B. C., and Chen, L., 2004, Geomorphic constraints on surface uplift, exhumation, and plateau growth in the Red River region, Yunnan Province, China: Geological Society of America Bulletin, v. 116, no. 7-8, p. 895-909, doi: 10.1130/b25364.1.

Whipple, K. X., and Tucker, G. E., 1999, Dynamics of the stream-power river incision model: Implications for height limits of mountain ranges, landscape response timescales, and research needs: Journal of Geophysical Research, v. 104, no. B8, p. 17661-17674, doi: 10.1029/1999jb900120.

Wobus, C., Whipple, K. X., Kirby, E., Snyder, N., Johnson, J., Spyropolou, K., Crosby, B., and Sheehan, D., 2006, Tectonics from topography: Procedures, promise, and pitfalls: Geological Society of America Special Paper, v. 398, p. 55-74, doi: 10.1130/2006.2398(04).

Supplementary tables

Table DR1. Topographic metrics of the active and relict landscape

Metric[1]	Active[2]		Relict[3]	
	mean	1σ	mean	1σ
Relief (m)	230	70	106	40
Slope (°)	20	2	14	4
normalized steepness index (k_{sn})	93	34.9	29.7	16.1
landslide frequency per km^2	0.84	0.47	0.28	0.35

[1] Metrics of mean relief, mean slope, mean channel steepness, and landslide frequency are from 24 tributary basins.
[2] Drainage basins with a mean elevation below 1150 m were categorized in the active landscape.
[3] Drainage basins with a mean elevation above 1150 m were categorized in the relict landscape

Table DR2. Statistics for the highest flight of knickpoints.

Knickpoint distance from divide (km)	Knickpoint distance from tributary mouth (m)	Knickpoint elevation (m)	Upstream drainage area (km^2)	Latitude (° N)	Longitude (° W)	Statistically significant regression
4.8	37.15	1191	4.8	35.07093	83.17401	yes
1.89	27.91	1187	1.6	35.13163	83.20761	yes
1.83	26.4	1188	1.64	35.10807	83.21677	yes
1.32	31.44	1202	0.67	35.08895	83.22121	yes
4.35	36.4	1182	7.36	35.09091	83.19406	yes
1.62	36.33	1159	1.17	35.07560	83.18929	yes
0.66	37.22	1201	0.28	35.04410	83.18891	no
0.52	31.84	1228	0.14	35.05541	83.24320	no
1.71	31.72	1235	1.09	35.04753	83.27156	yes
2.01	31.63	1225	1.03	35.05110	83.27854	yes
0.95	26.46	1209	0.3	35.08756	83.29835	no

Table DR3. Statistics of relict reach regressions and profile reconstructions

Stream[1]	Concavity (θ) of stream reach (±2σ)	Channel reach steepness (k_s)	Reference concavity (θ_{ref})	Channel reach normalized steepness index[2] (k_{sn} ± 2σ)	Mean reconstructed profile elevation at Cullasaja River confluence (m ± 2σ)[3]
trunk	0.56 ± 0.28	71.7	0.5	22 ± 4	—
1	0.55 ± 0.29	147	0.5	38.8 ± 4	1085 ± 10
2	0.53 ± 0.21	83.1	0.5	31.7 ± 3	1111 ± 6
3	0.25 ± 0.6	3.17	0.5	13.1 ± 12	1132 ± 48
4	0.43 ± 0.27	9.24	0.5	16.3 ± 3	1153 ± 3
5	0.47 ± 0.16	7.84	0.5	9.9 ± 1	1153 ± 2
6	0.65 ± 0.24	93	0.5	30.1 ± 3	1122 ± 12
7	0.59 ± 0.42	161	0.5	30.5 ± 6	1116 ± 20

[1] See Fig. DR2 for the location of stream reaches and profile reconstructions.
[2] Units are in $m^{0.9}$.
[3] Errors are associated with the calculation of the k_{sn} values.

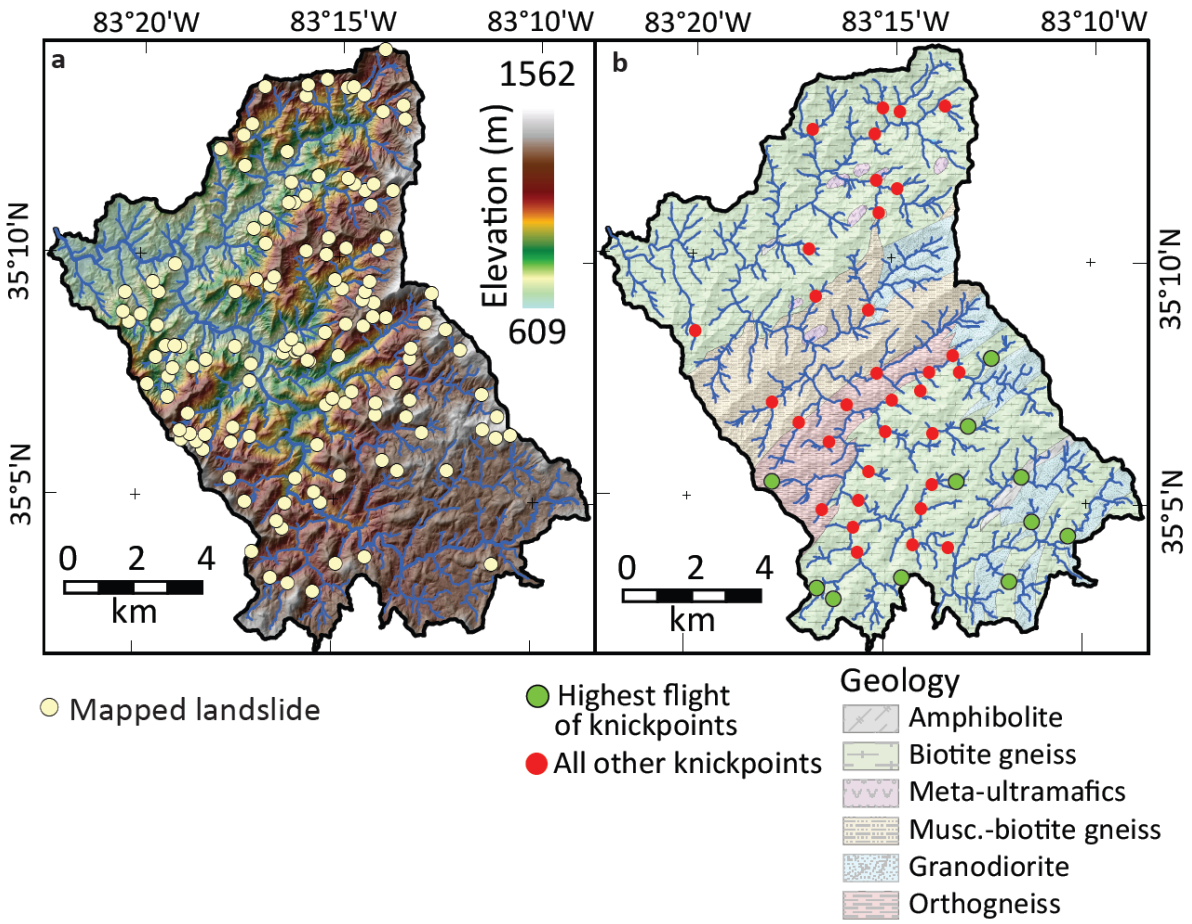

Figure DR1: **a**, Shaded relief map of the Cullasaja River basin with mapped landslide initiation points (Wooten et al., 2008). Note how there are fewer observed landslides in the relict-landscape portion of the basin. **b**, Geologic map of the Cullasaja River Basin. Shaded relief map over 1:200,000-scale U.S. Geologic Survey bedrock map (North Carolina Geological Survey, 1985). The majority of the lithologic units are gneisses. The regional foliation mimics lithologic contacts that strike northeast and dip moderately-to-steeply toward the southeast.

Figure DR2: Relict-reach regressions and profile reconstructions. Map of the location of the eight relict reaches (the trunk and seven tributary channels) that had sufficient data for least-squares regressions based on log slope-log drainage area data to determine ϑ and k_s. The longitudinal profiles and slope-area plots of each of these stream channels are shown. The linear least-squares regressions used to obtain θ and k_s for each relict reach is shown by the dark blue line on the log slope-log area data and the longitudinal profile. The forced linear regression through the slope-area data with a θ_{ref} of 0.5 was used to determine the k_{sn} value for each channel, and is shown in cyan on the log slope-log drainage area and longitudinal profile plots. Reconstructed stream profiles for the trunk and seven tributary channels are shown with their associated 2σ errors for each reconstructed profile. See Table DR3 for statistics.

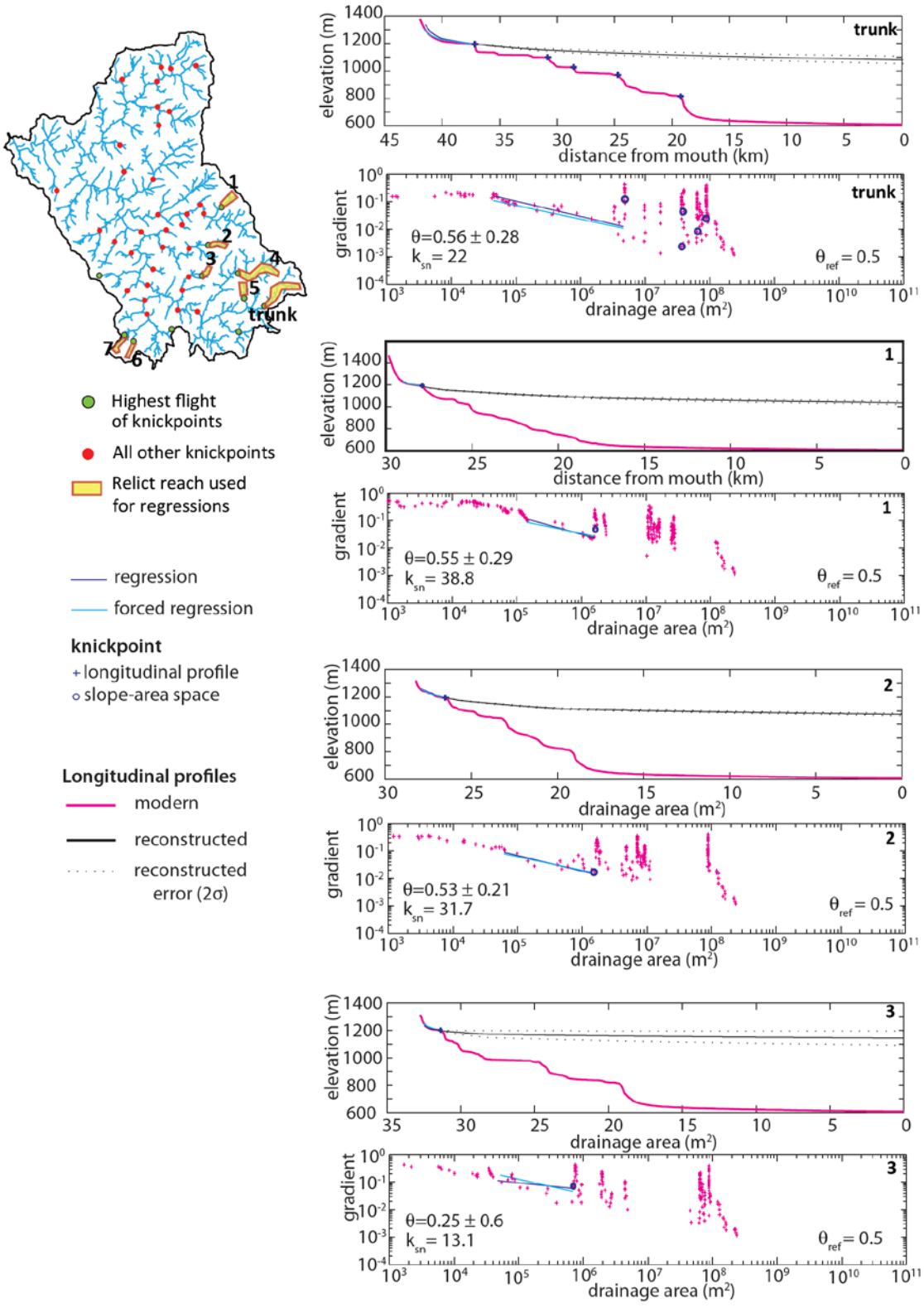
1
2
3
4
5
trunk
7
6
Highest flight of knickpoints
All other knickpoints
Relict reach used for regressions
regression
forced regression
knickpoint
+ longitudinal profile
o slope-area space
Longitudinal profiles
modern
reconstructed
reconstructed error (2σ)
elevation (m)
distance from mouth (km)
trunk
gradient
θ=0.56 ± 0.28
k_sn = 22
θ_ref = 0.5
drainage area (m²)
1
θ=0.55 ± 0.29
k_sn = 38.8
2
θ=0.53 ± 0.21
k_sn = 31.7
3
θ=0.25 ± 0.6
k_sn = 13.1

Figure DR2

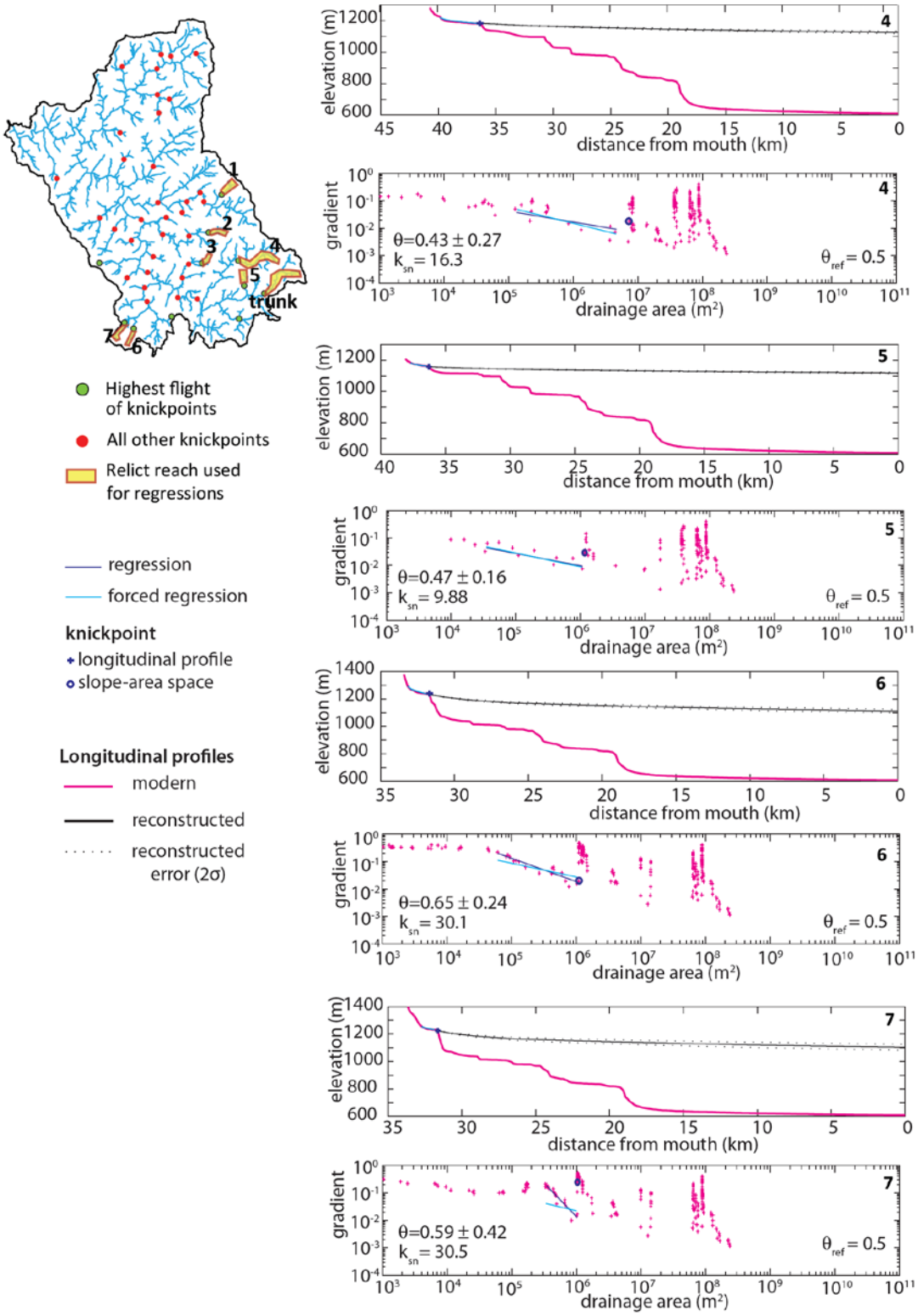

Figure DR2 continued

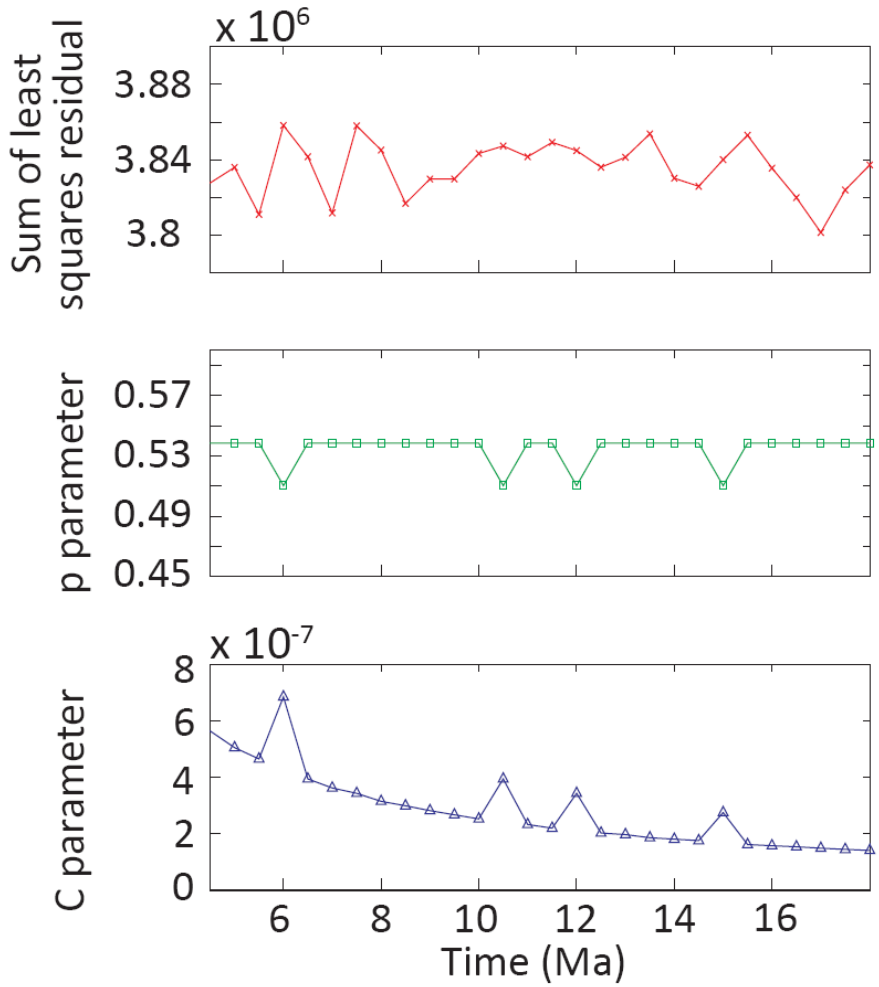

Figure DR3: Top plot shows the sum of square differences between the modeled and observed positions of the upper flight of knickpoints, assuming knickpoint initiation between 4.5 and 18 Ma. There is less than a 2% difference in the minimum residual for any of these model runs. Middle and bottom plots show the best fitting *p* and *C* parameter combination for each model run of knickpoint travel time, respectively. The *p* parameter varies little, while *C* varies over slightly more than an order of magnitude and progressively decreases to accommodate slower knickpoint travel times.

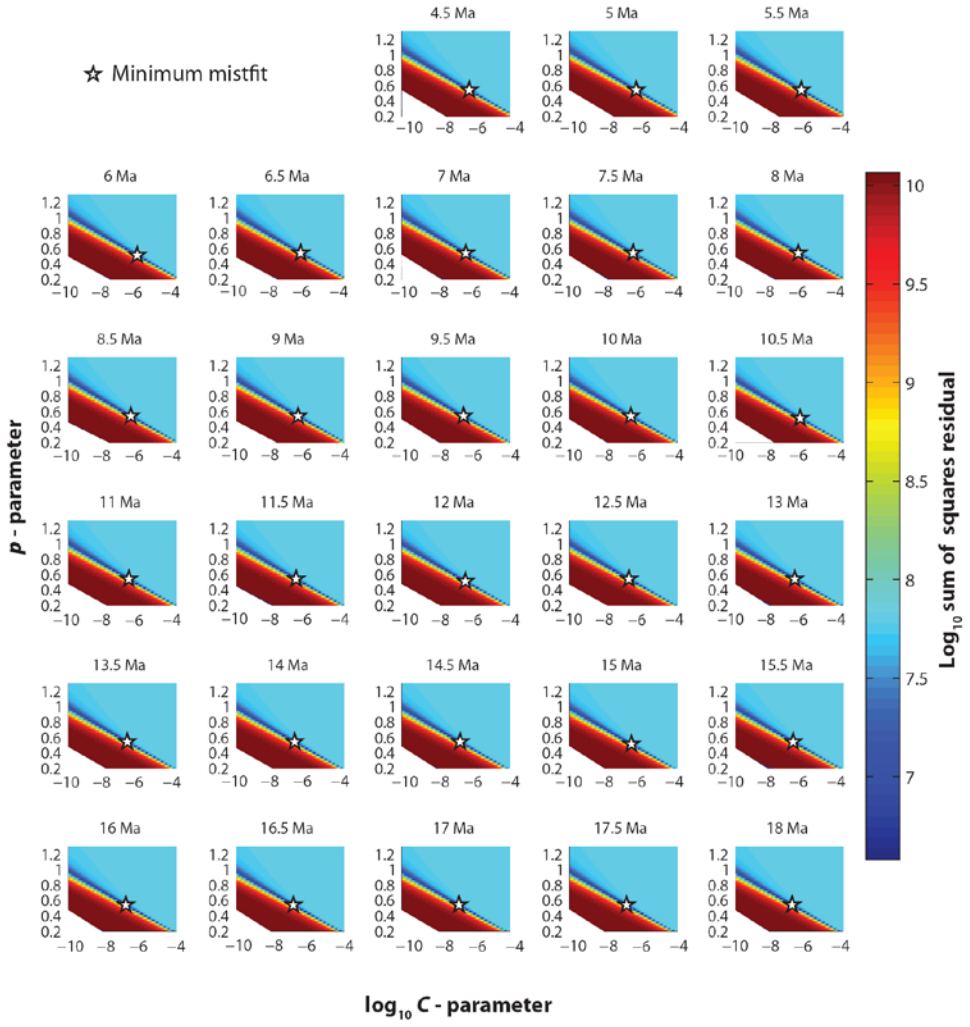

Figure DR4: Results from 28 numerical model runs of knickpoint positions using knickpoint travel times from 4.5 to 18 Ma at 0.5 Ma intervals. The data presented are the sum of squares residuals between observed and modeled knickpoint positions. The smallest residual value for each model run is indicated by a star. Minimum residual values fall within 2% of each other. Best fitting p values range between 0.51 and 0.54, and *C* varies over an order of magnitude, depending on the corresponding *p* value needed to reduce the misfit according to the input duration of the knickpoint travel time. Note that the misfits in each model run are minimized within a very narrow range similar to what Berlin and Anderson (2007) observed.

Chapter 2

Coastal Uplift and the Kinematics of the Hellenic Trough Faults: Tectonic Geomorphology of an Extending Forearc above a Retreating Subduction Zone, Crete, Greece

In preparation for submission to *Geophysical Journal International* with the following coauthors:

Wegmann, K.W.[1]; Bohnenstiehl, D.R.[1]; Pazzaglia, F.J.[2]; Brandon, M.T.[3]; Fassoulas, C.[4]

[2] Department of Marine, Earth and Atmospheric Sciences, North Carolina State University, Raleigh, NC, USA.

[3] Department of Earth and Environmental Sciences, Lehigh University, Bethlehem, PA, USA.

[4] Department of Geology and Geophysics, Yale University, New Haven, CT, USA.

[5] Natural History Museum of Crete, University of Crete, Heraklion, Greece.

Abstract

Syn-convergent extension above subduction zones generates spirited debate regarding the processes responsible for the juxtaposition of these contrasting crustal deformation styles. The Hellenic subduction zone serves as a prime example of syn-convergent extension, where more than 40-years of geologic and geophysical research have not led to consensus as to the geodynamic processes governing orogenesis. Central to resolving this controversy are the kinematics of an array of faults associated with the construction of a series of deep forearc basins, known as the Hellenic troughs. Early researchers designated the most southerly of the Hellenic troughs as the surface expression of the subduction thrust; but, it has since been recognized that the plate boundary lies ~ 150 km to the south, outboard of the Mediterranean Ridge accretionary complex. Accordingly, the Hellenic troughs are now generally considered to result from motion along a series of large intra-crustal faults. One hypothesis holds that these faults are south-dipping extensional-to-transtensional structures embedded in a subduction wedge where rock uplift driven primarily by underplating of material along the plate interface. The alternative hypothesis suggests that the faults are north-dipping contractional structures where mountain building is driven by primarily by frontal accretion. Which of these mutually-exclusive hypotheses is correct has important implications for the formation of forearc basins and regional seismic hazard analyses.

We present the combined results from a tectonic geomorphology and structural geology investigation of the south-central coastline of Crete, Greece. This location is ideally situated to test the kinematics of the Ptolemy fault, one of the Hellenic trough faults that daylights ~10 km south of Crete. Late Pleistocene marine terraces, optically stimulated luminescence dating, and correlations to the late Quaternary eustatic curve are used to synthesize the rates and patterns of uplift and fault

displacements. Fault-scaling relationships are used to constrain the three-dimensional geometry of a 55 km long range-front normal fault. Our reconstruction illustrates that late Quaternary slip along this fault is geometrically inconsistent with a north-dipping contractional Ptolemy fault; rather, the Ptolemy fault is synthetic to this active onshore structure. Review of the datasets used to argue that the other Hellenic troughs accommodate shorting indicates similarly indicates that the basin bounding faults are extensional, rather than contractional in nature. The simplest interpretation is that the Hellenic troughs are bound by southward dipping extensional-to-transtensional faults. These findings lead to the conclusion that orogenesis above the Hellenic Subduction zone is driven by underplating, while stretching in the overriding plate is the result of gravitational instability of the subduction wedge and lithospheric processes related to roll back of the African slab.

Uplift of the hanging and footwalls of active extensional faults in South-central Crete constrains the rate of regional secular uplift in the absence of extension to ~0.65 mm yr^{-1} during the late Quaternary. Results indicate that the rate of uplift has increased over the late Quaternary, a scenario that cannot be explained by changes in the rates of subduction or tectonism. Rather, we suggest that these rate changes are caused by horizontal advection of material through the subduction wedge that occurs in step with southward migration of the African slab. Crete is envisioned as a parcel of material fluxing through a southward propagating orogenic wave and uplift is driven by underplating, dynamic topography or both.

Introduction

The source of rapid uplift in extending forearcs above active subduction zones generates spirited debate. Such controversy is well-illustrated by geologic and geophysical investigations of the Hellenic margin in the Eastern Mediterranean. All subaerial forearc highs in this region show pervasive and active arc-parallel and arc-perpendicular extensional faulting with no active contractional structures observed at the surface. Offshore south of the forearc highs, the Hellenic troughs form a series of convex southward 2 to 4 km-high bathymetric escarpments and associated basins embedded in the forearc that overlies the Hellenic subduction zone (Fig. 1). Southwest of the Peloponnese the Ionian trough is a NW-SE trending seafloor lineament that rotates eastward, splaying off into three en echelon branches, the Ptolemy, Pliny, and Strabo troughs south of the island of Crete (Fig. 1; McKenzie 1978; Le Pichon *et al*. 1979; Le Pichon *et al*. 1982; Huguen *et al*. 2001; Kreemer & Chamot-Rooke 2004; Shaw & Jackson 2010). These prominent bathymetric features are recognized as the surface expression of large upper plate faults associated with historic and devastating seismicity in the region. Two hypotheses for the kinematics of these structures are invoked to explain the active tectonics and uplift above the Hellenic subduction zone; one describes these faults as south-dipping extensional-to-transtensional features (Fig. 2a; Ryan *et al*. 1982; Lallemant *et al*. 1994; Becket al. 2006, 2010; *and references therein*), where as the other portrays them as north-dipping thrust faults rooted in the subduction interface (Fig. 2b; Taymaz *et al*. 1990; Jackson, 1994; Shaw & Jackson, 2010; *and references therein*).

Despite more than 40-years of research in this region no consensus has been reached regarding the tectonic processes governing the development and kinematics of the Hellenic trough faults. Each of the competing hypotheses gathers support from different geologic and geophysical

Figure 1. Inset showing the major active and inactive convergent boundaries in the Mediterranean region and the North Anatolian Fault. Grey box shows the location of the map of the Eastern Mediterranean. The GPS velocity vectors (black arrows) are resolvable into a total convergence rate of ~ 36 mm/yr (Reilinger *et al.* 2006). Depth (km) to the subducting plate (dashed white line) is from the Benioff-zone seismicity (Papazachos *et al.* 2000), mico-seismicity (Meier *et al*. 2004; Becker *et al*. 2006), and upper mantle seismic velocity model (Gudmundsson & Sambridge 1998). The location of the cross-sections in figure 2 is shown by the line A – A'. The red box shows the location of Figure 3 a, b. IT, PtT, PlT and ST stand for the Ionian, Ptolemy, Pliny, and Strabos toughs, respectively. The location of the Hellenic Subduction zone and back thrust to the north that define the boundaries of the Mediterranean Ridge Accretionary complex is from Kreemer & Chamot-Rooke (2004). The location of the Deep Sea Drilling Project (DSDP) sites 127 and 128 in the Ionian trough is shown (Ryan *et al*. 1973).

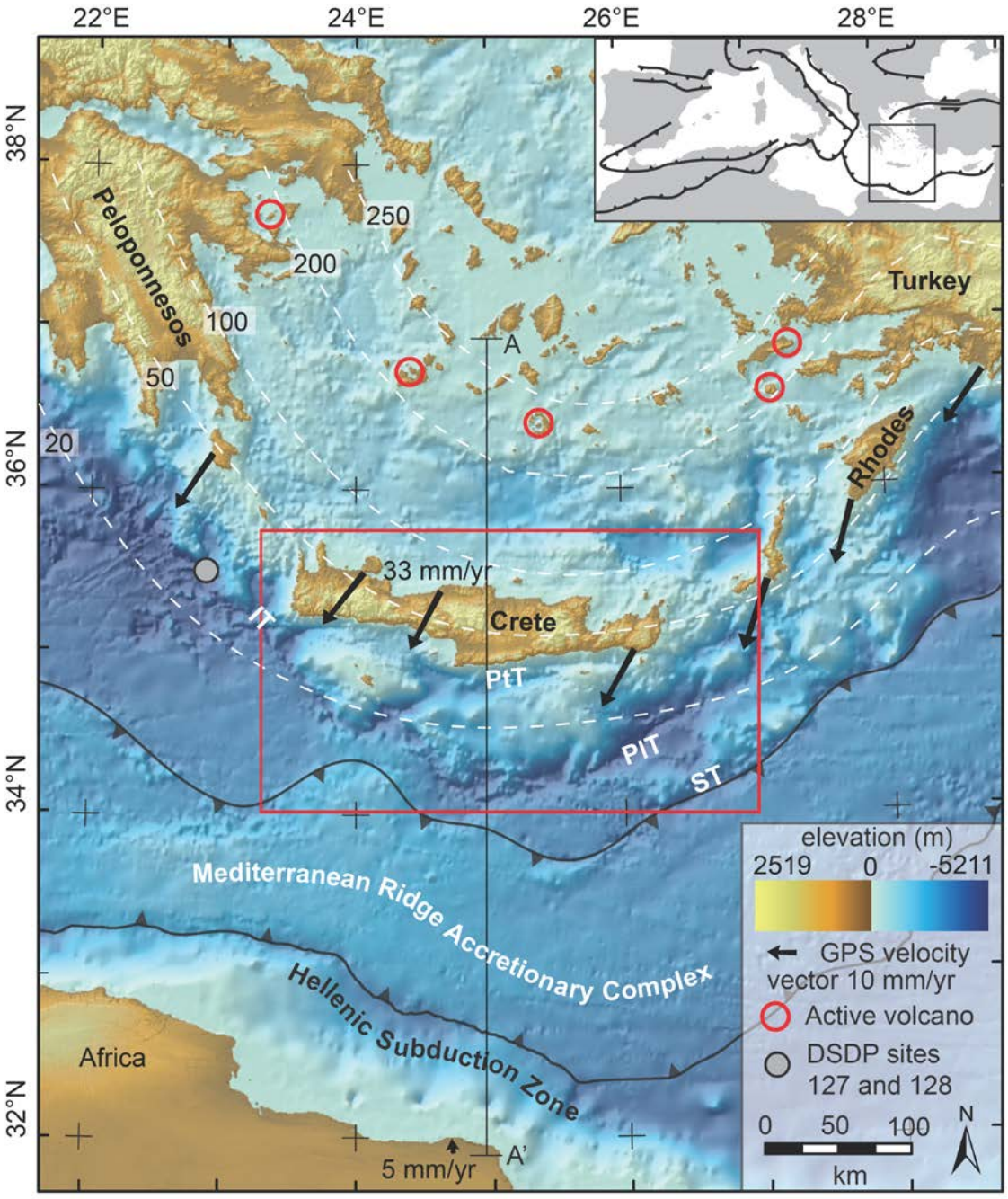
22°E
24°E
26°E
28°E
38°N
36°N
34°N
32°N
Peloponnesos
250
200
100
50
20
A
A'
Turkey
Rhodes
33 mm/yr
Crete
PtT
PIT
ST
IT
Mediterranean Ridge Accretionary Complex
Hellenic Subduction Zone
Africa
5 mm/yr
elevation (m)
2519
0
-5211
GPS velocity vector 10 mm/yr
Active volcano
DSDP sites 127 and 128
0
50
100
km
N

datasets. Which of these mutually exclusive hypotheses is correct has profound implications for our understanding of active orogenesis and uplift above the Hellenic subduction zone, seismic potential of the Hellenic trough faults, and the construction of forearc topography along the Hellenic margin (Fig. 2; see discussion below).

To address the current debate of the Hellenic trough faults, we conducted at detailed study of the tectonic geomorphology and structural geology of the south-central coastline of Crete to test the kinematics of the Ptolemy trough fault and document the rates and patterns of uplift along the coastline (Fig. 3). In this study, we provide an overview of the historical context of the Hellenic troughs in scientific literature and summarize the current models of their origins, followed by the new observations of our study, and a discussion of the results in the context of previously published literature. Our results show that active extensional faults in South-central Crete are geometrically inconsistent with one of the proposed north dipping contractional Hellenic trough faults, the Ptolemy fault. Rather, our results support an extensional-to-transtensional Ptolemy fault synthetic to active onshore structures, an interpretation consistent with the findings of many geophysical surveys as well as borehole data gathered from some of the other Hellenic troughs (e.g. Ryan *et al*. 1982; Lallemant *et al*. 1994; Kopf *et al*. 2003; Kreemer & Chamont-Rooke 2004; Meier *et al*. 2004, 2007; Chamont-Rooke *et al*. 2005; Becker *et al*. 2006, 2010). Further, our results indicate a rapid secular rate of uplift (ca. 0.65 mm yr^{-1}) in South-central Crete that is best explained by deep material underplating along the subduction interface or dynamic topography resulting from the encroaching Eurasian asthenospheric wedge or some combination of both processes. Based on these findings we present a geodynamic model for the Hellenic subduction zone that provides a basis for understanding the active tectonics and uplift of this rapidly deforming forearc over the late Cenozoic.

Historical Perspectives and Modern Controversy of the Hellenic Troughs

The topographic prominence of the Hellenic troughs lead many early studies to conclude that the outermost of these structures was the surface expression of the Hellenic subduction thrust or trench (e.g. Ryan *et al*. 1973; Hsü & Ryan 1973; and references therein). Early studies of earthquake focal mechanisms (McKenzie 1970) and intermediate depth earthquakes (Papazachos & Comninakis 1971) from the Eastern Mediterranean echoed this interpretation.

Inspired by these early studies and interpretations of the Hellenic subduction zone, the Deep Sea Ocean Drilling Project (DSDP - leg 13) carried out a combined bathymetric sonar and seismic reflection survey and drilled boreholes into the seabed at the base of the Ionian trough and regions southward (Fig. 1; Ryan *et al*. 1973). The goal of the project was to drill through the supposed plate boundary, and better characterize sea floor elevations, offshore stratigraphy and structures. This expedition found no evidence of a subduction thrust in the Ionian trough and identified the presence of an actively deforming accretionary wedge, the Mediterranean Ridge, outboard of the alleged plate boundary (i.e. Ryan *et al*. 1982; Kastens 1991; Lallemant *et al*. 1994).

It has been recognized since 1982 that the Hellenic troughs are *not* the plate boundary between Africa and Eurasia. Instead the surface expression of the subduction thrust is buried beneath a thick package of sediments outboard of the Mediterranean Ridge accretionary complex, ~ 150 km south of the Hellenic troughs (Fig. 1, 2; Ryan *et al*. 1982; Kastens *et al*. 1991; Lallemant *et al*. 1994; Chaumillon & Mascle 1997; Mascle & Chaumillon 1998; Huguen *et al*. 2001; Kreemer & Chamont-Rooke 2004; Chamont-Rooke *et al*. 2005; Snopek *et al*. 2007; Shaw & Jackson 2010; Yem *et al*. 2011). Nonetheless, numerous studies continue to misidentify the Hellenic troughs as the surface expression of the subduction thrust (Hall *et al*. 1984; Armijo *et al*. 1992; Stöckhert *et al*.

1999; Kahle *et al*. 2000; Wortel & Spakman 2000; Doutsos & Kokkalas 2001; Kokkalas & Doutsos 2001; Stiros *et al*. 2001; 2010; Laigle *et al*. 2002, 2004; Husson, 2006; Reilinger *et al*. 2006, 2010; Di Luccio & Pasyanos 2007; Papadimitriou & Karakostas 2008; Suckale *et al*. 2009; Royden & Papanikolaou 2011; Vassilakis *et al*. 2011, to name a few). Continued publication of this misconception needs to be addressed and discontinued because it leads to confusion in the literature, increases the likelihood of erroneous interpretations and serves as a barrier to future progress in understanding of the geodynamics and tectonics of the Eastern Mediterranean. One reason for the uncertainty in the location of the plate boundary in the Eastern Mediterranean comes from the fact that the term 'trench' is commonly used to describe the Hellenic troughs. In oceanography the term 'trench' is specifically defined as the surface expression of the subduction thrust, which the Hellenic troughs are not (Neuendorf *et al*. 2005). We therefore suggest that the use of the term 'trench' be abandoned in the literature when referring to the Hellenic troughs in order to avoid further confusion.

Most researchers now agree that the Hellenic troughs are the seafloor exposure of large-scale faults embedded in the upper-plate of Hellenic subduction zone; however, it is debated whether these structures accommodate extension-to-transtension on southward dipping faults that extend to approximately the brittle-ductile transition in the crust (Ryan *et al*. 1982; Lallemant *et al*. 1994; Le Pichon *et al*. 1995; 2002; Chaumillon & Mascle 1997; Mascle & Chaumillon 1998; Gautier *et al*. 1999; Bohnhoff *et al*. 2001; Huguen *et al*. 2001; Jolivet, 2001; Faccenna *et al*. 2003; Kopf *et al*. 2003; Kreemer & Chamont-Rooke 2004; Meier *et al*. 2004, 2007; Chamont-Rooke *et al*. 2005; Becker *et al*. 2006, 2010; Makris & Yegorava 2006; Alves *et al*. 2007; Jolivet & Brun 2010; Ring *et al*. 2010; Wegmann *et al*. 2010; Jolivet *et al.* 2012; Wegmann *et al*. in review) or shortening on northward dipping thrust and reverse faults rooted in the subduction interface (Taymaz *et al*. 1990; Jackson,

1994; Meulenkamp *et al*. 1988; 1994; Papazachos, 1996; Benetatos *et al*. 2004; Nyst & Thatcher 2004; Shaw *et al*. 2008; Shaw & Jackson 2010). In general, the two sides of the debate utilize different datasets. Those that favor the extensional-to-transtensional faulting hypotheses rely upon data from subaerial forearc highs (e.g. Crete and Rhodes) that exhibit widespread and active arc-parallel and arc-normal extensional faults with no active contractional faulting exposed at the surface today (e.g. Angelier, 1979; Angelier *et al*. 1982; Fassoulas *et al*. 1994; Fassoulas, 2001; ten Veen and Kleinspehn, 2003; Peterek & Schwarze 2004; Caputo *et al*. 2006). They also invoke data from bathymetric sonar and seismic reflection surveys that image structures to the south of Crete as horsts and grabens (e.g. Ryan *et al*. 1973; Le Pichon *et al*. 1982), micro-seismic surveys that suggest the Hellenic trough faults are steeply dipping southward (Meier *et al*. 2004, 2007; Becker *et al*. 2006, 2010) and evidence from DSDP drill sites 127 and 128 (Fig. 1; Ryan *et al*. 1973; 1982; Lallemant *et al*. 1994). Further, the regional trend of the GPS derived velocity field shows increasing vector length southward in the Aegean, indicating regional stretching of the overriding plate at least to the south-coast of Crete and indicate no strain accumulation in the vicinity of Crete (Le Pichon *et al*. 1995; McClusky *et al*. 2000; Nyst & Thatcher 2004; Reilinger *et al*. 2006, 2010).

Researchers that appeal to the thrust fault model draw heavily from focal mechanisms of earthquakes ≥ 4 M_w that have occurred during the instrumental record and are thought to be sourced in the upper ~ 20 km of the crust in the overriding plate (Taymaz *et al*. 1990; Papazachos, 1996; Benetatos *et al*. 2004; Nyst & Thatcher 2004; Shaw & Jackson 2010). Further support for the thrust hypothesis is garnered from an uplifted Holocene paleo-shoreline marker in south-western Crete that is up to nine meters above sea level (e.g. Pirazzoli, 1986; Pirazzoli *et al.* 1996). It is argued that this uplift occurred coseismically in a single event, a feat that is only feasible in a steeply dipping thrust or reverse fault (Shaw *et al*. 2008; Stiros 2010). A local GPS network of four stations on the

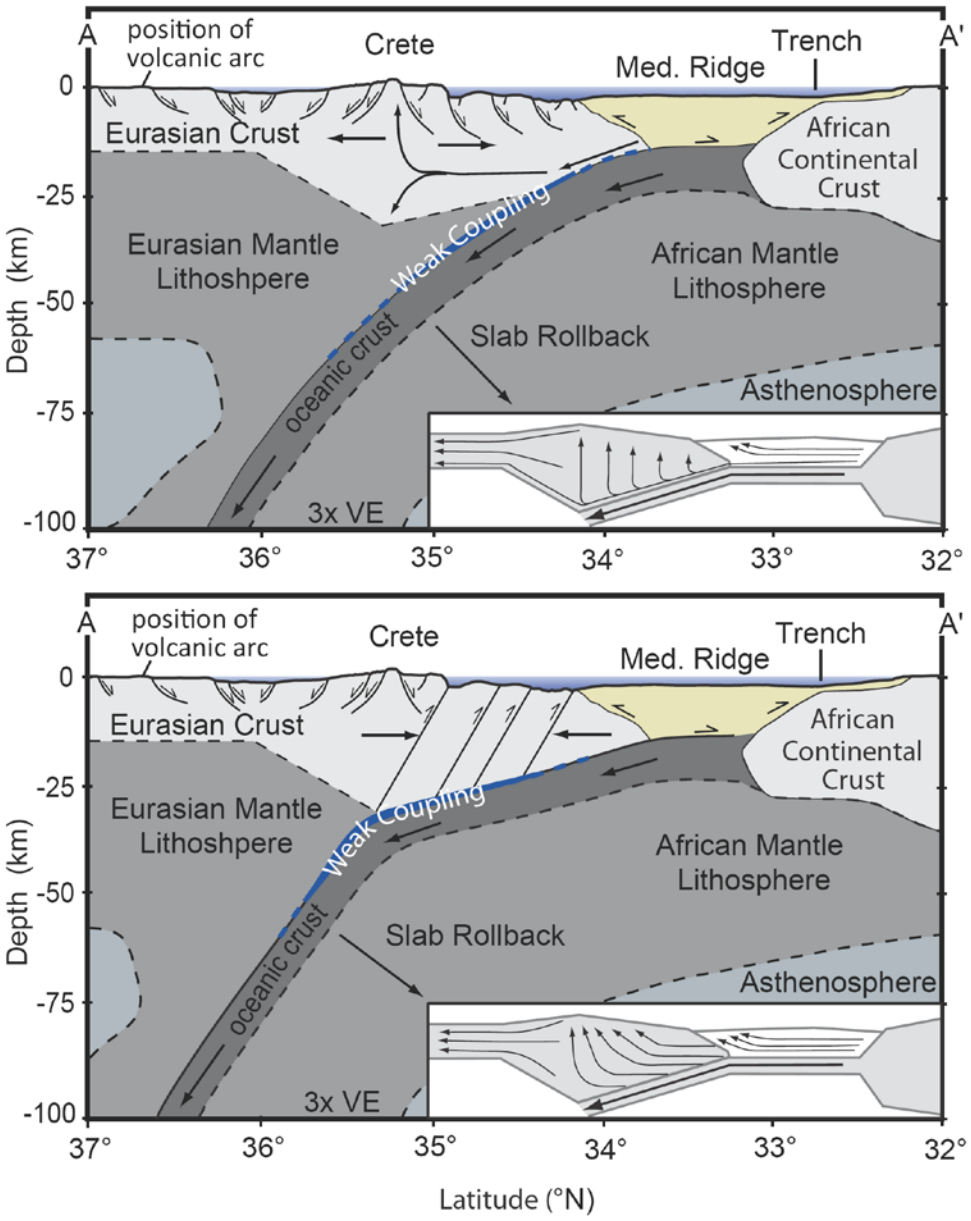

Figure 2. Profile and crustal and upper mantle cross-sections for the central Hellenic subduction zone along A – A' in figure 1 (modified after Meier *et al*. 2004). Thick blue line is inferred weak-coupling between ~ 15 and 45 km depth. Major forearc basins are abbreviated as MG (Messara graben), PtT (Ptolemy trough), and PlT (Pliny trough). (a) Illustrates the hypothesis that the entire forearc inboard of the Mediterranean Ridge Accretionary complex is experiencing arc perpendicular extension. (b) Shows the hypothesis that the forearc from Crete south to the subduction thrust is dominated by north-south directed compression.

Crete and the volcanic islands of Milos and Santorini indicate ~ 1mm yr^{-1} of contraction between the stations.

Each hypothesis predicts different mechanisms of orogenesis and earthquake potential in the region. The normal faulting hypothesis maintains that mountain building is largely driven by the basal accretion of material into the subduction wedge inboard of the actively deforming accretionary complex. In this model, upper crustal extension is driven by gravitational instability of a super-critical coulomb wedge (Angelier *et al*. 1982; Platt 1986) coupled with stretching of the Eurasian lithosphere resulting from southward upper plate retreat (Fig. 2a; Thomson *et al*. 1998; Faccenna *et al*. 2003; Alves *et al*. 2007; Jolivet & Brun 2010). Stretching of the upper-plate results in the development of horst-and-graben and pull-apart structures bound by steeply dipping (40-90°) extensional-to-transitional faults that extend approximately to the brittle ductile transition (Kreemer & Chamont-Rooke 2004; Meier *et al*. 2004, 2007; Becker *et al*. 2006, 2010). Fault scaling-moment magnitude relationships (e.g. Wells and Coppersmith, 1994) suggest the maximum moment magnitude of earthquakes expected on faults of this size is $M_w \leq 7.5$.

Proponents of the thrust fault model suggest that mountain building is accommodated primarily by frontal accretion of material into the orogenic wedge, a result of compressional strain accumulation in the upper-plate due to the continued convergence between the Eurasian and African plates (Fig. 2b; Meulenkamp *et al*. 1988; 1994; Shaw & Jackson 2010). Uplift in this model is driven by crustal shortening to shallow crustal depths. In this model the deep bathymetric depressions in the Hellenic forearc are the result of piggy-back basins due to loading imposed by contraction on 30° northward dipping thrust faults. In this model the Hellenic trough faults are rooted in the subduction interface, coupled with the proposed dip angle proposed faults are much higher than in the alternative hypothesis. The potential size of these structures suggests they are

likely to generate earthquakes $M_w \geq 8$ based on fault scaling-moment magnitude relationships (e.g. Wells and Coppersmith, 1994).

Determining the kinematics of the Hellenic trough faults is important for improving understanding of the geodynamics and tectonics of the Hellenic subduction system, because each hypothesis views active orogenesis, seismic potential of faults and the construction of forearc topography from a fundamentally different prospective (Fig. 2). They central purpose of this paper is to determine the kinematics and uplift of the Ptolemy trough fault. In doing so, we will shed light on the tectonic processes related to the construction of the dramatic forearc topography associated with the Hellenic troughs and gain insight into what geodynamic processes govern rapid and sustained uplift of the extending Hellenic forearc highs.

Background

Tectonic and Geodynamic Setting

The Hellenic margin overlies the largest, fastest, and most seismically active subduction zone in the Mediterranean. Here the African (Nubian) plate subducts beneath the Eurasian plate with a velocity of ~ 36 mm/yr with respect to a fixed European reference frame (Fig. 1; McClusky *et al*. 2000; Reilinger *et al*. 2006). A well-defined Benioff seismic zone illustrates that the subduction interface dips between 10 and 15° northward reaching a depth of 35 to 45 km beneath Crete, and is observed to depths of 150 to 180 km below the central Aegean (e.g. Papazachos *et al*. 1996, 2000; Knapmeyer, 1999). Seismic tomography investigations image the subducted slab to depths > 600km (Wortel & Spakman 2000); while Mesozoic to Cenozoic arc volcanism (Pe-Piper & Piper 2002) from the Aegean and Eastern Mediterranean provide evidence that the Hellenic subduction zone has been actively consuming the African plate since at least 100 Ma (Faccenna *et al*. 2003; van

Hinsbergen *et al*. 2005). The Hellenic margin has migrated southward since the Early Eocene as evidenced by the directional younging of both volcanic arc and high-pressure metamorphic rocks found throughout the Aegean along with the southward migration of the thrust front (Pe-Piper and Piper, 2002; Faccenna *et al*. 2003; Marchev, *et al*. 2004; Kounov *et al*. 2004; Jolivet & Brun 2010; Ring *et al*. 2010). The Hellenic subduction complex can thus be viewed as a southward migrating "orogenic wave" like other well-studied retreating subduction zones such as the Apennines of Italy (e.g. Thomson *et al*. 2010).

Long-lived subduction has resulted in the accretion and growth of a large south-facing subduction wedge that at present extends from the north coast of Crete to the southern boundary of the aseismic Mediterranean Ridge accretionary complex (Fig. 1b; e.g. Le Pichon *et al*. 1979, 1982; Kastens 1991; Kastens *et al*. 1992). Crete is often considered a "rigid backstop" to the Mediterranean Ridge accretionary complex (e.g., Le Pinchon *et al*. 1982, 2002; Kastens 1991; Kastens *et al.* 1992; Huguen *et al*. 2001; Kopf *et al*. 2003; Chamot-Rooke *et al*. 2005; Shaw & Jackson 2010). This interpretation, however, fails to account for the observed widespread and active deformation and uplift of this "backstop" since its formation ~ 40 Ma (e.g. Angelier 1978, 1979; Angelier *et al*. 1982; Fassoulas *et al*. 1994; Jolivet *et al*. 1996; Wegmann 2008; Jolivet and Braun, 2010; Strasser *et al.* 2011). This evidence indicates that Crete is still actively involved in orogenic processes at the Hellenic margin. We therefore favor a more encompassing view of the forearc that places Crete and adjacent forearc highs (e.g. the Peloponnese and island of Rhodes) within a larger subduction wedge (Fig. 2; e.g., Willett *et al*. 1993; Rahl *et al*. 2005; Fuller *et al*. 2006; Wegmann 2008).

Many of the observable features of the Hellenic margin are thought to be in part related to a plate-interface that accommodates tectonic motion predominantly by aseismic creep. Evidence to

support a weakly-coupled Hellenic subduction zone comes from four primary lines of evidence: (1) seismic-moment release records demonstrate that plate boundary seismicity can only account for ~ 13 mm yr^{-1} of the total ~ 36 mm yr^{-1} of convergence across the Hellenic subduction zone (Jackson & McKenzie 1988; Taymaz, *et al*. 1990; Shaw & Jackson 2010), (2) the occurrence of large high and low angle normal faults on all subaerial forearc highs (e.g. Angelier *et al*. 1982; Stewart & Hancock 1991; Stewart 1993; Fassoulas *et al*. 1994; Kontogianni *et al*. 2002; Caputo *et al*. 2006), (3) the presence of large under-filled forearc basins (e.g., Wells *et al.* 2003; Fuller *et al*. 2006) and (4) low strain accumulations rates derived from continues GPS surveys in the southern Aegean and Crete (Reilinger *et al*. 2010). This evidence suggests that the Hellenic subduction zone is an unlikely nucleation zone for large-to-great historic tsunamigenic earthquakes. Instead, historically-devastating seismicity is probably related to large-scale intra-crustal faults, some of which likely were spatially related to the Hellenic troughs (Shaw *et al*. 2008; Wegmann *et al*. 2010; Stiros, 2010; Wegmann *et al.* in review).

Geologic and Tectonic Summary of Crete

The island of Crete represents a prominent forearc high above the Hellenic subduction zone (Fig. 1). The construction of Crete initiated with nappe stacking between 40 to 15 Ma, after the initiation of slab retreat in the Eocene (e.g. van Hinsbergen *et al*. 2005). The geologic history of the Crete records the Oligocene to Miocene collision of the Adriatic (or Apula) microcontinent (Bonneau 1984). The earliest tectonic units accreted to the overriding plate were the more distal continental platform of Adria, known as the Pindos unit, and the shallower carbonate platform referred to as the Tripolitza unit (Bonneau *et al*. 1976). The Pindos, Tripolitza, and Uppermost ophiolitic mélange form the weakly metamorphosed and structurally highest units on the island today (Seidel *et al*.

1981). These upper nappes are in tectonic contact with the lower high-pressure (HP) low-temperature (LT) metamorphic units. The contact between upper and lower units is a prominent top to the north detachment fault related to the exhumation of the lower units. At the structural top of the HP-LT lower nappes, the Phyllite-Quartzite unit is interpreted as a sliver from the subducted Adria microcontinent (Krahl *et al*. 1983; Stöckhert *et al*. 1999). The lowest structural unit on Crete is the Plattenkalk, an assemblage of highly deformed clastic and carbonate units thought to be the cover of the southern edge of the colliding microcontinent (Bizon *et al*. 1976). The HP-LT units on Crete were subducted, underplated and rapidly exhumed during the Miocene (~24 to 20 Ma; Seidel *et al*. 1982; Fassoulas *et al*. 1994; Jolivet *et al*. 1996; Ring & Reischmann 2002; Rahl *et al*. 2005). Seismic surveys and borehole measurements show that the Cretan nappes continue south to at least the northern boundary of the Mediterranean Ridge accretionary complex (Aubouin *et al*. 1976; Le Pichon *et al*. 2002).

Following Miocene exhumation, both arc normal and parallel brittle extension occurred, and is continuing today as noted by numerous high (Bohnhoff *et al*. 2005; Caputo *et al*. 2006) and low-angle extensional faults (Fassoulas *et al*. 1994) that cut the Cretan nappes. Importantly, no active contractional faults are exposed on Crete today, and sea-beam and seismic reflection data suggest faults of similar orientation and dip to the extensional faults that crop out on the island continue offshore to the northern boundary of the Mediterranean Ridge accretionary complex (Angelier *et al*. 1982; Huguen *et al*. 2001; Meier *et al*. 2004, 2007; Becker *et al*. 2010). Brittle faulting opened extensional basins that filled with Miocene to Pliocene marine sediments. Today these grabens are exposed 100's of meters above sea-level, indicating long-lived uplift of the island (Meulenkamp *et al*. 1994; van Hinsbergen & Meulenkamp 2006; Zachariasse *et al.* 2008). Late Quaternary uplift of the island is observed in Pleistocene and Holocene paleo-shoreline markers found 10's to 100's of

meters above modern sea level (Flemming, 1978; Angelier, 1979; Pirazzoli *et al*. 1982; Meulenkamp *et al*. 1994; Shaw *et al*. 2008; Wegmann 2008; Strasser *et al*. 2011).

Studies of Pleistocene Marine Terraces on Crete

Marine terraces are ideally suited geomorphic markers from which to derive long-term (10^5 yrs) rock uplift rates with respect to the geoid (e.g. England & Molnar 1990) because they integrate the signal of tectonic uplift over multiple earthquake cycles (e.g. Lajoie 1986; Merrits & Bull 1989). Three important studies of the Pleistocene marine terrace along the southern Cretan coast have been conducted. Angelier (1979) investigated a 70-km stretch of the south-eastern coast from Tsoutsouras in the west to Asprolithos. He reported the occurrence of up to three broad strath terraces cut on Neogene marine sediments and mantled by beach cobbles to course-sand deposits. Angelier constrained the age of individual terraces with U-series geochronology of sub-fossil bivalves as well as identifying the occurrence of the warm-water index fossil *Strombus bubonius* (Table 1; Angelier, 1979) that in many circum-Mediterranean coastal sites identifies the last interglacial sea-level highstand (5e, ~125 kyr), known regionally as the Tyrrhenian shoreline (e.g. Ferranti *et al*. 2006). The geochronologic and fossil evidence led Angelier to conclude that the lowest of the three terrace straths was cut during the MIS 5e (Tyrrhenian) transgression. This stratigraphy was used to demonstrate localized occurrences of late Quaternary fault block motions and in calculating uplift rates between 0.25 to 0.4 mm/yr. Gaki-Papanastassiou *et al*. (2009) resurveyed the marine terraces mapped by Angelier (1979) along the coastline adjacent to Ierapetra (Fig. 3, site 18). Following the U-series geochronology of Angelier (1979), these authors confirmed many of the earlier findings, report the occurrence of several previously unrecognized terraces, and demonstrate that this

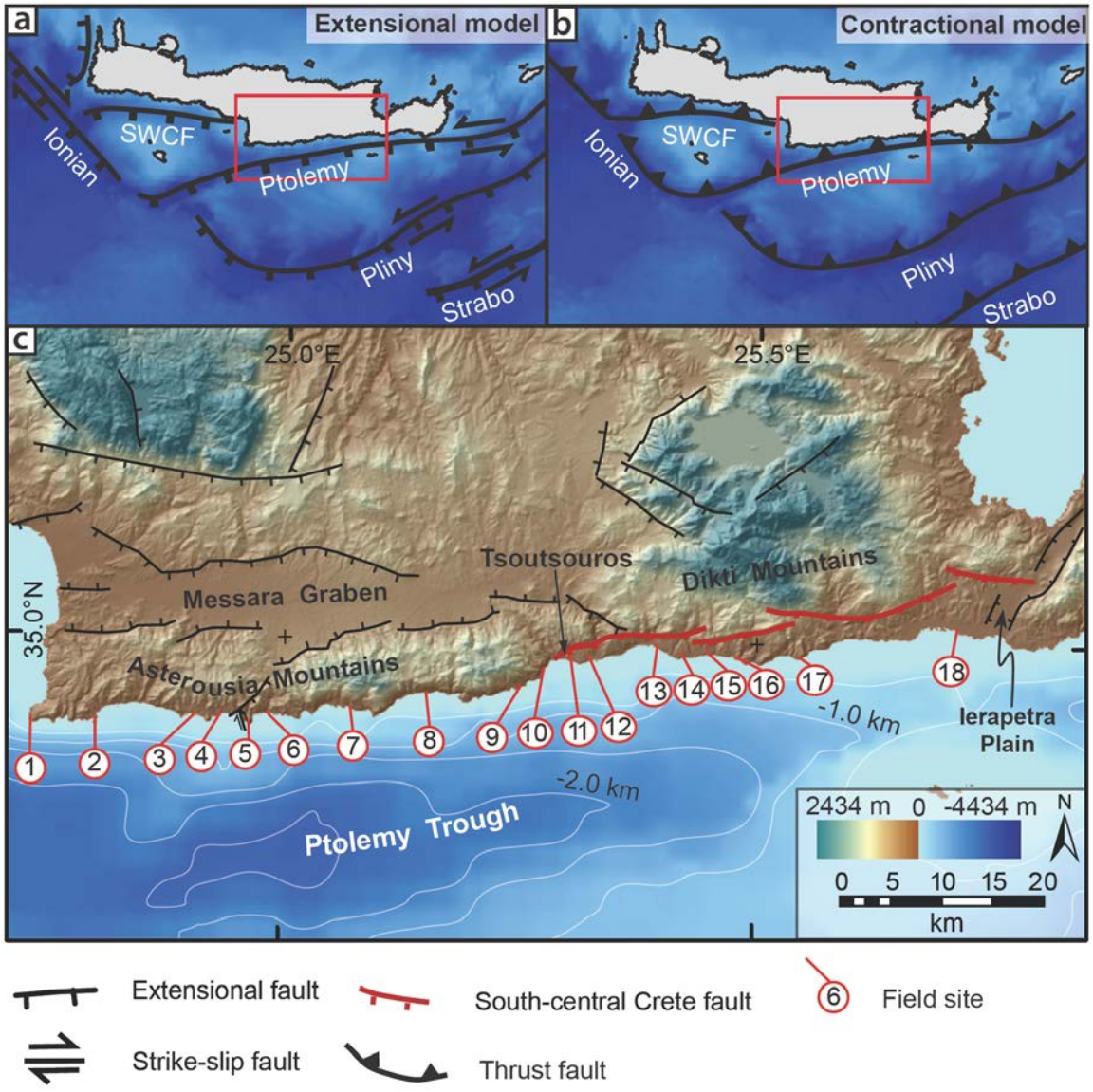

Figure 3. (a) and (b) show the two competing hypotheses for the style of faulting related to the construction of the Hellenic troughs and associated faults outboard of Crete and the approximate location of the area of study in this paper. Note the proximity of the study area to the Ptolemy fault. (c) Digital topography of south-central Crete with mapped active faults shown in black (Fassoulas 1994; Peterek & Schwarze 2004; Gaki-Papanastssiou *et al*. 2009). Study locations (1 – 18) are keyed to table 1. The dashed yellow boxes show the location of topographic swath profiles extracted from the digital topography shown in Figure 10 c.

Table 1: from Angelier (1979)

site	fauna	radiometric method	sample elev. (m asl)[1]	age (kyrs)[2]	assigned MIS[3]
14	*Pectendiae*	$^{230}Th/^{235}U$	10	$131 \pm 9/7$	5e
14	*Pectendiae*	$^{230}Th/^{235}U$	10	103 ± 6	5e
14	*Pectendiae*	$^{231}Pa/^{235}U$	10	$109 \pm 22/12$	5e
14	*Callista chione*	$^{230}Th/^{235}U$	10	$90 \pm 5/3$	5e
14	*Callista chione*	$^{231}Pa/^{235}U$	10	$130 \pm \infty/65$	5e
14	*Strombus bubonius*	N/A	10	N/A	5e
18	*Strombus bubonius*	N/A	20	N/A	5e
18	*Spondylus & Pectendiae*	$^{230}Th/^{235}U$	20	$114 \pm 15/7$	5e
18	*Spondylus*	$^{230}Th/^{235}U$	70	≥ 250	7

[1] Sample elevation in meters above sea level (m asl).

[2] Radiometric age in 1000's of years before present (kyrs).

[3] Marine isotope stage (MIS) sea level highstand assigned based on radiometric age or index fossil.

terrace sequence is offset by an east dipping extensional fault, known as the Ierapetra fault, with a mean late Quaternary vertical slip rate of 0.1 mm/yr.

Wegmann (2008) and Strasser *et al*. (2011) utilized Pleistocene marine terraces, bio-erosional notches and alluvial fans, combined with radiocarbon and optically stimulated luminescence (OSL) geochronology and correlation with the late Quaternary eustatic curve to synthesize the late Quaternary uplift history of the southern coastline west of the Messara Plain (cf. Merrits & Bull 1989). The terraces in this area, cut into carbonates and Phyllite-Quartzites, are considerably different from those described by Angelier (1979). These authors classified paleo-shoreline makers as either sediment-rich strath terraces comprised of beach cobbles and coarse-sand, or sediment poor bio-erosional notches with varying amounts of fringing calcareous algal reef material demarcating the maximum local paleo-sea level at the time of deposition. The deposits were found to inter-finger with alluvial fans with systematically varying degrees of soil development (e.g., Pope *et al.* 2008). Based on their geochronologic results, stratigraphic relationships, and correlations with the eustatic curve (i.e. Lajoie 1986; Merrits & Bull 1989) the ages of individual terraces were assigned, resulting in the determination of late Quaternary uplift rates for the southwestern coast of Crete between 1.0 and 1.5 mm yr^{-1}.

Fault-scaling

For many fault systems, properties including length, width, and displacement follow quasi-universal scaling relationships (Walsh & Watterson 1988; Cowie & Scholz 1992b; Dawers *et al*. 1993; Nicol *et al*. 1996; Schlische *et al*. 1996; Gupta & Scholz 2000; Davis *et al*. 2005). For example, compilation of global datasets of fault length (L) and maximum fault displacement (D_{max}) from

natural fault populations shows that the relationship between L and D_{max} obeys a power-law:

$$D_{max} = cL^n, \quad (1),$$

where *c* is the scaling constant and fault length is raised to the exponent *n* (Cowie & Scholz 1992a; Drawers *et al*. 1993). There is disagreement over the value of *n* due to scatter in different datasets, with proposed values ranging from 0.5 to 2. However, the best fit regression through the global composite dataset of fault measurements spanning eight orders of magnitude, combined with evidence from theoretical investigations, suggests that the value of *n* is close to 1 (Fig. 4; Walsh & Watterson 1988; Cowie & Scholz 1992a,b; Dawers *et al*. 1993; Schlische *et al*. 1996; Manighetti *et al*. 2001; Davis *et al*. 2005; Bergen & Shaw 2010). These findings have led to fault growth models where single isolated faults grow through repeated earthquakes in a self-similar fashion; propagating laterally at their tips while accumulating displacement maxima near their centers (Drawers *et al*. 1993).

Displacement profiles measured along individual faults exhibit some degree of variability in shape, ranging from elliptical to triangular. Similarly, the position of the displacement maxima varies from the center of the profile to highly asymmetric (Drawers *et al*. 1993; Drawers & Anders 1995; Manighetti *et al*. 2001, 2005). General characteristics do emerge, however, that are consistent with theoretical models of fault growth that predict elliptical or bell-shaped displacement profiles (Pollard & Segall 1987; Cowie & Scholz 1992a), in part because displacement along an individual fault must reach a minimum at the fault tips with a maximum value located between them (Fig. 4). The position of the displacement maximum is likely controlled by mechanical interactions with adjacent faults that distort the local stress field (Cartwright *et al*. 1995; Gupta & Scholz 2000).

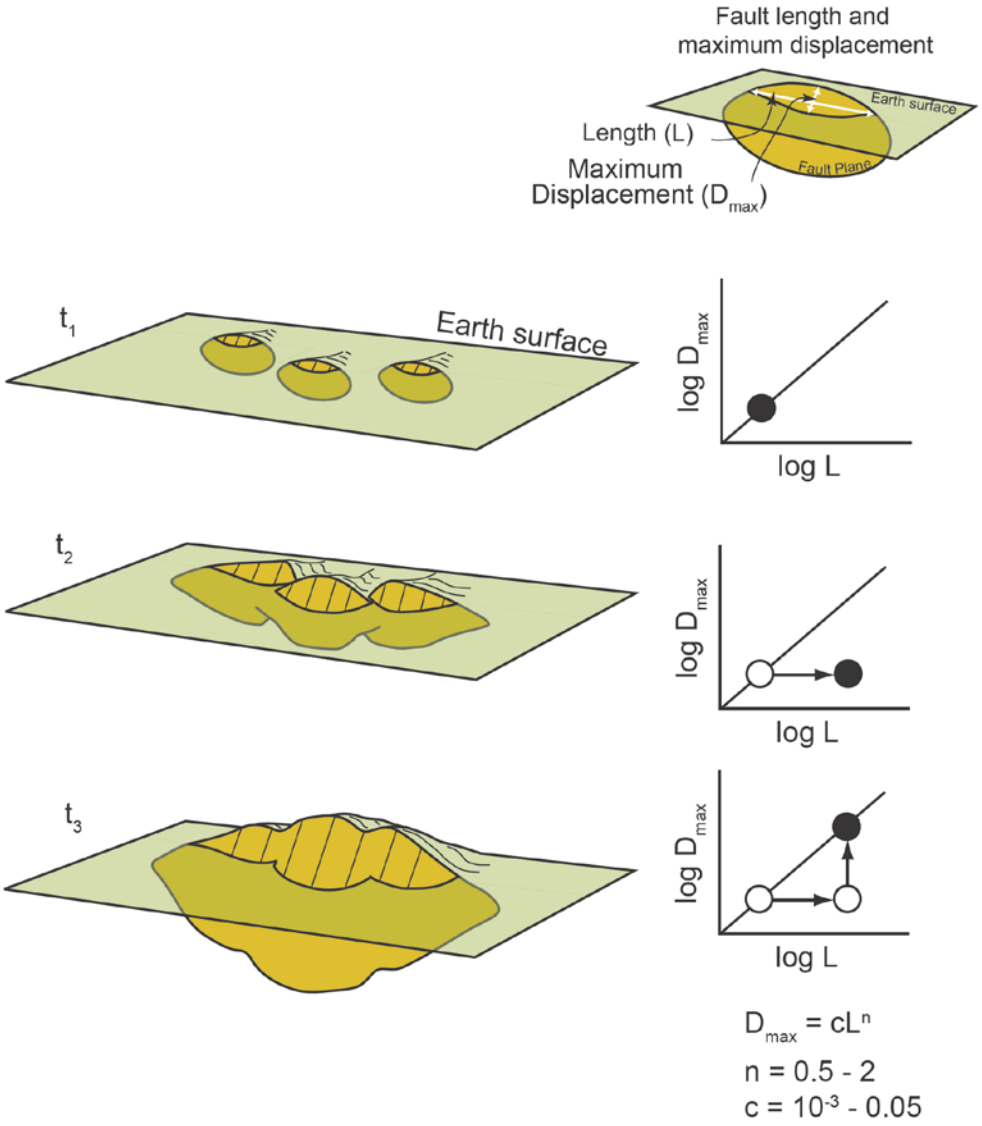

Figure 4. Schematic of different fault scaling relationship measurements. Upper right shows fault length to maximum displacement (After Drawers *et al*. 1993). The diagrams in the upper right show the fault dimension measurements used to determine fault scaling relationships. Cartoon in the left column showing the growth and linkage of normal faults and plots tracking the evolution of fault dimensions at three time steps from single isolated faults (t1) through interaction (t2) and finally hard linkage (t3). Note that post-hard linkage fault scaling relationships of the composite fault are similar to that for single isolated faults show in t1. Modified after Anders & Schlische (1994) and Nicol *et al*. (1996).

The history of fault-growth and linkage is often observable in displacement profiles of active faults (Fig. 4; Anders & Schlische 1994; Dawers & Anders 1995; Gupta & Scholz 2000; Manighetti *et al*. 2001, 2005; Hetzel *et al.* 2004; Davis *et al*. 2005). When adjacent faults begin to overlap their stress fields interact and fault displacement profiles temporarily deviate from predicted profiles for a singular fault (Fig. 4). Once hard linkage of overlapping faults is accomplished, the composite fault will begin to recover unrealized displacement (D_{max}), and the displacement profile will return to roughly the same pattern as that for a single isolated fault (Fig. 4; Cartwright *et al*. 1995).

Importantly, the predictability of fault behavior based on length-displacement scaling relationships and displacement profile characteristics allows for the determination of whether or not a segmented fault is hard linked at depth simply by measuring its length to maximum displacement ratio and assessing the composite displacement profile along all fault segments (Fig. 4). If the length to displacement ratio is less than expected and the displacement profile contains multiple maxima, hard-linkage is unlikely; however, if length to displacement ratios are consistent with the global dataset and the displacement profile contains a single peak near the center of the fault, it can be assumed that the fault that is segmented at the Earth's surface is linked at depth.

Fault-scaling relationships and fault shape similarities are not limited to the portions of a fault exposed at the Earth's surface (Nicol *et al*. 1996; Willemse *et al*. 1996; Willemse, 1997; Schulz & Fossen 2002; Walsh *et al.* 2003). This is not surprising given that it is the mechanical properties of the rocks in which the faults are embedded that largely dictate the process of fault growth (Benedicto *et al*. 2003; Soliva & Benedicto 2005; Soliva *et al*. 2006). Analyses of natural populations shows that isolated faults have strike-to-dip dimension ratios, or aspect ratios, of 0.5 to 3 (Fig. 4; Nicol *et al*. 1996; Soliva & Benedicto 2005).

When two adjacent faults commence linking, their aspect ratio often increases to as high as 3 to 5 (i.e. becoming more elliptical in the strike direction). However, this response is likely ephemeral because faults tend to accrue displacement, and hence increase size in the dip dimension, after hard linkage of individual faults is complete (Fig. 4; e.g. Cartwight *et al*. 1995; Willemse *et al*. 1996; Willemse 1997). Fault aspect ratios can be skewed to even higher values when growth in the dip dimension is restricted by changes in rock mechanical properties with depth, thus favoring fault growth towards the tip zones (e.g. Willemse 1997; Solvia *et al*. 2006). Nonetheless, in settings where fault growth remains unrestricted, the consistency of fault aspect ratios implies that these scaling relationships can be applied to help constrain the three-dimensional geometry of faults. Caution must be used when interpreting fault geometries based solely on scaling-relationships because obtaining measurements of the actual strike length of an active fault are difficult as most of the fault plane lies beneath the Earth's surface (Fig. 4). In general, fault geometry estimates based on scaling relationships represent a minimum of the true fault dimensions.

Methods

This investigation was conducted in three field seasons during 2010 and 2011 along a 100 km of coastline along the range fronts of the Asterousia and Dikti Mountains (Fig. 3c). We combine the sedimentology and optically stimulated luminescence (OSL) age-dating of terrace deposits, differential GPS surveys, soil profile characterization for the relative dating of geomorphic surfaces, and terrace correlation to the late Pleistocene eustatic curve in order to (1) calculate surface uplift rates, and (2) identify active faults along South-central Crete for the past 0.40 Ma.

Field Investigation

Vertical transects of marine terraces were carried out at 18 sites along the south-central coastline of Crete using a 2008 Trimble GeoXH differential GPS system (Fig. 3c). The inner shoreline angle (ISA) elevation, which approximates paleo-sea level at the time of terrace formation (Fig 5; Lajoie 1986; Merrits & Bull 1989), was measured for terraces at each site. ISA elevation measurement errors varied between 0.1 to 4 m, with mean and median errors of 1.6 and 1 m, respectively, after post-processing corrections were applied (Appendix 2.1). Terraces were correlated along the coastline by GPS survey elevations, mapping of stratigraphic relationships between marine terraces and alluvial fans, and the degree of soil development in overlying alluvial fans. Faults identified in the field that offset marine terraces were mapped and the orientations of their exposed surfaces measured. When available the trend and plunge of slicken lines were measured to assess the most recent near-surface direction of fault motion. Soil development profiles on alluvial fan deposits were described when natural exposures allowed.

Optically Stimulated Luminescence Geochronology

Fine-grained lenses of quartz-rich sediment from marine terraces and alluvial fans were targeted to determine the timing of sediment burial using optically stimulated luminescence (OSL). Samples were collected using a 3 cm diameter by 30 cm long steel tube hammered into the target horizon. Additional samples were collected for measurements of moisture content and natural background radiation. All samples were submitted to the Laber Scientific luminescence dating research laboratory. Each sample was treated with 10% hydrochloric acid (HCl) and 30% hydrogen peroxide (H_2O_2) to remove carbonates and organic materials, respectively. The sample was then sieved to the 90 to 150 μm size fraction, which was used for the equivalent dose (D_e)

determinations, measured in Grays (Gy; 1 Gy = 1 J kg^{-1}). The sieved grains were treated with 40% hydrofluoric acid (HF) for 40 minutes then with 10% HCl to remove fluoride precipitates. An automated Risø TL/OSL-20 reader was used to perform the quartz OSL measurements. Stimulations was carried out by a blue light-emitting diode (LED; $\lambda = 470 \pm 20$ nm) source for 40 s at 130 °C. Irradiation was carried out using a $^{90}Sr/^{90}Y$ beta source built into the reader and the OSL signal was detected by a 9235QA photomultiplier tube through a 7.5 mm thick U-340 filter.

The single aliquot regenerative-dose (SAR) protocol was adopted for the D_e measurements on twenty-four aliquots per sample (e.g. Rhodes 2011). The initial preheated temperature was 260 °C for 10 s, followed by 220 °C for 10 s. The final reported D_e is the average of all aliquots and the D_e error is the 1σ distribution. The cosmic ray dose rate was estimated as a function of depth, altitude and geomagnetic latitude. The concentration of uranium (U), thorium (Th) and potassium (K) was measured by neutral activation analysis in the laboratory and the elemental concentrations were then converted into annual dose rate, taking into account the water content effect. The sample OSL age is calculated by dividing D_e value by the mean dose rate:

$$\text{Age(yrs)} = D_e\text{(Gy)}\ [\text{dose rate (Gy yrs}^{-1})]^{-1} \qquad (2).$$

Rates of Coastal Uplift and Eustatic Correlations

The long-term (10^4 to 10^5 yr) uplift rate is determined by height-age relationships for the OSL-dated marine terraces. Following Lambeck *et al*. (2004) the uplift rate, *u* and its uncertainty, σ^2_u are calculated from the following, where:

$$u = \Delta H\, T_T^{-1}, \qquad (3)$$

and

$$\sigma^2_u = \sigma^2_{\Delta H}\, T_T^{-2} + (\Delta H\, T_T^{-2})^2\, \sigma_{TT}^2 \qquad (4).$$

The tectonic change in terrace elevation is found by:

$$\Delta H = H_T - \delta H_{SL} \quad (5),$$

where H_T is the height of the dated terrace shoreline above modern mean sea-level and δH_{SL} is the eustatic elevation for the dated terrace time interval. T_T is the 2σ calibrated radiocarbon age of the terrace with an uncertainty of σ_{TT}, where $\sigma^2_{\Delta H}$ is the uncertainty in the amount of tectonic uplift (= $\sigma^2 H_T + \sigma^2 \delta H_{SL}$).

It is often assumed that Pleistocene marine terraces form during periods of relative sea-level stability, such as during glacio-eustatic highstands (i.e. Lajoie 1986; Merritts & Bull 1989). Along coastlines uplifting at a uniform rate the periodic nature of eustatic highstands often results in the formation of flights of Pleistocene terraces with unique altitudinal spacing. Geochronologic dating of at least one of these terraces at a particular locality allows for local calibration of the entire terrace flight to the Late Pleistocene eustatic curve (Lambeck & Chappell 2001; Waelbroeck *et al*. 2002; Wegmann, 2008) and constrains the age of the other terraces in the sequence (i.e. Merritts & Bull 1989).

Results

Marine Terraces and Alluvial Fans

The eastern Mediterranean Sea has a small tidal range (< 0.2 m spring tide) and generally low wave energy. Nonetheless, marine terraces and bio-erosional notches are extensive and easily defined along the south coast of Crete, and have inner shoreline angle elevations varying between 1 and 260 m above mean sea level (amsl) across the study area (Appendix 2.1). Preserved paleo-shorelines separate into two general categories: 1) sediment-poor bedrock erosional features

typically associated with narrow biogenic “fringing reefs” and 2) sediment-rich deposits on bedrock planation surfaces (Fig. 5). Some terraces are buried by thick (>2 m) alluvial fan sediment, from which only a minimum inner shoreline angle (ISA) elevation estimate is attainable. Local geology plays an important role in the form and preservation of the terraces. Well defined and preserved terraces and paleo-shoreline notches are found where carbonates crop out. In contrast, terraces are almost completely absent from coastal areas where flysch and opholitic sequences crop out, due to the enhanced mass-wasting potential of these units in comparison to the Mesozoic carbonates. Portions of the study area underlain by Miocene to Pliocene turbidites are characterized by broad, easily identifiable marine terraces due to the weak lithification and erodibility of these units. Terraces developed on top of the Neogene sedimentary units typically have thick (> 1 m) deposits of mainly beach cobbles and pebbles.

We separate the Pleistocene paleo-sea level indicators into six classifications that allow us to develop a unique stratigraphic assemblage model for the south-central coastline of Crete (Fig. 5). Two assemblages are classified as sediment poor. Assemblage *A* consists of notches, small sea caves and sea arches that are attributed to mechanical and bio-erosional processes (Fig. 5a). Assemblage *B* consists of broad, vertically-draped calcareous algal reefs that typically reach a terminus just below the elevation of a bedrock planation surface (Fig. 5b).

Sediment-rich sea level indicators are subdivided into four assemblages (Fig. 5). Erosional features such as notches, sea caves and arches are sometimes accompanied by small pebble to cobble beach lag deposits that we classify as assemblage *C* (Fig. 5c). Assemblage *D* is similar to assemblage *C*, but is capped by solid calcareous algae reefs (Fig. 5d). The stratigraphy of assemblage *D*, beach rock capped by algae reef, indicates that the terrace planation surfaces and overlying

Figure 5. Top schematic of the six assemblages (A – F) of paleo-shore line markers found along the south-central coastline of Crete and the letters are keyed to the digital photos below. Note that this is not a representation of an actual terrace sequence. Digital photographs (a – f) of examples of the six different marine terrace assemblages. (a) Assemblage A- bioerosional notch at Cape Trekalo. (b) Assemblage B – bioerosional notch and fringing algal reef at Cape Trekalo. (c) Assemblage C – bioerosional notch and pebbly beach-lag couplet at Lentas. (d) Assemblage D – Beach rock and abrasion platform west of Tsoutsouros. (e) Assemblage E – transgressive algal reef on beach rock overlain by an alluvial fan at Agios Ioannis. (f) Assemblage F – Beach rock and abrasion platform buried by an alluvial fan at Trypiti gorge.

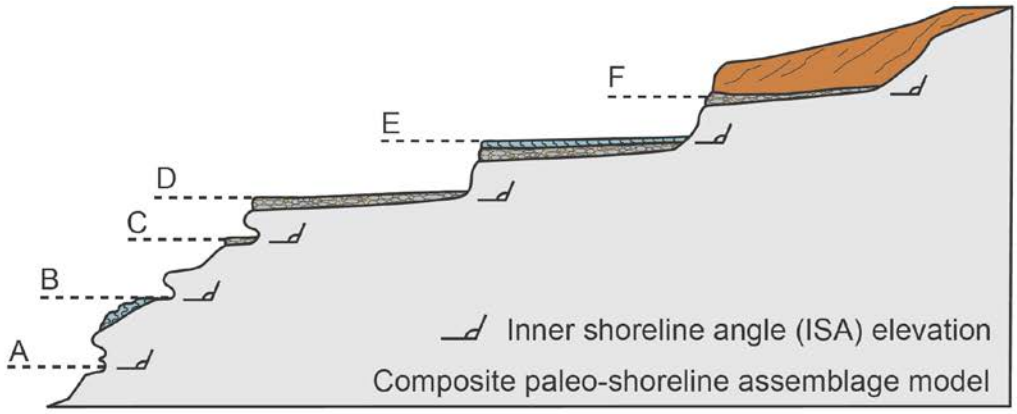
F
E
D
C
B
A
Inner shoreline angle (ISA) elevation
Composite paleo-shoreline assemblage model


a
Assemblage A
wave cut notch

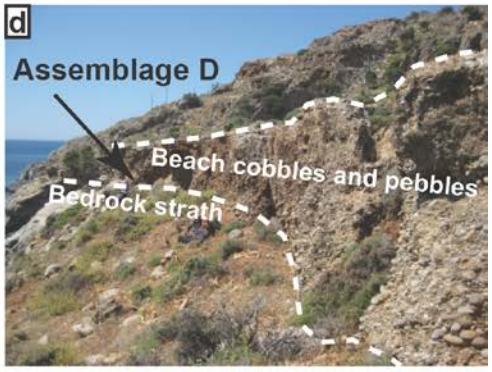
d
Assemblage D
Beach cobbles and pebbles
Bedrock strath

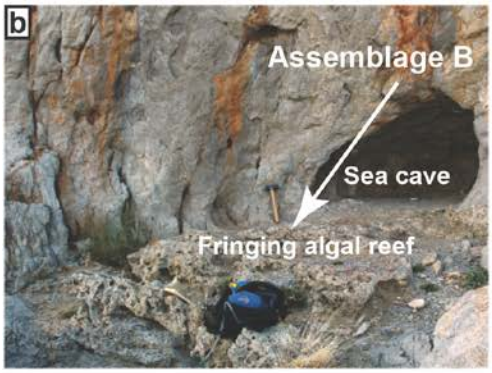
b
Assemblage B
Sea cave
Fringing algal reef

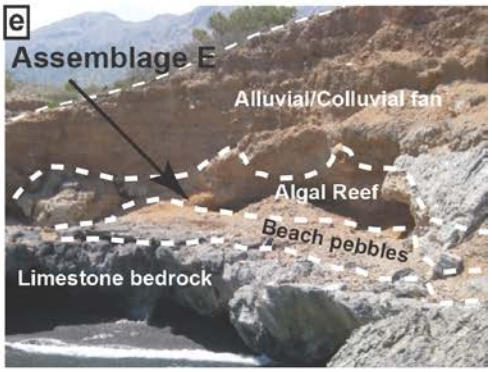
e
Assemblage E
Alluvial/Colluvial fan
Algal Reef
Beach pebbles
Limestone bedrock


c
Assemblage C
Sea cave
wave cut notch
Beach lag (pebbles)

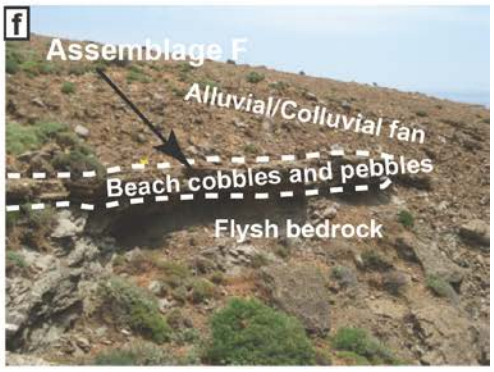
f
Assemblage F
Alluvial/Colluvial fan
Beach cobbles and pebbles
Flysh bedrock

deposits formed during local transgressive to highstand intervals. Assemblage *E* consists of a pebble-to-cobble beach lag unconformably overlying broad bedrock planation surfaces (Fig. 5e). Assemblage *F* is similar to assemblage *E*, but is buried by alluvial fan detritus. Stratigraphic relationships for assemblage *F* may be exposed along road and/or stream cuts, or along sea cliffs (Fig. 5f).

Many of the marine terraces of the South-central Crete coast are buried by alluvial fans (Fig. 6), which allows for the correlation and relative dating of terraces between study sites (Fig. 3c). We distinguish three distinct fan types, based largely upon the degree and nature of soil development, and additionally on sedimentologic and stratigraphic characteristics (Fig. 6a-c). Fan types *1* and *2A* are found along the Asterousia coastline, west of Tsoutsouros (Fig. 6, 7). Type *1* fans have thin A horizons, weakly-developed illuvial horizons (Bt_w), and occasional incipient calcic horizons (Bk_w; Fig. 6a; Appendix 2.2). Type *2A* fans have a diagnostic petrocalcic horizon (Bk) that may or may not be capped by a thin soil A horizon (Fig. 6b; Appendix 2.2). Both are comprised of angular gravel locally-derived from flysch and carbonate outcrops (Fig 6a, b). Type *1* is inset in to Type *2A,* indicating that it is relatively younger (Figs. 6a, b). This is supported by the relatively less well-developed soil of Type *1* and 2A fans, which are otherwise indistinguishable from each other based upon their sedimentology and stratigraphy. Type *2B* alluvial fans are only found along the range front of the Dikti Mountains (Fig. 6, 7). They exhibit soils with thin, well-developed A horizons and thick, red Bt horizons (Fig. 6c; Appendix 2.2). Type 2B fan deposits are generally thicker and composed of smaller and more rounded clasts than fans of Type *1* or *2A*. All of the south-central coastline alluvial fans are graded to a base level far lower than present-day sea level, indicating that the timing of fan progradation likely occurred during periods of eustatic drawdown.

Figure 6. (a-c) Photos of alluvial fans and soil horizons. (d-g) Photos of the fan and terrace stratigraphy. Asteroussia fault block at site 10 original photo (d) and mapped fan units and marine terrace inner shore line elevations (dashed white lines) with elevations in meters shown (e). Note the inset relationship between fan type 1 and type 2a. Coastal stratigraphy found in the hanging wall of the South-Central Crete fault at site 11, original photo (f) and mapped fans with the inner shore line elevations of the marine terrace denoted and elevations above sea level are doted as above (g).

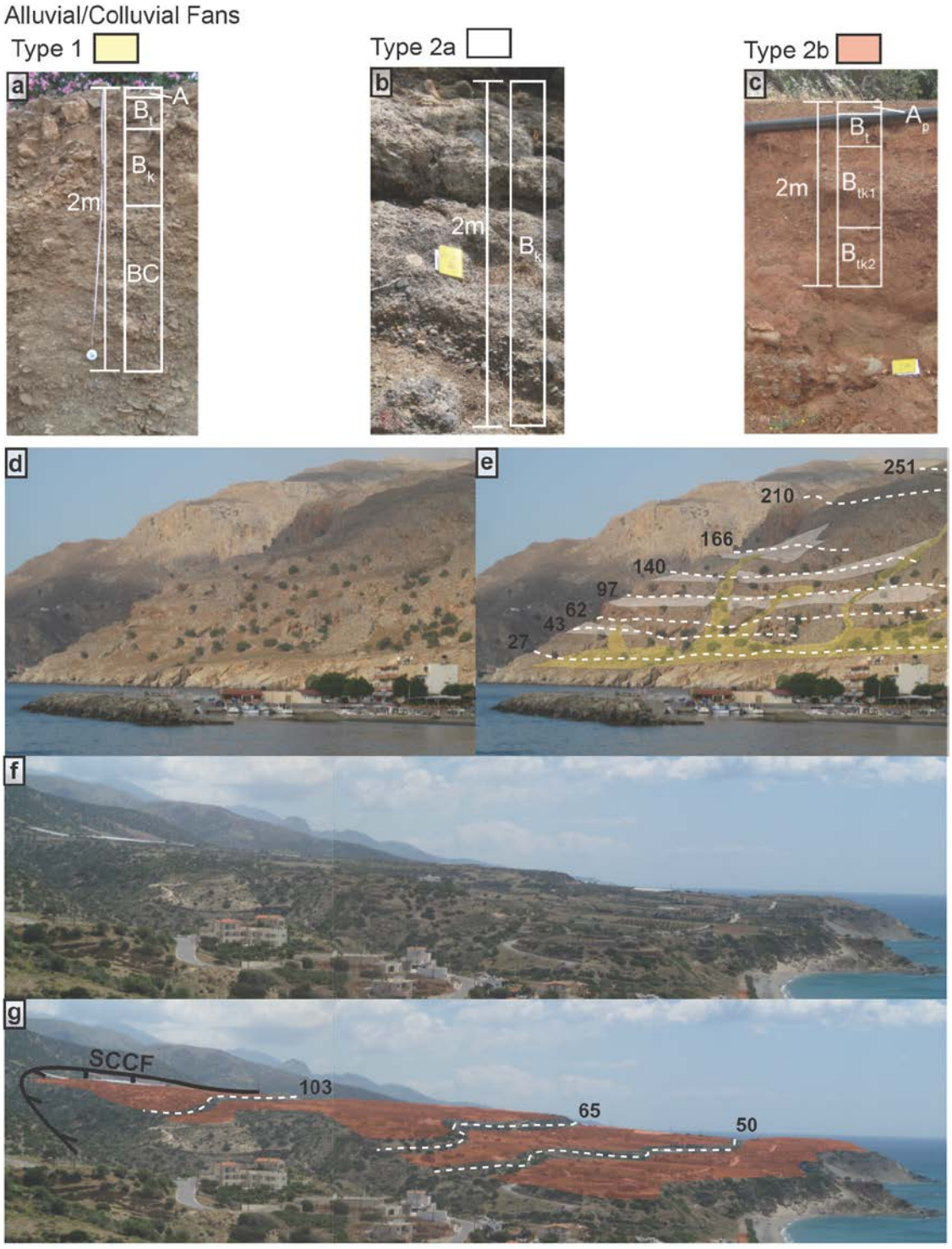
Alluvial/Colluvial Fans
Type 1
Type 2a
Type 2b
a
A
B_t
B_k
2m
BC
b
2m
B_k
c
A_p
B_t
2m
B_{tk1}
B_{tk2}
d
e
251
210
166
140
97
62
43
27
f
g
SCCF
103
65
50

Faults

Two faults were identified that offset Pleistocene marines terraces and extend offshore, dividing the study area into three distinct fault blocks; the eastern and western Asterousia blocks and the South-central Crete fault hanging-wall block (Fig. 7). The more westerly of the two, the Lentas fault, crops out onshore 3 km to east of the town Lentas, strikes ENE and dips 45° south-southeast (Fig. 7). No slip direction indicators were observed on this fault (Fig. 7b). The Lentas fault vertically offsets the lowest terraces in the sequence by 14.5 ± 1 m. A smaller near-vertical conjugate fault, with slickensides indicating highly-oblique right-lateral dipslip motion, also offsets Pleistocene terraces (Fig. 7b).

The more easterly South-central Crete fault extends offshore at Tsourtsouros, forms the segmented front of the Dikti Mountains, and terminates somewhere in the Ierapetra Plain about 55 km to the east of where it first crops out onshore (Figs. 3, 7). The South-central Crete fault juxtaposes Mesozoic flysch and carbonates in the footwall against Neogene turbidites in the hanging wall. The South-central Crete fault has four main segments striking east-northeast that dip 40 to 50° towards the south southeast. Exposed fault planes contain slicken lines demonstrating that near-surface slip has been predominantly dip-slip with lesser components of left-lateral motion (Fig 7c); both of which are consistent with focal mechanisms derived from shallow earthquakes sourced a few kilometers to the south (e.g. Bohnhoff et al., 2005). The South-central Crete fault unequivocally offsets late Quaternary marine terraces. Well preserved fault scarps are found along the footwalls of all fault segments, and bedrock knickpoints are common immediately upstream from the surface fault trace, providing further evidence of recent activity along the entire length of the fault. Late Pleistocene marine terraces offset and preserved in both the hanging and footwalls of the Lentas

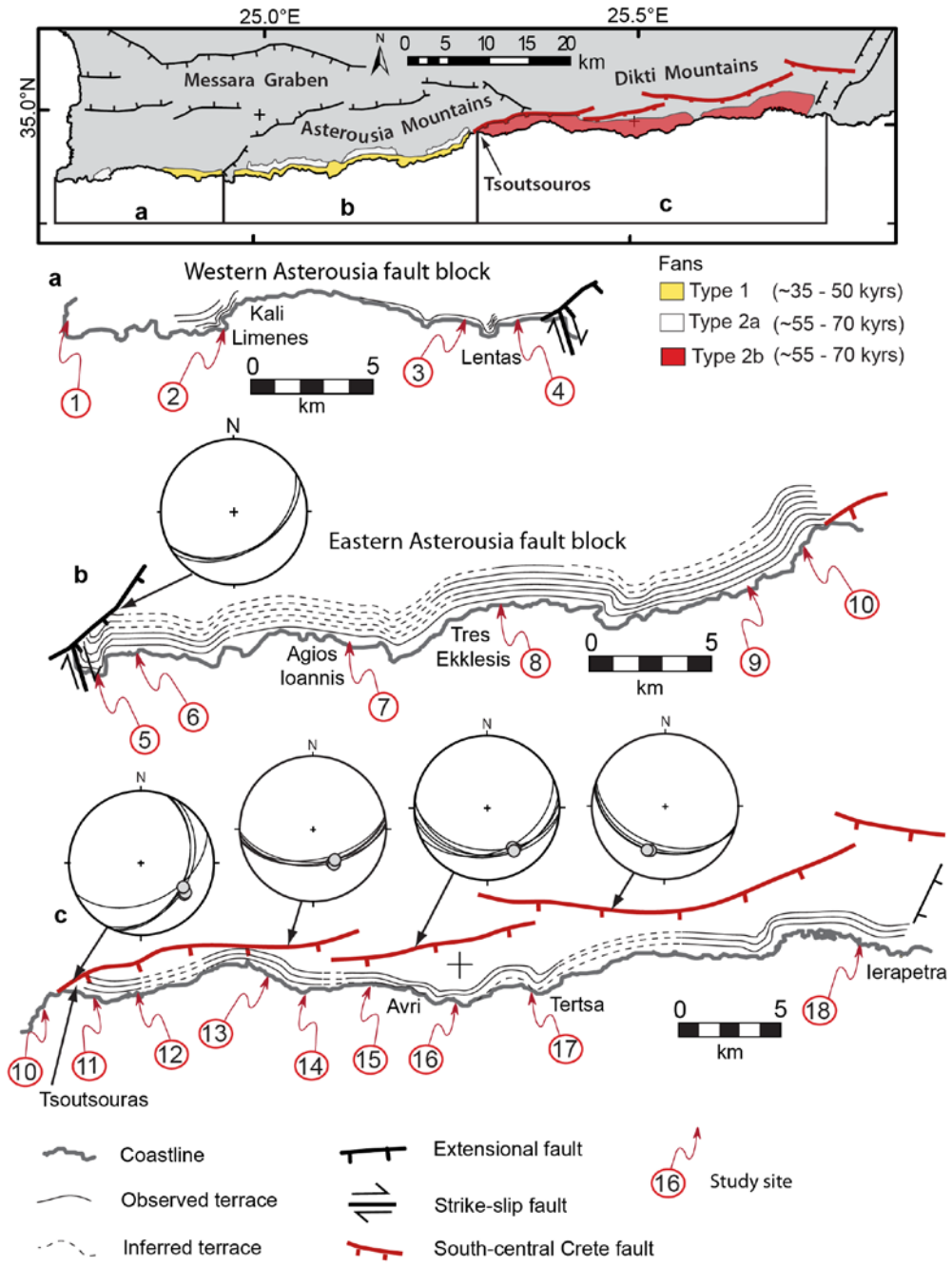

Figure 7. Map of south-central Crete with the approximate geographic distribution of alluvial/colluvial fans observed in the field (fan map units not to scale). (a – c) Along coast lateral distribution of Pleistocene marine terraces south-central Crete. Note that this figure is not to scale and does not indicate the actual vertical distribution of terraces. Sites (1 – 18) keyed to tables 1 and 2 and Appendix 2.1, 2.2, and 2.3.

and South-central Crete faults highlights the fact that southern Crete is simultaneously extending and uplifting.

The marine terraces and alluvial fans in South-central Crete form a unique coastal stratigraphy with substantial differences between the three fault-bounded blocks (Fig. 6, 7). West of the Lentas fault, two robust terrace sequences preserve four terraces each that range in elevation from 0 to 94 m above mean sea level (amsl; Fig. 7a). The lowest terrace in this combined sequence is laterally extensive and buried by a thick (> 3m) Type *1* alluvial fan. It is at a maximum elevation of 19 m amsl at the Lentas fault, tilted to the west and can be traced for ~ 10 km before it is no longer preserved due to mass-wasting within ophiolitic units between sites 2 and 3 (Fig. 7a). The most western marine terraces are found near Kali Limenes, where the higher terraces are buried by a type 2a alluvial fan (Fig. 7 – site 2). At the western end of the Asterousia (west of Kali Limenes), the shore is a ria coast, marine terraces are not preserved and submergered roman structures have been identified (Mourtzas 1988, 2012a,b; Peterek & Shawarze 2004). This evidence indicates either long-term stability or subsidence of this coastline, at least during the most recent portion of the Holocene.

The eastern Asteroussia block maintains the highest in elevation and greatest number of identified terraces along the south-central coastline (Fig. 7b). The lowest terrace from this sequence can be traced nearly continuously from the Lentas fault to the South-central Crete fault, rising in elevation from 4 to 25 m amsl (Fig. 7b). The facies of the lowest terrace varies along the coast, but it is always buried by a Type *1* alluvial fan. Higher terraces are generally less prominent and poorly preserved, with the exception of the fourth highest terrace. The fourth terrace in the sequence is traceable in an unbroken fashion for 30 km to the west of the South-central Crete fault, where it is buried by both Type *1* and *2* alluvial fans, reappearing again just to the east of the Lentas fault (Fig.

7b). All of the eastern Asterousia block terraces increase in altitude and inter-terrace spacing in an eastward direction, away from the Lentas fault.

Terraces preserved in the hanging wall of the South-central Crete fault hanging wall are distinct in form and number in comparison to those in the adjacent footwall (site 10 – Figs. 6d-g, 7c). Hanging wall terraces are broad, slope gently seaward, and are typically found as a flight of three (Fig. 6f-g, 7c). These terraces are dissected where streams drain the Dikti range front, yet can be traced for tens of kilometers along the coastline between Tsoutsouras and Tertsa (sites 11 to 17), where their preservation is reduced due to mass-wasting along coastal cliffs. These three terraces decline in elevation from the South-central Crete fault (site 11) to Arvi, where they steadily increase in elevation until they are truncated by the N-S striking Ierapetra fault (Anglier 1979; Gaki-Papanastassiou *et al*. 2009).

Geochronology

We report five new OSL age-dates from South-central Crete, two from the lowest terrace (Fig. 7b – sites 8 & 10), two from alluvial fans in the Asteroussia Mountains (Fig. 7a, b – sites 4 & 8) and one from the lowest terrace in the hanging wall of the South-central Crete fault (Fig. 7c – site 12; Table 2). The quartz OSL was fast component dominated. Recycle ratios were between 0.9 to 1.1 and recuperation was negligible. The lowest marine terrace is continuously exposed along the coastline between sites 8 and 10, a distance of 20 km. The OSL sample from site 10 (LS1254), collected from the footwall adjacent to the South-central Crete fault, yielded a sediment burial age of 72 $\pm$ 8 kyr (Table 2). The second sample from this terrace, OSL sample from site 8 (LS1251), yielded a burial age of 78 $\pm$ 8 kyr. The two OSL burial ages obtained from the lowest marine terrace

Table 2

Site (Fig. 3)	sample	deposit	depth (m)	Elevation (m asl)[1]	D (Gy kyr^{-1})[2]	Aliquot no.	D_e (Gy)[3]	water content (%)	OSL age (kyrs)[4]	assigned MIS[5]
4	LS1252	Alluvial fan	2	17.8	1.79 ± 0.13	24	77 ± 4	15 ± 5	43 ± 4	3
8	LS1256	Alluvial fan	3	26	1.07 ± 0.08	24	37.5 ± 3.1	15 ± 5	35.1 ± 4	3
8	LS1251	Marine terrace	3	23	1.50 ± 0.10	24	107 ± 9	15 ± 5	72 ± 8	4/5
10	LS1254	Marine terrace	3	25	1.13 ± 0.08	24	40.8 ± 3.2	15 ± 5	78 ± 8	4/5
11	LS1255	Marine terrace	2	35	1.55 ± 0.11	24	197 ± 15	15 ± 5	127 ± 13	5e

1 Sample elevation in meters above sea level (m asl).

2 Background dose rate (D) in Grays per 1000 yrs.

3 Equivalent dose (D_e) in Grays.

4 Optically stimulated luminescence (OSL) age in 1000's of years before present (kyrs).

5 Marine isotope stage (MIS) assigned based on age. 4/5 indicates the sea level highstand that occurred during the transition between MIS 4 and 5.

in the eastern Asteroussia fault block yield ages that overlap within error indicating OSL results are consistent, repeatable and thus reliable ages for terrace construction (Table 2).

Two OSL samples were obtained from alluvial fan sediments that bury the lowest terrace on either side of the Lentas Fault (sites 4 and 8, respectively). The burial ages of fine-grained lenses from these alluvial fans are 40.8 $\pm$ 3.2 and 37.5 $\pm$ 3.1 kyr, respectively (Table 2). Stratified sediments immediately above the bedrock strath from the lowest marine terrace in the hanging wall of the South-central Crete fault, just east of Tsourtsouras (site 12) yielded an OSL age of 127 $\pm$ 13 kyr. This OSL burial date supports earlier geochronology based upon index fossils (*Strombus bubonius*) and shell $^{230}Th/^{235}U$ and $^{231}Pa/^{235}U$ age-dates of various fauna extracted from the two lowest terraces above the South-central Crete fault hanging wall (Tables 1, 2; Angelier 1979b). The consistency of these results indicates that OSL is a viable method for the dating of late Quaternary surficial deposits in the eastern Mediterranean as has been found previously (e.g., Pope *et al*. 2008; Macklin *et al*. 2010).

Discussion

Coastal Chronostratigraphy

Based on the geochronology, this terrace was deposited over a relatively short interval during the eustatic highstand that occurred during the transition from MIS 4 to 5 (Lisiecki & Raymo 2005; Fig. 8a; Table 2; Appendix 2.1). The overlying alluvial fan has an OSL age of ~ 35 to 43 kyr, consistent with deposition during climatic transitions associated with MIS 3 (Fig. 8a; Table 2). The alluvial fans overlying the lowest terrace on both the western and eastern Asteroussia blocks exhibit a nearly identical sedimentology, stratigraphy, and soil development, in addition to having OSL burial ages that overlap within error (Fig. 6a, b; Table 2). These findings lead to the conclusion that

the Type *1* alluvial fan in the western block was deposited contemporaneously with the Type *1* alluvial fan in the eastern block and the lowest terrace buried by this fan is of the same age on either side of the Lentas fault.

The Type *2A* alluvial fans were deposited during MIS 4. This interpretation is based upon available geochronology, soil development and landscape position. The MIS 4 assignment for the Type 2 fans is consistent with the development of a petrocalcic soil horizon, a feature not observed on the younger, inset Type *1* fans. In addition, the Type *2A* fans unconformably overlie marine terrace deposits correlated with eustatic highstands during MIS 5 (see below), and their surface slopes project to a base level far lower than present-day base sea level (Fig. 6d, e).

The OSL date from the lowest marine terrace in the hanging wall of the South-central Crete fault (127 ± 13 kyr) indicates that terrace formation occurred during either the transgression to, or concurrent with the MIS 5e eustatic highstand, consistent with the interpretations of previous studies (Table 2; Fig. 8b; Angelier 1979; Gaki-Papanastassiou *et al*. 2009). The burial of this and higher terraces by Type *2B* alluvial fans indicates that fan deposition occurred post-MIS 5e, likely during MIS 4. Older alluvial fans may in fact be present on the higher, pre-MIS 5e terraces in this sequence; however, it is beyond the scope of this study to assess the detailed stratigraphy of alluvial fan progradation along the Asterousia and Ditki Mountain fronts. The difference in soil development between Type *2A* and *2B* alluvial fans, which are interpreted to be the same age, is most likely a function of the contrasting parent material lithology between the two fault blocks. Type *2A* fans are located in limestone-rich areas, and thus carbonate is readily available for the development of calcic soil horizons; whereas Type *2B* fans are located in areas underlain by Miocene-to-Pliocene marine sediments that contain abundant clay-rich horizons that promote the accumulation of pedogenic (Bt) clays in their soils.

The geochronologic results and interpretations of fan depositional timing presented here are consistent with the work of Pope *et al.* (2008), who proposed a soil development and OSL-based chronology of alluvial fan aggradation and incision from the Sfakia region of southwestern Crete. These authors identified five different phases of alluvial fan deposition. The Type *2A* and *2B* fans described in this study are synchronous with stage 2B (ca. 75 to 175 kyr) of Pope *et al*. (2008), while Type *1* fans are contemporaneous with their stage 2C fans (ca. 12 to 75 kyr; Table 2). Stratigraphic and age-control data are consistent with the interpretation that the marine terraces of the South-central Crete coastline were cut and emplaced during transgressive-to-highstand conditions associated with warmer interglacial periods and lends credibility to the correlation of terraces to specific late Pleistocene eustatic highstands. This chronology suggests that alluvial fans prograded outward to a base level far lower than present-day sea level during periods relatively cooler than today that experience high frequency climate fluctuations (e.g. MIS 3), as well as possibly during glacial intervals (e.g. MIS 4). This coastal chronostratigraphy is consistent with the general timing and eustatic-climatic correlations arrived at in previous studies of marine terraces (Angelier 1979; Wegmann 2008; Strasser *et al*. 2011) and alluvial fans (Pope *et al*. 2008) on the island of Crete.

Terrace Correlations and Vertical Coastal Motions

OSL burial dating, previously published geochronology, stratigraphic and sedimentologic relationships, soil profile development and the physical continuity of terraces along the coastline allows us to anchor the terrace sequences to the late Quaternary eustatic curve at 18 sites (Figs. 7, 8; Tables 1, 2; Appendix 2.1, 2.3). The present altitudinal distribution of each terrace sequence is compared to the predicted terrace elevations derived from correlation to the late Quaternary

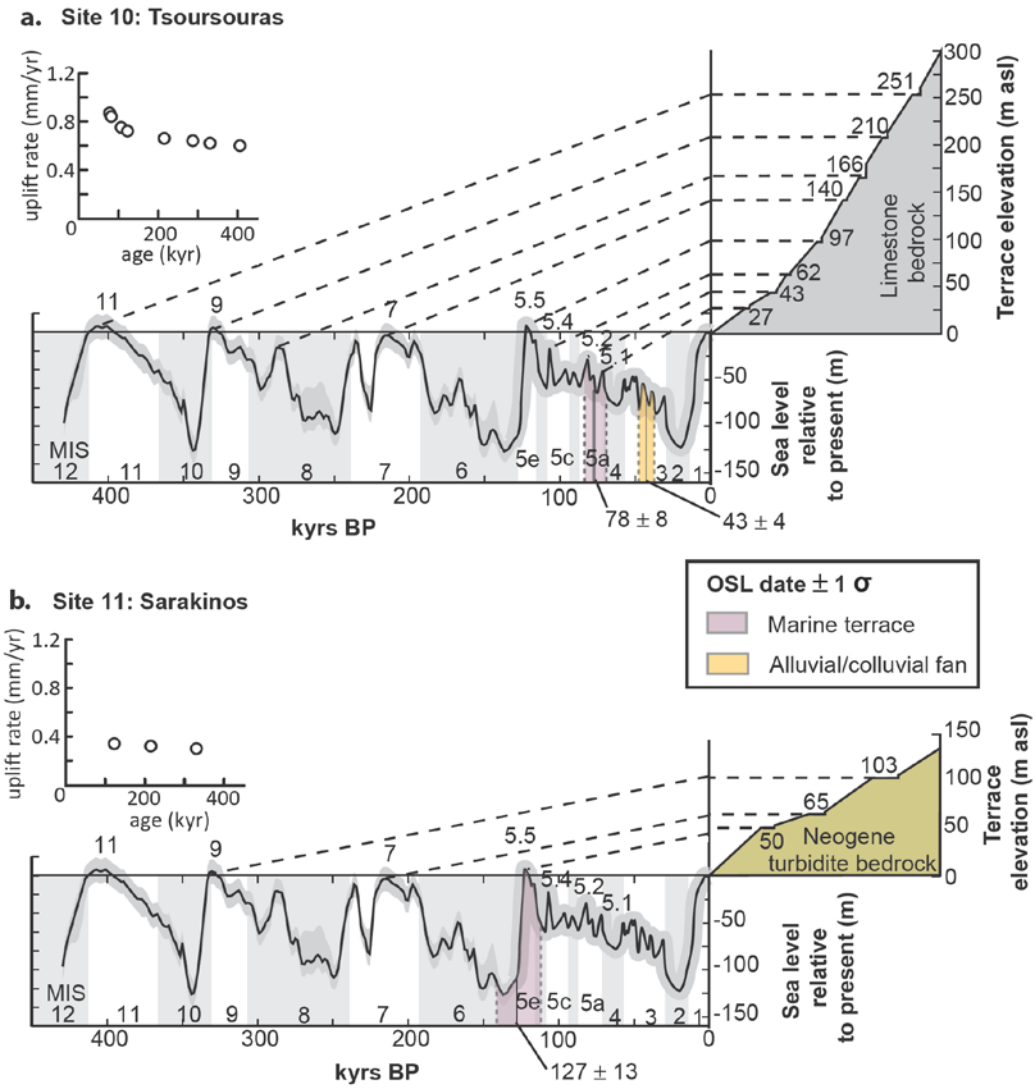

Figure 8. Correlation of the Tsoutsouros (a) and Sarakinos (b) terrace sequences to the Late Quaternary global sea level curve. The sea level curve was compiled from 0 to 125 kyrs from Lambeck & Chappell (2000) and from 125 to 450 kyrs from Waelbroek *et al*. (2002). Marine isotope stage (MIS) boundaries are from Lisiecki & Raymo (2005). Each terrace sequence is anchored to the sea level curve with an optically simulated luminescence (OSL) burial age of fine sand collected from marine terraces. The Tsoursouros sequence shows the OSL age of a fan overlying the lowest terrace in the sequence. Inset diagrams show uplift rates for individual terraces versus assigned terrace age determined using equations (3) and (4). Associated errors are smaller than the symbols at the scale of these diagrams.

eustatic curve assuming uniform and/or time-variant rates of rock uplift along the coast (c.f., Merritts & Bull 1989). The west Tsoutsouros sequence contains the greatest number of terraces and yields the most complete record of coastal uplift along the entire south coast of Crete for the last ~ 0.40 Ma (Fig. 6d-e, 8a). Every significant sea level highstand during MIS 5, with the exception of 5c is represented in this sequence along with those that that occurred during MIS 7, 8, 9 and 11 (Fig. 8a). The rate of coastal uplift has steadily increased through time, similar to the findings from southwestern Crete (Fig. 8a; Wegmann 2008; Strasser *et al*. 2011). West of Tsoutsouros, terrace elevations in all sequences show a general decrease in elevation with respect to modern mean sea level westward toward the Lentas Fault where they are offset by the fault (Fig. 9b). The average rate of late Quaternary uplift of the eastern Asteroussia block, between the Lentas and South-central Crete faults, is 0.5 to 1.0 mm yr^{-1} (Fig. 9). This estimate is slightly lower but comparable to the late Pleistocene uplift rates of southwestern Crete, to the north and west of the Messara plain (Wegmann 2008; Strasser *et al*. 2011).

Correlation of terraces by age along the Asterousia coastline reveals a consistency in the pattern of uplift over the late Quaternary (Fig. 9b). Total uplift is highest approaching the South-central Crete fault in the east and declines westward to the Lentas Fault (Fig. 9b). The similar pattern of uplift recorded from each of the marine terraces is indicative of characteristic earthquake rupture on an offshore fault (e.g. Schwartz & Coppersmith 1984). This finding is important because it suggests that ruptures on the Ptolemy Fault probably result in similarly-sized large earthquakes with relatively few intervening moderate earthquakes.

The ages of the terraces at the western end of the Asterousia Mountains (Sites 1 & 2) are unknown. Assuming the tilt for the lowest terrace between Sites 3 and 4 (0.15°) increases with

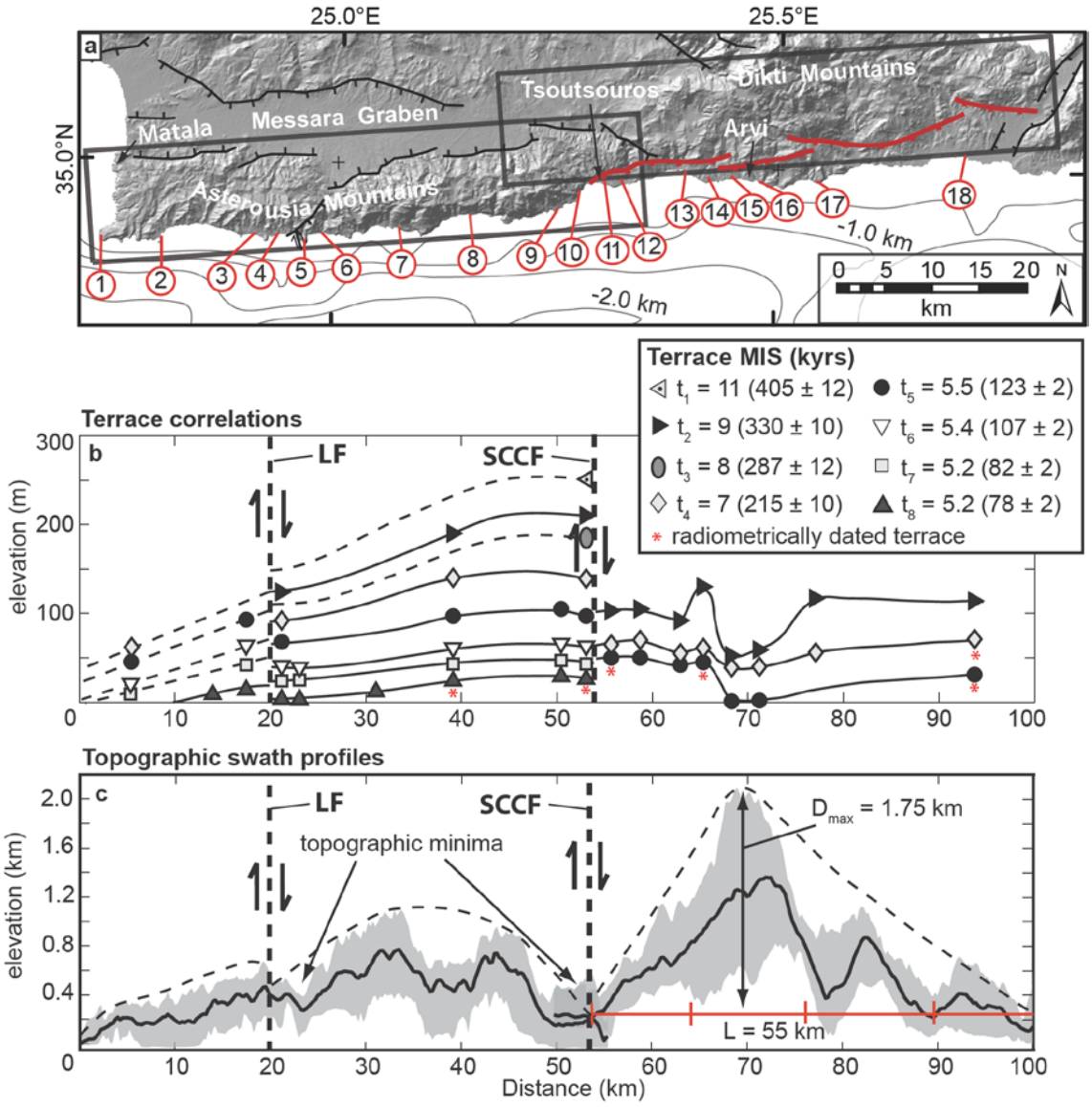

Figure 9. (a) Map of south-central Crete showing the location of the study sites and swath profiles shown in (d). (b) Correlations of terraces of same age along the south-central coastline of Crete. (c) Swath profiles taken along the Asteroussia and Dikti Mountains. Dashed lines indicate the profile of maximum displacement as determined by correlation of the highest peaks in the respective fault blocks. Horizontal red line indicates the approximate elevation and length of the South-Central Crete fault and the vertical red lines indicate the approximate horizontal extent of each fault segment. Vertical bold-dashed lines in b & c show the approximate location where the Lentas fault (LF) and South-Central Crete fault (SCCF) cross the coastline.

higher terraces, as would be expected for a fault that produces characteristic earthquakes (Schwartz and Coppersmith 1984), the higher and older terraces at site 4 can be projected to Site 2 (Fig. 9b). This assumption allows the lowest terrace at site 2 to be anchored to the sea-level curve at highstand 5.2 (ca. 80 kyr) and the correlation of successively higher terraces to older sea-level highstands, thus yielding a proposed temporal pattern of uplift consistent with other sites in the Asterousia (Fig. 9b). West of Site 2, the coastline is either stable or slowly subsiding, at least over the late Quaternary. This interpretation is supported by the lack of marine terrace deposits between Sites 1 and 2, despite the fact that the coast here is underlain by carbonates, the development of a highly indented (rias) shoreline, commonly associated with subsidence at least over the Holocene, and archeological evidence of submerged Roman tombs at Matala (Fig. 9a; Mourtzas 1988, 2012a).

To the east of Tsoutsouros, independent geochronologic and fossil evidence leads to the conclusion that the lowest terrace in the hanging wall sequence of the South-central Crete fault formed during MIS 5e and that the higher older terraces formed during earlier eustatic highstands during MIS 7 and 9, consistent with the findings of Angelier (1979)(Figs. 8b; 9b). The three terraces in the South-central Crete fault hanging wall are traceable for several kilometers along some coastal reaches, but are dissected by streams draining the Dikti range front, and are locally absent in other sections due to mass-wasting (Fig. 7c). The elevation of these terraces is more variable with distance from the South-central Crete fault, but a broad down warping is observed with a minimum approaching the center of the fault near the town of Arvi (Fig. 9b). While these is some scatter in the data, likely due to displacement on small subsidiary N-S striking faults embedded in the hanging wall, the first order synclinal deformation observed in these terraces is consistent with a mechanically linked South-central Crete fault (e.g. Cartwright *et al*. 1995).

The average late Quaternary uplift rate of the South-central Crete fault hanging wall is between 0.1 and 0.4 mm/yr, consistent with previous studies of the marine terraces here (Angelier, 1979). These rates are comparable to, but slightly faster than, the average Neogene rates of uplift of 0.14 to 0.2 mm yr^{-1} for the Messara and Iraklion basins determined form faunal assemblages of marine deposits now 100's of meters above sea level (Meulenkamp, 1994; van Hinsbergen & Meulenkamp 2006; Zachariasse *et al.* 2008).

Active faulting in South-central Crete

We utilize our eustatic correlation of terraces in the footwalls and hanging walls of both the Lentas and South Central Crete faults to estimate the spatial pattern of fault activity and late Quaternary slip rates (Figs. 8; 9b, c). Both Type *1* fans and the lowest terrace from the western and eastern Asteroussia fault blocks are offset by the Lentas fault, indicating that it has been active during the late Quaternary. The lowest terrace on either side of the Lentas fault is interpreted to have formed during the MIS 4/5 transition sea level highstand, making it a robust geomorphic marker from which to determine slip rates on the Lentas fault. Moreover, offset of the higher – older terraces permits slip accumulation to be determined since 72 to 123 kyr. The mean slip rate of the Lentas fault is 0.21 mm yr^{-1} over the late Quaternary, and from available constraints appears to have remained near constant (Fig. 9b). The South-central Crete fault offsets marine terraces associated with MIS 5.5, 7, and 9 terraces by 47 m, 74 m, and 107 m, respectively at Tsoutsouros (Site 10), indicating that the average slip rate on this portion of the fault is 0.35 mm yr^{-1} during the late Pleistocene. These findings are important for three primary reasons: (1) both the Lentas and South-central Crete faults should be considered seismically active and hazardous, not only for local ground accelerations induced by future earthquakes, but also because both faults extend offshore

into the Ptolemy trough, where they have the potential to generate tsunamis; (2) activity along these mostly east-to-west trending faults indicated that north-to-south (arc-normal) extension from the central Hellenic forearc is active into the late Quaternary; and (3) modest increases in the rates of fault slip are not sufficient to account for the increasing rate of late Quaternary uplift observed in the marine terraces along the coastline of the Asteroussia mountains. We address each of these issues in greater detail in the next sections.

Assessing linkage of the South-central Crete fault

Fresh fault scarp exposures and the presence of knickpoints along the streams draining the Dikti Mountains suggest that the entirety of the South-central Crete fault is active. The broad down-warping of marine terraces in the hanging wall of the fault is consistent with patterns of displacement predicted for a series of active and mechanically linked fault segments (Fig. 9b; e.g. Cartwright *et al*. 1995). The pattern of displacement, as defined by the maximum envelope of topography along the Dikti Mountains, is a broadly elliptical, or triangular profile, with a maximum near the fault center and accumulation of deficits along the profile that are spatially coincident with segment overlap zones (Fig. 9c; e.g. Drawers *et al*. 1993, Drawers & Anders 1995; Manighetti *et al*. 2001, 2005). The observed Dikti Mountains topographic profile is consistent with theoretical and empirical patterns of displacement across isolated faults or linked faults that behave mechanically act as isolated faults.

The length to maximum displacement ratio in the footwall of the South-central Crete fault is consistent with what is expected for a mechanically linked fault based on fault scaling properties, as expressed by Equation (1) (Figs. 4, 9d). The onshore portion of the South-central Crete fault is 55 km long. From this, fault scaling relationships predict that the maximum displacement is about 1.65 km.

A minimum estimate on the total footwall displacement across a fault can be determined using the maximum envelope of range front topography (Fig. 9c; i.e. Anders & Schlische 1994; Hetzel *et al*. 2004). The maximum elevation of the Dikti Mountains is ~1.75 km above the surface trace of the South-central Crete fault, in close agreement with the analytical prediction from fault scaling parameters alone (Fig. 9c). Collectively, these findings lead to the conclusion that the South-central Crete fault is mechanically linked at depth, and when coupled with the evidence of offset and warped late Quaternary marine terraces signifies that the South-central Crete fault represents significant seismic and tsunamigenic hazards to populations on Crete and throughout the eastern Mediterranean.

Three-dimensional constraints on the South-central Crete fault

The close proximity between the onshore South-central Crete and offshore Ptolemy trough faults is advantageous to ongoing discussions regarding the role of extension versus contraction in the formation of topography, basins, and earthquake hazards in the vicinity of Crete. The depth to which the South-central Crete fault penetrates, estimated using fault aspect ratios, is useful in assessing the kinematics of the Ptolemy fault, which is located only 10 km south from the trace of the South-central Crete fault (Fig. 3). As discussed above, linked faults that are mechanically unrestricted will exhibit aspect ratios between 1 and 5 (Fig. 4; Nicol *et al*. 1996; Willemse *et al*. 1996; Willemse 1997; Soliva & Benedicto 2005; Soliva *et al*. 2006). The seismogenic crust is 15 to 20 km thick beneath the south coast of Crete (Becker *et al*. 2006). We conservatively estimate that the down-dip height of the South-central Crete fault is between 11 and 18 km when a fault aspect ratio of 3 to 5 is considered for the exposed surface length of the fault. The fault depth is likely 5 to 16 km depending upon the assigned dip angle (40° to 90°; Fig. 10). We emphasize that these are

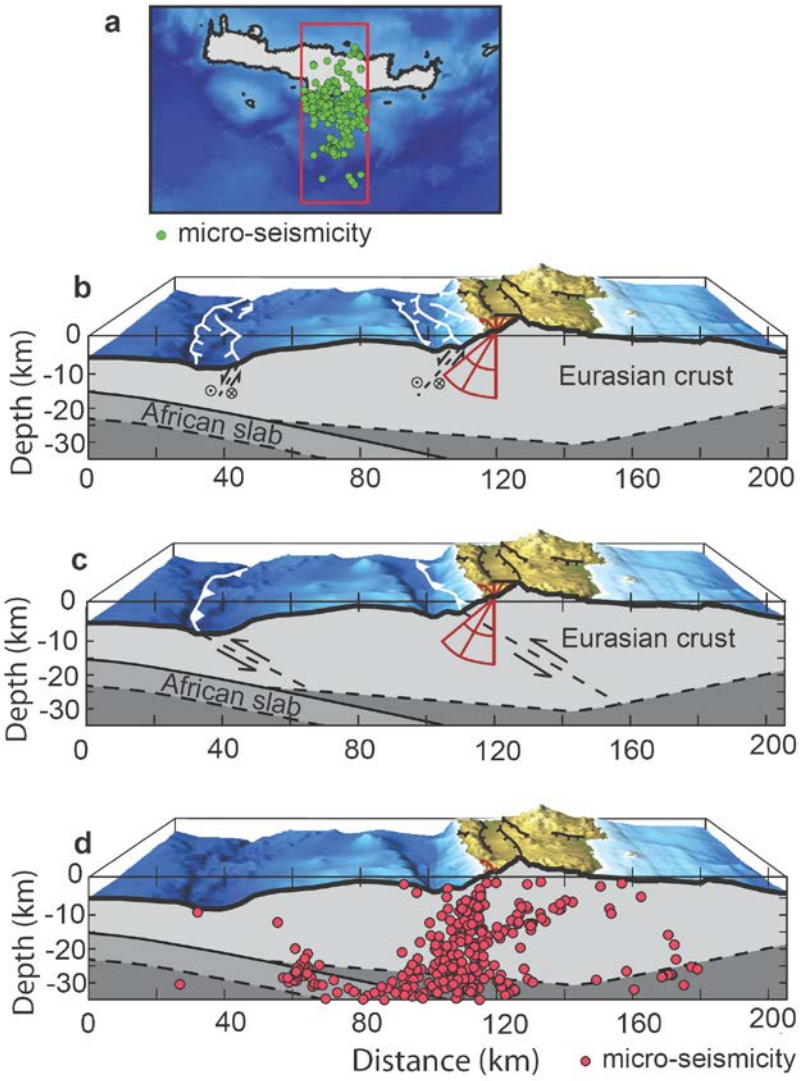

Figure 10. (a) Location (red box) of perspective views looking westward at digital topography (3 x vertical exaggeration) and crustal and upper mantle cross-sections (no vertical exaggeration) based on Meier *et al.* (2004) shown in b - c. (b) Shows the three-dimensional geometry of the South-Central Crete fault determined using probable and measured fault plane dip angles and fault aspect ratios with respect to the proposed orientation of a south-dipping extensional-to-transtensional Ptolemy fault. (c) South-Central Crete fault is the same as in (b), but the Ptolemy fault is shown as a 30° North dipping thrust fault. This scenario is geometrically impossible. (d) Mico-seismic hypocenters from Becker *et al.* 2006. Not the consistency with the pattern of seismicity and the geometry of the faults shown in (b).

minimum estimates for the depth of fault penetration into the crust because we utilize the surface length, as exposed on land, of the fault rather than the total strike length of the fault at depth in estimating its down-dip dimensions. From these considerations, we conclude that the South-central Crete fault likely extends to depths at or near the brittle-ductile transition. The South-central Crete fault is not a shallow superficial fault, but it is an important deep-seated structure that is in large part responsible for the rise of the Dikti Mountains.

Kinematics of the Ptolemy Fault

Researchers that support the thrust fault hypothesis suggest that the Ptolemy fault splays off the subduction interface, dips to the north at approximately 30°, and reaches the Earth's surface in the Ptolemy trench (Fig. 2b; 10c; Shaw & Jackson 2010). However, a fault of this geometry would intersect the active South-central Crete fault; a scenario that is geometrically impossible as both faults cannot be active at the same time (e.g. Scholz & Contreas, 1998). Instead, we favor a model whereby the fault that has generated the Ptolemy trough is synthetic to the South-central Crete fault (Fig. 10b). This fault geometry is consistent with the spatial pattern of micro-earthquakes beneath the south-central coast of Crete (Fig. 10c; Becker *et al*. 2006). Field mapping and the pattern of uplift along the Asteroussia coastline provide further evidence that the northern border fault of the Ptolemy trough is a south-dipping extensional structure.

The South-central Crete fault takes a sharp bend seaward as it extends offshore near the town of Tsoutsouros (Fig. 7c). Bends in fault systems are often interpreted as locations where previously isolated faults have linked (Cartwright *et al*. 1995). Swath topographic profiles from the Asterousia and Dikti Mountains contain low elevation sections that coincide spatially with this bend, indicating a localized slip deficit across the zone where previously isolated faults have linked (Fig. 9c;

Anders & Schlische 1994; Cartwright *et al*. 1995). We interpret these observations as evidence that the South-central Crete fault extends offshore west of Tsoutsouros and that it is linked with the segment of Ptolemy fault that forms the subaqueous range front of the Asterousia Mountains. Moreover, the more or less smooth westward decline in the late Quaternary marine terrace uplift pattern that is most easily explained if it is assumed the South-central Crete fault extend offshore into the Ptolemy trough (Fig. 9b).

Similar arguments can be extended to the Lentas fault, which we interpret as the onshore extension of the western-most segment of the Ptolemy fault (Fig. 3c, 9). It too is an active extensional fault with an average late Quaternary slip rate of ~0.20 mm yr^{-1}. In addition, the position of this fault corresponds to topographic minima along the Asteroussia Mountains (Fig. 9c). These findings support the hypothesis that the Lentas fault is a linked segment of the Ptolemy fault. An apparent smooth decline in the rate of marine terrace uplift from Lentas to the western end of the Asteroussia serve as additional evidence that the fault kinematics do not change as the fault extends offshore at Lentas (Figs. 9b, c). We suspect that stability-to-subsidence of the western most portions of the Asteroussia is the result of reaching the western tip-zone of the Ptolemy fault in combination with the increasingly important role that the next large fault to the north, the Southwestern Crete fault (e.g. Peterek & Schwarze 2004), plays with respect to the vertical motions of the Asteroussia horst (Fig. 3).

In sum, the geometric considerations of the active South-central Crete fault, field mapping and the pattern of uplift along the south-central Coastline of Crete are most consistent with a south-dipping extensional Ptolemy fault. This interpretation maintains that the Ptolemy trough is a graben or half-graben embedded in a rapidly uplift forearc, suggesting this bathymetric depression is the offshore equivalent of the onshore Messara Graben (Fig. 3).

Evaluating the Kinematics of the Hellenic Troughs

The results and discussion of the kinematics of Ptolemy trough fault presented above call into question the hypothesis that the Hellenic troughs are contractional structures. In lieu of these findings, we briefly reexamine the datasets used to support the competing hypotheses for the kinematics of the Hellenic troughs. The goal of this discussion is to reconcile the controversy over the kinematics of these faults in the context of the results presented in this study.

The primary body of evidence to support contractional faulting in the upper plate of the Hellenic subduction zone between Crete and the Mediterranean Ridge accretionary complex comes from earthquake focal mechanisms ≥ 4 M_w that have occurred from throughout the instrumental record (e.g. Taymaz *et al*. 1990; Jackson 1994; Papazachos 1996; Shaw & Jackson 2010). In the most recent of these investigations, this interpretation is supported by five focal mechanisms that have anomalously steep dips (~ 30°) relative to the angle of the subducting slab (Shaw & Jackson 2010). Four of the five earthquakes are sourced on the plate interface and the one that appears to be sources in the upper plate lies is within error of the subduction zone (see Fig. 7 of Shaw & Jackson 2010). Uncertainties in the dips of the best fit focal mechanisms are reported at $\pm$ 20°. Collectively, these uncertainties in depth and dip of earthquake focal mechanism indicate that these events may have been sourced on the subduction interface and not along faults embedded in the upper plate.

A local GPS network of four stations indicates ~ 1 mm yr^{-1} of convergence between the volcanic islands of Milos and Santorini and Crete (Shaw *et al*. 2008). This evidence is used, in part, to support a model where regions south of Crete are dominated by shortening. Conversely, more dense regional GPS networks in the Aegean indicate the upper plate is stretching on a regional scale (e.g. Le Pichon *et* al. 1995; McClusky *et al*. 2000; Reilinger *et al*. 2006) and no strain accumulation is observed in the vicinity of Crete (Reilinger *et al*. 2010). A possible explanation for these contrasting

datasets is that the small local network suffers from motion on creeping faults or deep-seated landslides, common on Crete and the Aegean. Moreover, the volcanic arc where two of these stations are located is active and observed to be inflating (e.g. Newman *et al*. 2012). Slip on local features or inflation of the Earth's surface above active magma bodies result in apparent convergence between GPS stations.

The Holocene paleo-shoreline marker in southwestern Crete up to nine meters above present-day sea level is often cited as evidence for the existence of historic great earthquakes (≥ 8 M_w) generated on large contractional faults within the upper plate of the Hellenic subduction zone (e.g. Pirazzoli, 1986; Pirazzoli *et al.* 1996; Drakos & Stiros, 2001; Shaw *et al.* 2008; Stiros 2010). This interpretation, however, hinges on the assumption that all of the observed uplift occurred coseismically in a single event in AD 365 (e.g. Shaw *et al*. 2008). Independent archeological (Price *et al*. 2002) and geochronologic (Wegmann *et* al. 2010) evidence from southwestern Crete illustrate that this paleo-shoreline marker was not uplifted in a single event, but was uplifted in multiple earthquake events throughout the Holocene. It is, thus, entirely plausible that multiple ruptures on extensional faults bounding the southwestern coast of Crete are responsible for this uplift Holocene shoreline.

Nearly every seismic reflection and bathymetric survey carried out between Crete and the Mediterranean Ridge accretionary complex interprets the forearc topography as the product of horst-and-graben and pull-apart structures (e.g. Ryan *et al*. 1982; Chaumillon & Mascle 1997; Mascle & Chaumillon 1998; Huguen *et al*. 2001; Le Pichon *et al*. 2002; Kopf *et al*. 2003; Kreemer & Chamont-Rooke 2004; Chamont-Rooke *et al*. 2005; Alves *et al*. 2007). This interpretation is echoed by micro-seismic surveys (Meier *et al*. 2004, 2007; Becker *et al*. 2006, 2010) that elucidate the geometry of the structures associated with the Hellenic troughs as dipping southward and find no evidence of

north dipping structures in the upper plate. Such interpretations are consistent with the geology observed on the forearc highs (e.g. Angelier *et al*. 1982; Stewart & Hancock 1988; Stewart 1993; Fassoulas 1999, 2001; ten Veen & Kleinspehn 2003; Peterek & Schwarze 2004; Caputo *et al*. 2006) and the findings presented in this study.

Some of the most compelling evidence related to the kinematics of the Hellenic trough faults comes from the borehole data collected at sites 127 and 128 of the DSDP – leg 13 (Fig. 1; Ryan *et al*. 1973). While the goal of the project was to drill through the supposed plate boundary, this expedition found no evidence of a subduction thrust. Initially, the results of the four boreholes were interpreted as interpreted as ambiguous (Hsü & Ryan 1973); however, it was soon realized that the data revealed a south-dipping fault plane and stratigraphy consistent with syn-depositional extension in the adjacent forearc basin (the Ionian tough; i.e. Ryan *et al*. 1982; Kastens 1991; Lallemant *et al*. 1994).

We find no compelling physical evidence to support the hypothesis that active thrust faults exists within the upper-crust in the Hellenic forearc north of the Mediterranean Ridge accretionary complex (Fig. 2b). Based on the result presented in this study, the numerous geophysical investigations conducted south of Crete that do not rely entirely on focal mechanisms that identify the Hellenic troughs as south dipping extensional-to-transtensional faults (Lallemant *et al*. 1994; Le Pichon *et al*. 1995; 2002; Chaumillon & Mascle 1997; Mascle & Chaumillon 1998; Gautier *et al*. 1999; Huguen *et al*. 2001; Faccenna *et al*. 2003; Kopf *et al*. 2003; Kreemer & Chamont-Rooke 2004; Chamont-Rooke *et al*. 2005; Makris & Yegorava 2006; Alves *et al*. 2007), and the findings from the DSDP sites 127 and 128 we interpret all of the Hellenic troughs as south-dipping extensional-to-transtensional structures embedded in the Hellenic forearc (Fig. 11). This interpretation leads to the conclusion that forearc basins between Crete and the Mediterranean Ridge accretionary complex

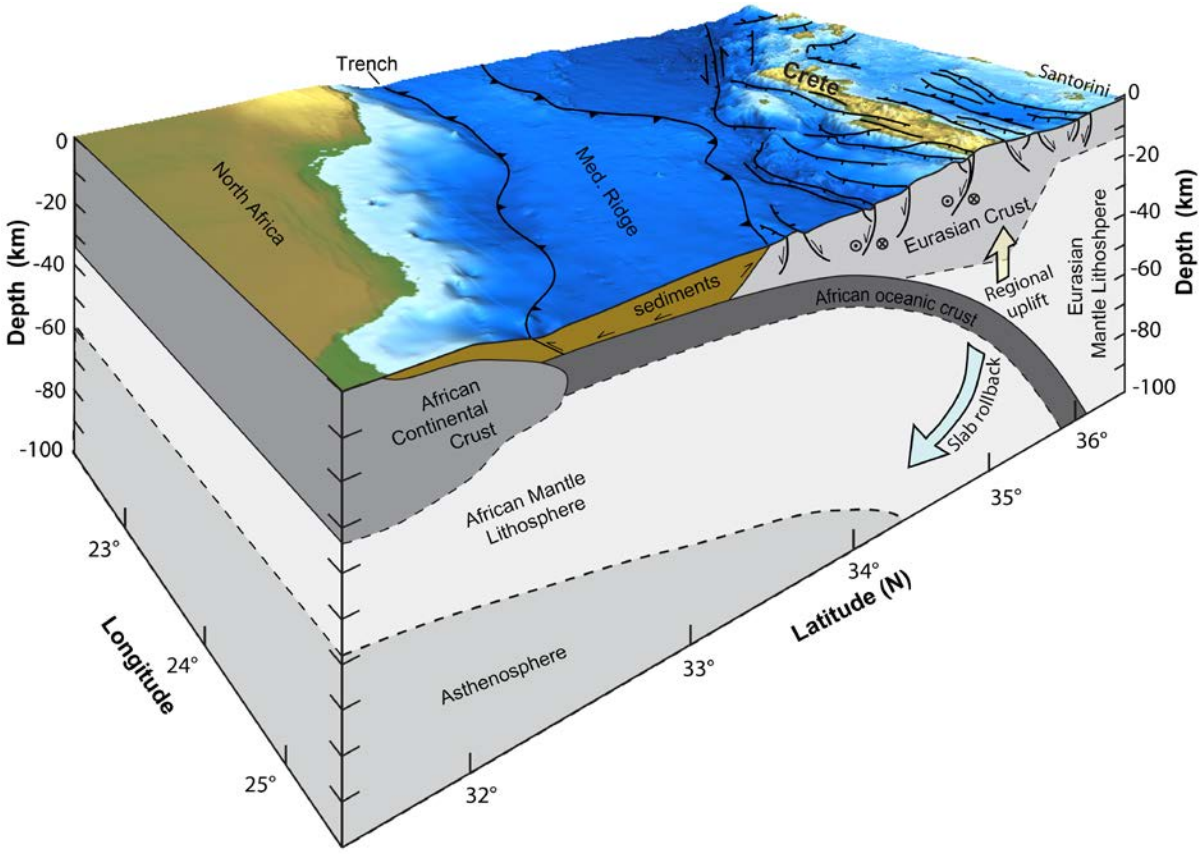

Figure 11. Northwest oriented perspective view of digital topography of the central Hellenic forearc and crustal and upper mantle cross-section (Modified after Meier *et al.* 2004). Based on the results of this study strain in the Hellenic Forearc likely vertically partitioned; convergence is accommodated at lower crustal levels by duplexing and/or ductile folding, which at least in part drives uplift at the Earth's surface (see text for details). Extension at upper crustal levels is driven by gravitational instability of a super critical coulomb wedge coupled with stretching of the overriding plate related to lithospheric processes related to slab roll back. This interpretation is consistent with figure 2a.

are graben or half-grabens and deformation in the upper-crust is the result of by pervasive stretching of the upper plate (Fig. 11).

Implications for Seismic Hazards

The historic and destructive seismicity that has occurred throughout the region is a testament to such hazards (e.g. Ambraseys 2009). The findings of this study are relevant to all who are interested in the seismic potential of faults in the Eastern Mediterranean and especially those on Crete. The extensional-to-transtensional model suggests that the faults associated with the Hellenic troughs have steeper dips and extend to shallower depths than those proposed by the thrust fault hypothesis. Thus, which hypothesis is correct has direct implications for size and maximum magnitude of earthquakes that could be generated on these faults (Fig. 2). The conclusion reached in this study is that the Ptolemy fault and all other faults of similar topographic expression in the Hellenic forearc are extensional-to-transtensional structures (Fig. 11). This interpretation implies that the seismic threats posed by this series of faults is nearly an order of magnitude less than suggested by the thrust fault hypothesis (e.g. Shaw *et al*. 2008; Shaw & Jackson 2010; Stiros 2010) from strictly a potential energy-release perspective.

The results from field investigation coupled with fault scaling properties allow us to determine the geometry and size of the South-central Crete fault. Using empirically derived fault size – earthquake magnitude scaling relationships (e.g. Wells and Coppersmith, 1994), we estimate that a single segment rupture of the South-central Crete fault will have moment magnitudes of M_w 5 to 6.5, while rupture of the entire fault system will produce an earthquake of M_w 7 to 7.5. These maximum estimates for the South-central Crete fault are likely applicable to the Hellenic trough faults, suggesting that the seismic hazards in the Eastern Mediterranean may be overestimated in

some studies. While our results suggest that the seismic threats posed by the Hellenic trough faults are exaggerated by some researchers, we emphasize that these fault still pose a significant threat to the Eastern Mediterranean.

Implications for Active Tectonics and Geodynamics

The results presented in this paper combine earlier efforts by other research groups with new data in demonstrating that the upper crust of the Hellenic forearc is dominated by extension-to-transtension (Fig. 2a; 12; Ryan *et al*. 1982; Anglier *et al*. 1982; Le Pichon *et al*. 1982; Lallemant *et al*. 1994; Huguen *et al*. 2001; Meier *et al*. 2004, 2007; Kreemer & Chamot-Rooke 2004; Chamont-Rooke *et al*. 2005; Becker *et al*. 2006; Meier *et al*. 2007; Wegmann 2008; Ring *et al.* 2010; Wegmann *et al*. 2010; Becker *et al*. 2010; van Hinsbergen & Schmid 2012; Wegmann *et al*. in review). A regional signal of uplift rapid enough to outpace upper-crustal extension has persisted since at least the Pliocene on Crete indicated by basins containing Neogene marine sediments 100's of meters above sea level (Meulenkamp *et al*. 1994; van Hinsbergen & Meulenkamp 2006; Zachariasse *et al.* 2008). The data presented in this paper illustrate that regional uplift of the southern coastline of central Crete continued during the Quaternary evidenced by marine terraces uplifted in the hanging walls and footwalls of active extensional faults (Fig. 9, 10).

With some simplifying assumptions, the marine terraces preserved in the hanging walls and footwalls of the Lentas and South-central Crete faults can be used to isolate the pace of regional uplift in the absence of localized upper-crustal extension during the late Quaternary. Assuming that the displacement across an active extensional fault is partitioned over geologic time into 80% hanging wall subsidence and 20% footwall uplift (e.g. Stein *et al.* 1998) the elevations of terraces offset by the Lentas and South-central Crete faults can be predicted in the absence of a regional

uplift signal. First, terrace elevations relative to sea level at time of terrace formation are determined utilizing the magnitude of terrace displacement across the fault (Fig. 12a, b). These values are then compared to the present-day elevation of the terraces in order to derive the regional rates of late Quaternary uplift (Fig. 12a-c).

Using the same approach for the Lentas fault from offset MIS 4/5 to 5e terraces, we again find that the regional rate of uplift has increased from 0.65 to 0.8 mm yr^{-1} for the interval between ~72 kyr to 123 kyr (Fig. 12d). Importantly, the average regional uplift rates calculated since the MIS 5e highstand are statistically the same at both sites indicating that our results are repeatable. Taken together, the results from the South-central Crete and Lentas faults imply that increasing rates of late Quaternary uplift along the south-central coast of Crete is primarily a response to increased secular uplift, rather than the escalation of fault slip rates.

Two end-member models can be called upon to explain rapid and sustained uplift that outpaces upper-crustal extension in the Hellenic forearc. In the first model strain is vertically partitioned in the overriding plate of the Hellenic subduction zone (Fig. 11; Le Pinchon & Angelier 1981, Le Pinchon *et al*. 1982; Angelier *et al*. 1982). Lower crustal levels accommodate convergence between Africa and Eurasia via the addition of material by duplexing, or ductile folding that inflates the subduction wedge, while the upper crust is in a state of widespread extension driven by gravitational instability and lithospheric processes related to slab rollback (Fig. 11; Angelier *et al*. 1982; Platt 1986; Thompson *et al*. 1998; Ring *et al.* 2010). The alternative hypothesis is that the Eurasian asthenospheric wedge propagates southward instep with the backward rolling African oceanic lithosphere. The encroachment of the asthenospheric wedge beneath Crete induces surface uplift via dynamic topography. Stretching of the upper plate in this model is almost entirely driven by southward retreat of the upper plate (Fig. 13). These models are not mutually exclusive

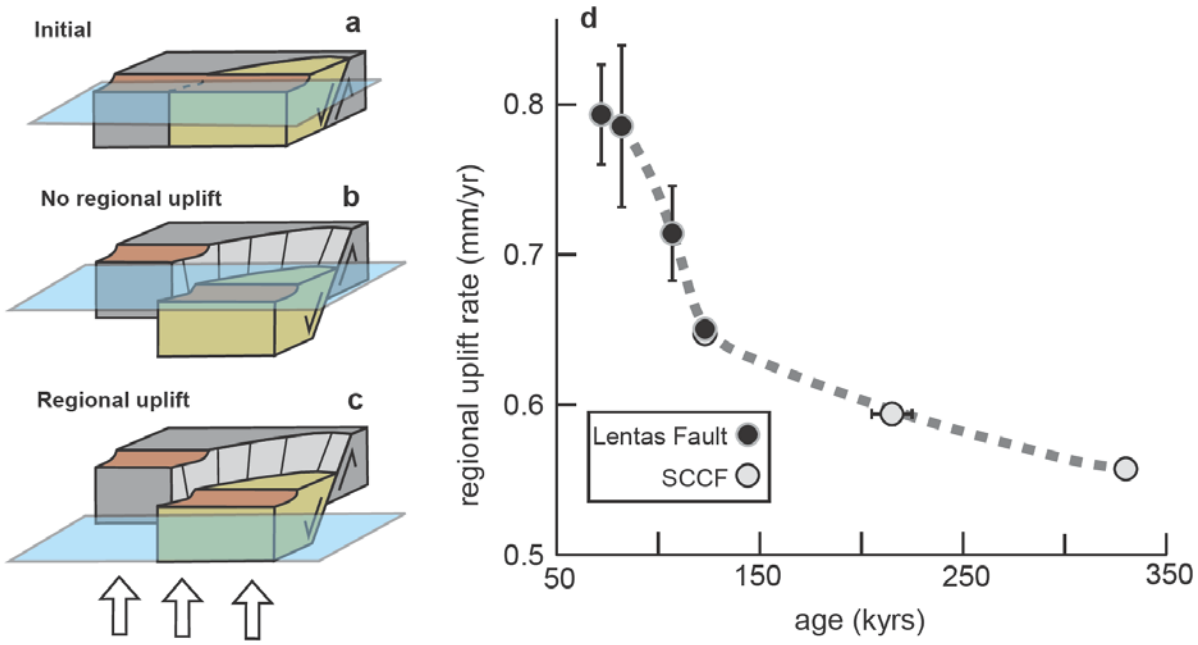

Figure 12. Schematic illustration of a marine terrace offset by an extensional fault. (a) Terrace is initially cut across the fault. (b) Multiple fault ruptures separate terraces. Terrace uplift in the footwall is ~ 20% of fault displacement and terrace subsidence is ~ 80% of fault displacement in the hanging wall. (c) Regional uplift raises both foot-and-hanging walls above sea level. Plot above shows the results of this analysis applied to the Lentas and South-Central Crete faults and reveals an increasing rate of regional uplift over the late Quaternary. This signal of uplift is interpreted as the result of deep underplating along the subduction interface or dynamic topography due to the encroaching Eurasian asthenospheric wedge or both.

and are likely working in concert to contribute to surface uplift of Crete and other Hellenic forearc highs.

We have documented that the rates of regional uplift for the past 400 kyr, despite localized upper-crustal extensional faulting, are unsteadily increasing through time (Fig. 12d), and this uplift is not isolated only to the Asterousia and Dikti Mountain fronts, but also to the west along the coastline of southwestern Crete (Wegmann 2008; Strasser *et al.* 2011). We interpret this finding in the context of regional considerations affecting at least the entire southern coastline of Crete. The amount of convergence between the African and Eurasian plates and the subduction velocity have remained approximately steady since the Eocene (e.g. Faccenna *et al.* 2003; Jolivet & Brun 2010; Ring *et al.* 2010); and therefore, changes in tectonic or subduction velocities are unlikely candidates to drive increases in uplift rates. Rather, we envision that the increasing rate of late Quaternary uplift observed from southern Crete is a reflection of changes in the horizontal position of the island relative to the southward propagating Hellenic orogenic wave (Fig. 13). The kinematics of deformation will vary with respect to the rates of vertical motions for different positions along the orogenic wedge (Fig. 13). In our conceptual framework, a parcel of material moving through the wedge will experience increasing rates of uplift due to underplating and dynamic topography before reaching the crest, or kinematic boundary of the orogenic system (Fig. 13). Crete is envisioned as such a "parcel", that we exploit to track vertical material velocities as it moves horizontally through the orogen. Today, the island of Crete spans the approximate apex of the orogenic system, with the Lefka Ori, Psiloritis, and Dikti Mountains defining the crest of the orogenic wave and demarcating the boundary between orogenic accretion to the south and excretion to the north (Fig. 13b).

Figure 13. Conceptual model of the geodynamic evolution of the Hellenic Subduction Zone in the late Cenozoic. Crete is envisioned as a parcel of material passing through a southward migrating orogenic wave. (a) In the past (~ 5 Ma) modern-day Crete occupied a position inboard of the apex of the orogen allowing the filling of the Messara graben and other adjacent forearc basins to fill with Neogene age turbidites. (b) Crete was subsequently uplifted as the orogenic wave propagated southward and former topographic highs were laterally extended and excreted to the north into the Aegean Sea. (c) In the future(~ 5 Ma) the Asteroussia Mountains (A) and Ptolemy Trough will occupy similar topographic positions to the modern day Psilorities (P) Mountains and Messara Graben (MG), respectively, that will be extended and excreted out of the orogen. This model is based on tectonic reconstructions that show the subduction zone as a southward migrating "orogenic wave" and provides the framework from which to explain the increasing rates of regional uplift over the late Quaternary when tectonic rates of convergence and subduction have remained approximately constant.

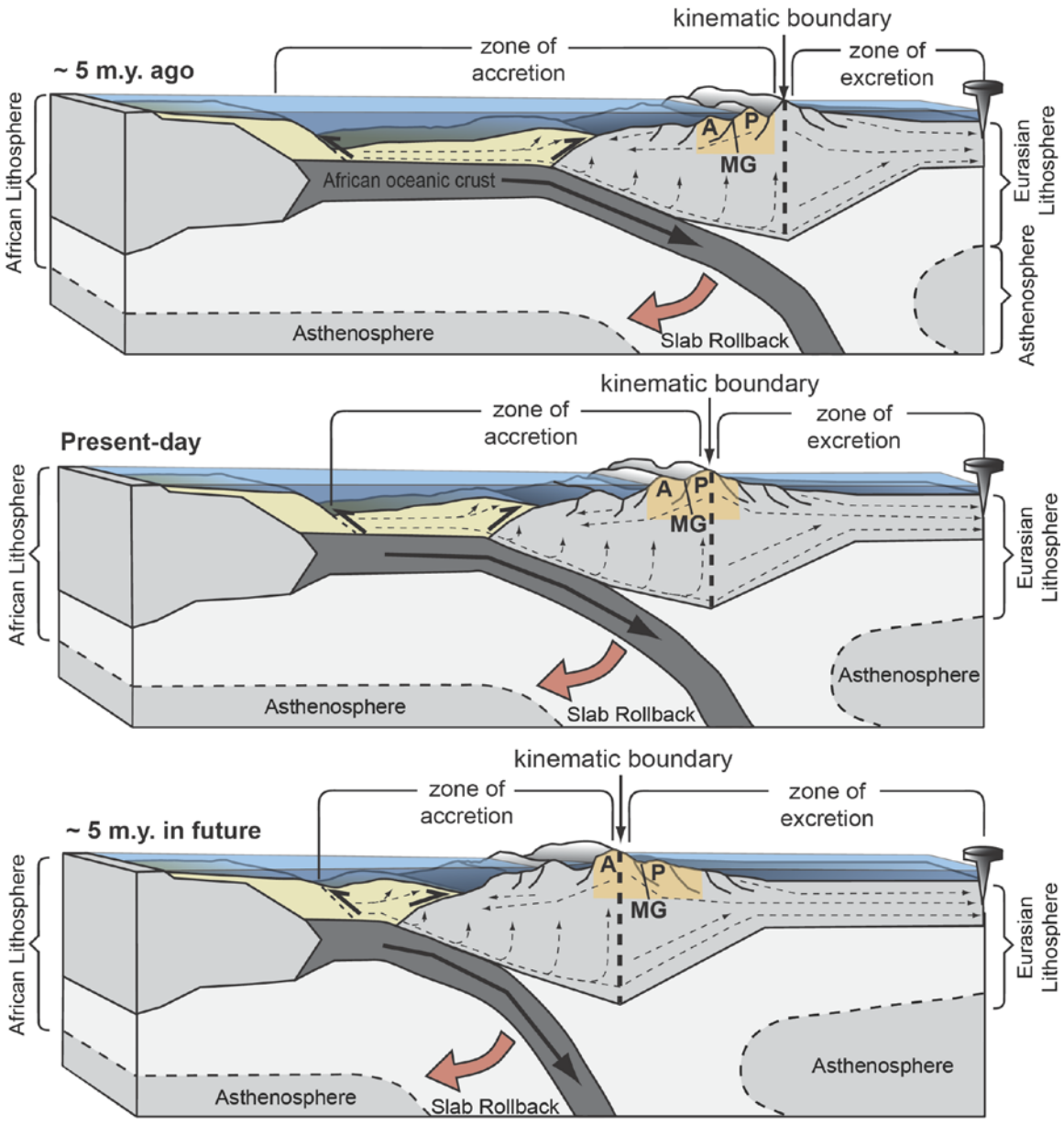
~ 5 m.y. ago
kinematic boundary
zone of accretion
zone of excretion
African Lithosphere
African oceanic crust
A
P
MG
Eurasian Lithosphere
Asthenosphere
Asthenosphere
Slab Rollback
Present-day
kinematic boundary
zone of accretion
zone of excretion
African Lithosphere
A
P
MG
Eurasian Lithosphere
Asthenosphere
Asthenosphere
Slab Rollback
~ 5 m.y. in future
kinematic boundary
zone of accretion
zone of excretion
African Lithosphere
A
P
MG
Eurasian Lithosphere
Asthenosphere
Asthenosphere
Slab Rollback

The view of the Hellenic orogenic system presented here implies that present day Crete probably occupied a subaqueous position in the past, while topographic highs to the north existed that fed sediment into the actively subsiding extensional basins, such as the Messara graben (Fig. 13a). For a modern analogue to this scenario one simply needs to look ~ 20 to 30 km south of Crete. The islands of Gavdos, Chrysi, and Koyfonisi will become the highest peaks in a large subaerial mountain range in the future, while the southwest Cretan and Ptolemy toughs will become elevated forearc basins, like the Messara graben is today. The present subaerial topography of Crete will be excreted (tectonically denuded) to the north, as it transitions to attenuated subaqueous continental crust underlying the southward expanding Aegean Sea (Fig. 13c).

Our geodynamic model not only provides a simple explanation for the temporal evolution of Cretan topography, it also explains the macromorphology of the island. The north-south oriented topographic profile of Crete is often argued to resemble that of a back-tilted fault block above a thrust fault and is commonly used as evidence in support of the existence of thrust faulting in the Ptolemy and south-west Crete troughs (Muelenkamp *et al*. 1988, 1994; Shaw & Jackson 2010). The model presented here indicates that the topographic profile of Crete is rather a reflection of the contemporary position of the island spanning the crest, or kinematic boundary of the Hellenic orogenic wave. The south coast is currently enjoying relatively rapid uplift due to material underplating while the north coast is probably subsiding due to deceased rates of material accretion and an increased influence of lithospheric stretching related to slab rollback.

Conclusions

The results from this study of the tectonic geomorphology and structural geology of the south-central coastline of Crete are contradictory with the hypotheses of a north-dipping thrust in

the Ptolemy tough, but are consistent with a south-dipping extensional-to-transtensional fault in this location. An active South-central Crete fault is physically incompatible with an active north dipping thrust 10 km to the south (Fig. 10). Numerous extensional faults extend offshore, suggesting linkage with subaqueous fault segments of the Ptolemy fault. The pattern of uplift along the south-central coastline does not contain abrupt changes that would indicate a switch in fault kinematics offshore (Fig. 10). These findings illustrate that the Ptolemy trough is an extensional forearc basin, analogous to its northern onshore neighbor, the Messara graben. The arguments used to illustrate that the Ptolemy fault is not contractional can be applied to the Southwestern Crete fault to the west and north, suggesting it too is an extensional-to-transtensional fault. This interpretation is consistent with numerous studies that identify all of the Hellenic trough faults as extensional-to-transtensional structures (Ryan *et al*. 1982; Lallemant *et al*. 1994; Chaumillon & Mascle 1997; Mascle & Chaumillon 1998; Gautier *et al*. 1999; Bohnhoff *et al*. 2001; Huguen *et al*. 2001; Jolivet, 2001; Kopf *et al*. 2003; Chamont-Rooke *et al*. 2005; Le Pichon *et al.* 2002; Kreemer & Chamont-Rooke 2004; Meier *et al*. 2004, 2007; Becker *et al*. 2006, 2010; Makris & Yegorava 2006; Alves *et al*. 2007; Jolivet *et al*. 2010, 2012; Ring *et al*. 2010; Wegmann *et al*. 2010; Mourtzas 2012b; Wegmann *et al*. in review).

The findings presented here call into question the validity of the interpretation that the Hellenic trough faults accommodate shortening on north-dipping thrusts (Taymaz *et al*. 1990; Jackson 1994; Meulenkamp *et al*. 1988, 1994; Papazachos 1996; Benetatos *et al*. 2004; Nyst & Thatcher 2004; Shaw *et al*. 2008; Shaw & Jackson 2010). Uncertainties associated with the depth and dip angles of earthquake focal mechanisms south of Crete limit the strength of interpretations drawn from such datasets. Moreover, GPS monument convergence can be caused by local movement of faults and Price *et al*. (2002) and Wegmann *et al*. (in review) have shown that

coseismic uplift of Holocene geomorphic markers in southwestern Crete likely occurred during multiple events, rather than a single anomalously large fault rupture. A thrust fault offshore of south-western Crete is thus not required to coseismically raise this Holocene shoreline to its present elevation of 9 m above present sea level.

These results have important implications for seismic hazards in the region. First, the South-central Crete fault was previously not identified as active. Evidence presented here shows unambiguously that it is. It is situated just north and west of one of Crete's largest population centers, Ierapetra. As such, civil and hazard planners in Crete must be aware of and prepare for seismicity associated with the South-central Crete fault. Second, as discussed above, the seismic potential of the extension-to-transtensional faults associated with the Hellenic troughs is expected to be nearly an order of magnitude less than what is proposed by researchers who favor the thrust fault hypothesis. We emphasize that the Hellenic trough faults do still pose a significant threat to the Eastern Mediterranean, as evidenced by the historic and destructive seismicity that has occurred throughout the region (e.g. Ambraseys 2009).

Finally, our findings have broad implications for the active tectonics and geodynamics of the Hellenic subduction zone. In the absence of thrust faulting in the shallow crust (< 20 km) north of the Mediterranean Ridge accretionary complex the Hellenic forearc is simultaneously uplifting and extending, indicating that strain is vertically partitioned in the subduction wedge. Rates of this background region uplift are about 0.6 mm yr^{-1} and are probably driven by deep underplating in the subduction wedge (Angelier *et al*. 1982) coupled with dynamic topography associated with the Eurasian asthenospheric wedge encroaching beneath Crete. Active extensional faulting in the upper crust of this portion of the forearc is likely caused by the coupled response to an over-thickened and gravitationally unstable coulomb-style subduction wedge and stretching of the overriding plate

caused by lithospheric processes related to the southerly rollback of the African slab. Increasing regional rates of uplift observed for the southern coastlines of Crete cannot be explained by changes in the rates of tectonic convergence or subduction. Increasing vertical rock uplift velocity is best explained in the framework of a southward migrating orogenic wave in which vertical motions vary with position in the orogenic system. As such we envision Crete as a parcel of material fluxing through the orogenic wave, where it currently occupies a position near the crest of the orogenic wave that demarcates a southern zone of accretions from a northern zone of excretion. This conceptual framework can explain the patterns of late Quaternary uplift throughout the island of Crete as well as its macro-geomorphic expression in cross section.

Acknowledgments

Acknowledgment is made to the Donors of the American Chemical Society Petroleum Research Fund for primary support of this research under grant #50792-DNR8. Additional support was provided by the National Science Foundation Continental Dynamics program awards #0208652 and #0207980, and a 2010 Geological Society of America Graduate Student Research Grant to Gallen. We would like to thank Dirk Becker and Thomas Meier for generously sharing their micro-seismic data that allowed us to construct Figure 10d. We would also like to thank the Institute of Geology & Mineral Exploration in Greece for granting us permission to carry out field work on Crete.

References

Alves, T., Lykousis, V., Sakellariou, D., Alexandri, S. & Nomikou, P., 2007. Constraining the origin and evolution of confined turbidite systems: southern Cretan margin, Eastern Mediterranean Sea (34°30–36°N), *Geo-Mar. Lett.,* **27,** 41-61.

Ambraseys, N., 2009. *Earthquakes in the Mediterranean and Middle East: a multidisciplinary study of seismicity up to 1900,* Cambridge University Press, Cambridge, UK.

Anders, M.H. & Schlische, R.W., 1994. Overlapping faults, intrabasin highs, and the growth of normal faults, *J. Geol.,* **102,** 165.

Angelier, J., 1978. Tectonic evolution of the Hellenic arc since the late Miocene, *Tectonophysics,* **49,** 23-36.

Angelier, J., 1979. Recent quaternary tectonics in the Hellenic arc; examples of geological observations on land; recent crustal movements, *Tectonophysics,* **52,** 267-275.

Angelier, J., Lybéris, N., Pichon, X.L., Barrier, E. & Huchon, P., 1982. The tectonic development of the Hellenic arc and the sea of Crete: A synthesis *Tectonophysics,* **86,** 159-196.

Armijo, R., Lyon-Caen, H. & Papanastassiou, D., 1992. East-west extension and Holocene normal-fault scarps in the Hellenic arc, *Geology,* **20,** 491-494, doi:10.1130/0091-7613(1992)020<0491:eweahn>2.3.co;2.

Aubouin, J., Bonneau, M., Davidson, J., Leboulenger, P., Matesco, S. & Zambetakis, A., 1976. Esquisse structurale de l'Arc egeen externe; des Dinarides aux Taurides. Structural section of the outer Aegean Arc, from the Dinaric Alps to the Taurus Mountains, *B. Soc. Geol. Fr.,* **108,** 327-336.

Becker, D., Meier, T., Bohnhoff, M. & Harjes, H.P., 2010. Seismicity at the convergent plate boundary offshore Crete, Greece, observed by an amphibian network, *J. Seismol.,* **14,** 369-392, doi:10.1007/s10950-009-9170-2.

Becker, D., Meier, T., Rische, M., Bohnhoff, M. & Harjes, H.-P., 2006. Spatio-temporal microseismicity clustering in the Cretan region, *Tectonophysics,* **423,** 3-16.

Benedicto, A., Schultz, R.A. & Soliva, R., 2003. Layer thickness and the shape of faults, *Geophys. Res. Lett.,* **30,** 2076, doi:10.1029/2003gl018237.

Benetatos, C., Kiratzi, A., Papazachos, C. & Karakaisis, G., 2004. Focal mechanisms of shallow and intermediate depth earthquakes along the Hellenic Arc, *J. Geodyn.,* **37**(2)**,** 253-296.

Bergen, K.J. & Shaw, J.H., 2010. Displacement profiles and displacement-length scaling relationships of thrust faults constrained by seismic-reflection data, *Geol. Soc. Am. Bull.,* **122**(7-8)**,** 1209-1219, doi. 10.1130/b26373.1.

Bizon, G., Bonneau, M., Leboulenger, P., Matesco, S. & Thiébault, F., 1976. Sur la signification et l'extension des "massifs cristallins externes" en Péloponnèse méridional et dans l'Arc égéen, *B. Soc. Geol. Fr.,* **18**, 337-345.

Bohnhoff, M., Harjes, H.-P. & Meier, T., 2005. Deformation and stress regimes in the Hellenic subduction zone from focal Mechanisms, *J. Seismol.,* **9,** 341-366.

Bohnhoff, M., Makris, J., Papanikolaou, D. & Stavrakakis, G., 2001. Crustal investigation of the Hellenic subduction zone using wide aperture seismic data, *Tectonophysics,* **343,** 239-262.

Bonneau, M., 1976. Esquisse structurale de la Crète alpine, *B. Soc. Geol. Fr.,* **18**, 351-353.

Bonneau, M., 1984. Correlation of the Hellenide nappes in the south-east Aegean and their tectonic reconstruction, *Geological Society, London, Special Publications,* **17,** 517-527, doi:10.1144/gsl.sp.1984.017.01.38.

Burbank, D.W. & Anderson, R.S., 2011. *Tectonic geomorphology,* 2nd edn, Wiley-Blackwell, Hoboken, NJ, USA.

Caputo, R., Monaco, C. & Tortorici, L., 2006. Multiseismic cycle deformation rates from Holocene normal fault scarps on Crete (Greece), *Terra Nova,* **18**, 181-190.

Cartwright, J.A., Trudgill, B.D. & Mansfield, C.S., 1995. Fault growth by segment linkage: an explanation for scatter in maximum displacement and trace length data from the Canyonlands Grabens of SE Utah, *J. Struct. Geol.,* **17**(9)**,** 1319-1326.

Chamot-Rooke, N., Rangin, C., Le Pichon, X. & group, D.w., 2005. DOTMED: Deep Offshore Tectonics of the Mediterranean, *Les Mémoires de la Société Géologique de France,* **177**, 64.

Chaumillon, E. & Mascle, J., 1997. From foreland to forearc domains: New multichannel seismic reflection survey of the Mediterranean ridge accretionary complex (Eastern Mediterranean), *Mar. Geol.,* **138,** 237-259.

Cowie, P.A. & Scholz, C.H., 1992. Displacement-length scaling relationship for faults: data synthesis and discussion, *J. Struct. Geol.,* **14,** 1149-1156.

Cowie, P.A. & Scholz, C.H., 1992. Physical explanation for the displacement-length relationship of faults using a post-yield fracture mechanics model, *J. Struct. Geol.,* **14,** 1133-1148.

Davis, K., Burbank, D.W., Fisher, D., Wallace, S. & Nobes, D., 2005. Thrust-fault growth and segment linkage in the active Ostler fault zone, New Zealand, *J. Struct. Geol.,* **27,** 1528-1546.

Dawers, N.H. & Anders, M.H., 1995. Displacement-length scaling and fault linkage, *J. Struct. Geol.,* **17,** 607-614.

Dawers, N.H., Anders, M.H. & Scholz, C.H., 1993. Growth of normal faults: Displacement-length scaling, *Geology,* **21,** 1107-1110, doi:10.1130/0091-7613(1993)021<1107:gonfdl>2.3.co;2.

Di Luccio, F. & Pasyanos, M.E., 2007. Crustal and upper-mantle structure in the Eastern Mediterranean from the analysis of surface wave dispersion curves, *Geophys. J. Int.,* **169,** 1139-1152, doi:10.1111/j.1365-246X.2007.03332.x.

Doutsos, T. & Kokkalas, S., 2001. Stress and deformation patterns in the Aegean region, *J. Struct. Geol.,* **23,** 455-472.

Drakos, A. & Stiros, S.C., 2001. The A.D. 365 earthquake. From legend to modeling, *Bulletin of the Geological Society of Greece,* **XXXIV,** 1417-1424.

Engdahl, E.R., van der Hilst, R. & Buland, R., 1998. Global teleseismic earthquake relocation with improved travel times and procedures for depth determination, *B. Seismol. Soc. Am.,* **88,** 722-743.

England, P. & Molnar, P., 1990. Surface uplift, uplift of rocks, and exhumation of rocks, *Geology,* **18,** 1173-1177, doi:10.1130/0091-7613(1990)018<1173:suuora>2.3.co;2.

Faccenna, C., Jolivet, L., Piromallo, C. & Morelli, A., 2003. Subduction and the depth of convection in the Mediterranean mantle, *J. Geophys. Res.,* **108,** 2099, doi:10.1029/2001jb001690.

Fassoulas, C., 1999. The structural evolution of central Crete: insight into the tectonic evolution of the south Aegean (Greece), *J. Geodyn.,* **27,** 23-43.

Fassoulas, C., 2001. The tectonic development of a Neogene basin at the leading edge of the active European margin: the Heraklion basin, Crete, Greece, *J. Geodyn.,* **31**(1)**,** 49-70.

Fassoulas, C., Kilias, A., Mountrakis, D., 1994. Postnappe stacking extension and exhumation of high-pressure/low-temperature rocks in the Island of Crete, Greece, *Tectonics,* **13**(1)**,** 125-138.

Ferranti, L., Antonioli, F., Mauz, B., Amorosi, A., Dai Pra, G., Mastronuzzi, G., Monaco, C., Orrù, P., Pappalardo, M., Radtke, U., Renda, P., Romano, P., Sansò, P. & Verrubbi, V., 2006. Markers of the last interglacial sea-level high stand along the coast of Italy: Tectonic implications, *Quatern. Int.,* **145-146,** 30-54.

Flemming, N.C., 1978. Holocene Eustatic Changes and Coastal Tectonics in the Northeast Mediterranean: Implications for Models of Crustal Consumption, *Philos. T. R. Soc. Lond. Series A, Mathematical and Physical Sciences,* **289,** 405-458.

Fuller, C.W., Willett, S.D. & Brandon, M.T., 2006. Formation of forearc basins and their influence on subduction zone earthquakes, *Geology,* **34,** 65-68., doi: 0.1130/G21828.1.

Gaki-Papanastassiou, K., Karymbalis, E., Papanastassiou, D. & Maroukian, H., 2009. Quaternary marine terraces as indicators of neotectonic activity of the Ierapetra normal fault SE Crete (Greece), *Geomorphology,* **104,** 38-46.

Gautier, P., Brun, J.-P., Moriceau, R., Sokoutis, D., Martinod, J. & Jolivet, L., 1999. Timing, kinematics and cause of Aegean extension: a scenario based on a comparison with simple analogue experiments, *Tectonophysics,* **315,** 31-72.

Gudmundsson, O. & Sambridge, M., 1998. A regionalized upper mantle (RUM) seismic model, *J. Geophys. Res.,* **103,** 7121-7136.

Gupta, A. & Scholz, C.H., 2000. A model of normal fault interaction based on observations and theory, *J. Struct. Geol.,* **22,** 865-879.

Hall, R., Audley-Charles, M.G. & Carter, D.L., 1984. The significance of Crete for the evolution of the eastern Mediterranean; Geological Society Special Publications, vol.17, pp.499-517, 1984. *in The geological evolution of the eastern Mediterranean*, pp. 499-517, ed Dixon, J.E.R., Robertson, A.H.F., Geological Society of London, London, UK.

Hetzel, R., Tao, M., Niedermann, S., Strecker, M.R., Ivy-Ochs, S., Kubik, P.W. & Gao, B., 2004. Implications of the fault scaling law for the growth of topography: mountain ranges in the broken foreland of north-east Tibet, *Terra Nova,* **16,** 157-162, doi. 10.1111/j.1365-3121.2004.00549.x.

Hsü, K.J. & Ryan, W.B.F., 1973. Initial reports of the Deep Sea Ocean Drilling Project: Summary of the evidence for extensional and compressional tectonics in the Mediterranean, pp. 1011-1019 Government Printing Office, Washignton, D.C.

Huguen, C., Mascle, J., Chaumillon, E., Woodside, J.M., Benkhelil, J., Kopf, A. & Volkonskaïa, A., 2001. Deformational styles of the eastern Mediterranean Ridge and surroundings from combined swath mapping and seismic reflection profiling, *Tectonophysics,* **343,** 21-47.

Husson, L., 2006. Dynamic topography above retreating subduction zones, *Geology,* **34,** 741-744, doi:10.1130/g22436.1.

Jackson, J., 1994. Active Tectonics of the Aegean Region, *Ann. Rev. Earth planet Sci.,* **22,** 239-271, doi:doi:10.1146/annurev.ea.22.050194.001323.

Jackson, J. & McKenzie, D., 1983. The geometrical evolution of normal fault systems, *J. Struct. Geol.,* **5,** 471-482.

Jolivet, L., 2001. A comparison of geodetic and finite strain pattern in the Aegean, geodynamic implications, *Earth planet. Sci. Lett.,* **187,** 95-104.

Jolivet, L. & Brun, J.P., 2010. Cenozoic geodynamic evolution of the Aegean, *Int. J. Earth Sci.,* **99,** 109-138, doi:10.1007/s00531-008-0366-4.

Jolivet, L., Faccenna, C., Huet, B., Labrousse, L., Le Pourhiet, L., Lacombe, O., Lecomte, E., Burov, E., Denele, Y., Brun, J.-P., Philippon, M., Paul, A., Salaun, G., Karabulut, H., Piromallo, C., Monie, P., Gueydan, F., Okay, A.I., Oberhansli, R., Pourteau, A., Augier, R., Gadenne, L. & Driussi, O., *in press,* 2012. Aegean tectonics: Strain localisation, slab tearing and trench retreat, *Tectonophysics*.

Jolivet, L.G., B; Monie, P; Truffert-Luxey, C; Patriat, M; Bonneau, M, 1996. Miocene detachment in Crete and exhumation P-T-t paths of high-pressure metamorphic rocks, *Tectonics,* **15,** 1129-1153.

Kahle, H.G., Cocard, M., Peter, Y., Geiger, A., Reilinger, R., Barka, A. & Veis, G., 2000. GPS-derived strain rate field within the boundary zones of the Eurasian, African, and Arabian Plates, *J. Geophys. Res.,* **105,** 23353-23370, doi:10.1029/2000jb900238.

Kastens, K.A., 1991. Rate of outward growth of the Mediterranean ridge accretionary complex, *Tectonophysics,* **199,** 25-50.

Kastens, K.A., Breen, N.A. & Cita, M.B., 1992. Progressive deformation of an evaporite-bearing accretionary complex: SeaMARC I, SeaBeam and piston-core observations from the Mediterranean Ridge, *Mar. Geophys. Res.,* **14,** 249-298, doi:10.1007/bf01203620.

Knapmeyer, M., 1999. Geometry of the Aegean Benioff Zone, *Annali di Geofisica,* **42**(1)**,** 27-38.

Kokkalas, S. & Doutsos, T., 2001. Strain-dependent stress field and plate motions in the south-east Aegean region, *J. Geodyn.,* **32,** 311-332.

Kontogianni, V.A., Tsoulos, N. & Stiros, S.C., 2002. Coastal uplift, earthquakes and active faulting of Rhodes Island (Aegean Arc): modeling based on geodetic inversion, *Mar. Geol.,* **186,** 299-317.

Kopf, A., Mascle, J. & Klaeschen, D., 2003. The Mediterranean Ridge: A mass balance across the fastest growing accretionary complex on Earth, *J. Geophys. Res.,* **108,** 2372, doi:10.1029/2001jb000473.

Kounov, A., Seward, D., Bernoulli, D., Burg, J.P. & Ivanov, Z., 2004. Thermotectonic evolution of an extensional dome: the Cenozoic Osogovo–Lisets core complex (Kraishte zone, western Bulgaria), *Int. J. Earth Sci.,* **93,** 1008-1024, doi:10.1007/s00531-004-0435-2.

Krahl, J., Kauffmann, G., Kozur, H., Richter, D., Förster, O. & Heinritzi, F., 1983. Neue Daten zur Biostratigraphie und zur tektonischen Lagerung der Phyllit-Gruppe und der Trypali-Gruppe auf der Insel Kreta (Griechenland), *Geol. Rundsch.,* **72,** 1147-1166, doi:10.1007/bf01848358.

Kreemer, C. & Chamot-Rooke, N., 2004. Contemporary kinematics of the southern Aegean and the Mediterranean Ridge, *Geophys. J. Int.,* **157,** 1377-1392, doi:10.1111/j.1365-246X.2004.02270.x.

Laigle, M., Hirn, A., Sachpazi, M. & Clément, C., 2002. Seismic coupling and structure of the Hellenic subduction zone in the Ionian Islands region, *Earth planet. Sci. Lett.,* **200,** 243-253.

Laigle, M., Sachpazi, M. & Hirn, A., 2004. Variation of seismic coupling with slab detachment and upper plate structure along the western Hellenic subduction zone, *Tectonophysics,* **391,** 85-95.

Lajoie, K.R., 1986. Coastal tectonics. *in Active Tectonics*, pp. 95-124, ed. Wallace, R. National Academy Press, Studies in Geophysics Series, Geophysics Research Forum, Washington, D.C.

Lallemant, S., Truffert, C., Jolivet, L., Henry, P., Chamot-Rooke, N. & de Voogd, B., 1994. Spatial transition from compression to extension in the Western Mediterranean Ridge accretionary complex, *Tectonophysics,* **234**, 33-52.

Lambeck, K., Antonioli, F., Purcell, A. & Silenzi, S., 2004. Sea-level change along the Italian coast for the past 10,000 yr, *Quatern.Sci. Rev.,* **23,** 1567-1598.

Lambeck, K. & Chappell, J., 2001. Sea Level Change Through the Last Glacial Cycle, *Science,* **292,** 679-686, doi:10.1126/science.1059549.

Le Pichon, X. & Angelier, J., 1981. The Aegean Sea, *Philos. T. R. Soc. Lond.,* **300**, 357-372.

Le Pichon, X., Angelier, J., Aubouin, J., Lyberis, N., Monti, S., Renard, V., Got, H., Hsü, K., Mart, Y., Mascle, J., Matthews, D., Mitropoulos, D., Tsoflias, P. & Chronis, G., 1979. From subduction to transform motion: a seabeam survey of the Hellenic trench system, *Earth planet. Sci. Lett.,* **44,** 441-450.

Le Pichon, X., Chamot-Rooke, N., Lallemant, S., Noomen, R. & Veis, G., 1995. Geodetic determination of the kinematics of central Greece with respect to Europe: Implications for eastern Mediterranean tectonics, *J. Geophys. Res.,* **100,** 12675-12690, doi:10.1029/95jb03170.

Le Pichon, X., Lallemant, S.J., Chamot-Rooke, N., Lemeur, D. & Pascal, G., 2002. The Mediterranean Ridge backstop and the Hellenic nappes, *Mar. Geol.,* **186,** 111-125.

Le Pichon, X., Lybéris, N., Angelier, J. & Renard, V., 1982. Strain distribution over the east Mediterranean ridge: A synthesis incorporating new Sea-Beam data, *Tectonophysics,* **86,** 243-255, 259-274.

Lisiecki, L.E. & Raymo, M.E., 2005. A Pliocene-Pleistocene stack of 57 globally distributed benthic δ18O records, *Paleoceanography,* **20,** PA1003, doi:10.1029/2004pa001071.

Macklin, M.G., Tooth, S., Brewer, P.A., Noble, P.L. & Duller, G.A.T., 2010. Holocene flooding and river development in a Mediterranean steepland catchment: The Anapodaris Gorge, south central Crete, Greece, *Global Planet. Change,* **70,** 35-52.

Makris, J. & Yegorova, T., 2006. A 3-D density-velocity model between the Cretan Sea and Libya, *Tectonophysics,* **417,** 201-220.

Manighetti, I., Campillo, M., Sammis, C., Mai, P.M. & King, G., 2005. Evidence for self-similar, triangular slip distributions on earthquakes: Implications for earthquake and fault mechanics, *J. Geophys. Res.,* **110,** B05302, doi:10.1029/2004jb003174.

Manighetti, I., King, G.C.P., Gaudemer, Y., Scholz, C.H. & Doubre, C., 2001. Slip accumulation and lateral propagation of active normal faults in Afar, *J. Geophys. Res.,* **106,** 13667-13696, doi:10.1029/2000jb900471.

Marchev, P., Raicheva, R., Downes, H., Vaselli, O., Chiaradia, M. & Moritz, R., 2004. Compositional diversity of Eocene-Oligocene basaltic magmatism in the Eastern Rhodopes, SE Bulgaria: implications for genesis and tectonic setting, *Tectonophysics,* **393,** 301-328.

Mascle, J. & Chaumillon, E., 1998. An overview of Mediterranean Ridge collisional accretionary complex as deduced from multichannel seismic data, *Geo-Mar. Lett.,* **18,** 81-89, doi. 10.1007/s003670050056.

McClusky, S.B., S; Barka, Aykut; Demir, C; Ergintav, S; Georgiev, I; Gurkan, O; Hamburger, M; Hurst, K; Kahle, H; Kastens, K; Kekelidze, G; King, R; Kotzev, V; Lenk, O; Mahmoud, S; Mishin, A; Nadariya, M; Ouzounis, A; Paradissis, D; Peter, Y; Prilepin, M; Reilinger, R; Sanli, I ; Seeger, H ; Tealeb, A ; Toksoz, M N; Veis, G, 2000. Global positioning system constraints on plate kinematics and dynamics in the eastern Mediterranean and Caucasus, *J. geophys. Res.,* **105,** 5695-5719.

McKenzie, D.P., 1970. Plate Tectonics of the Mediterranean Region, *Nature,* **226,** 239-243.

McKenzie, D.P., 1978. Active tectonics of the Alpine–Himalayan belt: the Aegean Sea and surrounding regions, *Geophys. J. Roy. Astr. S.,* **55,** 217-254.

Meier, T., Becker, D., Endrun, B., Rische, M., Bohnhoff, M., Stockhert, B. & Harjes, H.-P., 2007. A model for the Hellenic subduction zone in the area of Crete based on seismological investigations, *Geological Society, London, Special Publications,* **291,** 183-199, doi:10.1144/sp291.9.

Meier, T., Rische, M., Endrun, B., Vafidis, A. & Harjes, H.P., 2004. Seismicity of the Hellenic subduction zone in the area of western and central Crete observed by temporary local seismic networks, *Tectonophysics,* **383,** 149-169.

Merritts, D. & Bull, W.B., 1989. Interpreting Quaternary uplift rates at the Mendocino triple junction, northern California, from uplifted marine terraces, *Geology,* **17,** 1020-1024, doi:10.1130/0091-7613(1989)017<1020:iqurat>2.3.co;2.

Meulenkamp, J.E., van der Zwaan, G.J. & van Wamel, W.A., 1994. On late Miocene to recent vertical motions in the Cretan segment of the Hellenic arc *Tectonophysics,* **234,** 53-72.

Meulenkamp, J.E., Wortel, M.J.R., van Wamel, W.A., Spakman, W. & Hoogerduyn Strating, E., 1988. On the Hellenic subduction zone and the geodynamic evolution of Crete since the late Middle Miocene, *Tectonophysics,* **146,** 203-215.

Mourtzas, N.D., 1988. Neotectonic evolution of Messara's Gulf – Submerged archaeological constructions and use of the coast during the prehistoric and historic periods. *in The engineering geology of ancient works, monuments and historical sites; preservation and protection*, pp. 1565-1573, eds. Marinos, P. G. & Koukis, G. C. A. A. Balkema, Rotterdam.

Mourtzas, N.D., 2012a. Archaeological indicators for sea level change and coastal neotectonic deformation: the submerged Roman fish tanks of the gulf of Matala, Crete, Greece, *J. Archaeol. Sci.,* **39,** 884-895.

Mourtzas, N.D., 2012b. Fish tanks of eastern Crete (Greece) as indicators of the Roman sea level, *J. Archaeol. Sci.,* **39,** 2392-2408.

Neuendorf, K.K.E., Mehl Jr, J.P. & Jackson, J.A., 2005. 5th ed. Glossary of Geology: American Geological Institute, *Alexandria, Virginia*.

Newman, A.V., Stiros, S., Feng, L., Psimoulis, P., Moschas, F., Saltogianni, V., Jiang, Y., Papazachos, C., Panagiotopoulos, D., Karagianni, E. & Vamvakaris, D., 2012. Recent geodetic unrest at Santorini Caldera, Greece, *Geophysical Research Letters,* **39**(6)**,** L06309, doi. 10.1029/2012gl051286.

Nicol, A., Watterson, J., Walsh, J.J. & Childs, C., 1996. The shapes, major axis orientations and displacement patterns of fault surfaces, *J. Struct. Geol.,* **18,** 235-248.

Nyst, M. & Thatcher, W., 2004. New constraints on the active tectonic deformation of the Aegean, *J. Geophys. Res.,* **109,** B11406, doi:10.1029/2003jb002830.

Papadimitriou, E. & Karakostas, V., 2008. Rupture model of the great AD 365 Crete earthquake in the southwestern part of the Hellenic Arc, *Acta Geophys.,* **56,** 293-312, doi:10.2478/s11600-008-0001-6.

Papazachos, B.C., 1996. Large seismic faults in the Hellenic Arc, *Annali di Geofisica,* **39,** 891-903.

Papazachos, B.C. & Comninakis, P.E., 1971. Geophysical and Tectonic Features of the Aegean Arc, *J. geophys. Res.,* **76,** 8517-8533.

Papazachos, B.C., Karakostas, V.G., Papazachos, C.B. & Scordilis, E.M., 2000. The geometry of the Wadati-Benioff zone and lithospheric kinematics in the Hellenic arc, *Tectonophysics,* **319,** 275-300.

Pe-Piper, G. & Piper, D.J.W., 2002. *The igneous rocks of Greece: the anatomy of an orogen,* pp. 645, Gebrüder Borntraeger, Berlin.

Peterek, A. & Schwarze, J., 2004. Architecture and Late Pliocene to recent evolution of outer-arc basins of the Hellenic subduction zone (South-central Crete, Greece), *J. Geodyn.,* **38,** 19-55.

Pirazzoli, P.A., Thommeret, J., Thommeret, Y., Laborel, J. & Montag-Gioni, L.F., 1982. Crustal block movements from Holocene shorelines: Crete and Antikythira (Greece), *Tectonophysics,* **86,** 27-43.

Pirazzoli, P.A., 1986. The early Byzantine tectonic paroxysm: Dating Mediterranean shorelines, *Z. Geomorphol.,* **62**, 31-49.

Pirazzoli, P.A., Laborel, J. & Stiros, S.C., 1996. Earthquake clustering in the Eastern Mediterranean during historical times, *J. Geophys. Res.,* **101,** 6083-6097.

Platt, J.P., 1986. Dynamics of orogenic wedges & the uplift of high-pressure metamorphic rocks, *Geol. Soc. Am. Bull.,* **97,** 1037-1053, doi:10.1130/0016-7606(1986)97<1037:doowat>2.0.co;2.

Pollard, D. & Segall, P., 1987. Theoretical displacements and stresses near fractures in rock: with applications to faults, joints, veins, dikes, and solution surfaces, *Fracture mechanics of rock***,** 277-349.

Pope, R., Wilkinson, K., Skourtsos, E., Triantaphyllou, M. & Ferrier, G., 2008. Clarifying stages of alluvial fan evolution along the Sfakian piedmont, southern Crete: New evidence from analysis of post-incisive soils and OSL dating, *Geomorphology,* **94,** 206-225.

Price, S., Higham, T., Nixon, L. & Moody, J., 2002. Relative Sea-Level Changes in Crete: Reassessment of Radiocarbon Dates from Sphakia and West Crete, *The Annual of the British School at Athens,* **97,** 171-200, doi. 10.2307/30073187.

Rahl, J.M., Anderson, K.M., Brandon, M.T. & Fassoulas, C., 2005. Raman spectroscopic carbonaceous material thermometry of low-grade metamorphic rocks: Calibration and application to tectonic exhumation in Crete, Greece, *Earth planet. Sci. Lett.,* **240,** 339-354.

Reilinger, R., McClusky, S., Paradissis, D., Ergintav, S. & Vernant, P., 2010. Geodetic constraints on the tectonic evolution of the Aegean region and strain accumulation along the Hellenic subduction zone, *Tectonophysics,* **488,** 22-30.

Reilinger, R., McClusky, S., Vernant, P., Lawrence, S., Ergintav, S., Cakmak, R., Ozener, H., Kadirov, F., Guliev, I., Stepanyan, R., Nadariya, M., Hahubia, G., Mahmoud, S., Sakr, K., ArRajehi, A., Paradissis, D., Al-Aydrus, A., Prilepin, M., Guseva, T., Evren, E., Dmitrotsa, A., Filikov, S.V.,

Gomez, F., Al-Ghazzi, R. & Karam, G., 2006. GPS constraints on continental deformation in the africa-arabia-eurasia continental collision zone and implications for the dynamics of plate interactions, *J. geophys. Res.,* **111,** 26, doi:10.1029/2005JB004051

Rhodes, E.J., 2011. Optically Stimulated Luminescence Dating of Sediments over the Past 200,000 Years, *Ann. Rev. Earth planet Sci.,* **39,** 461-488, doi:10.1146/annurev-earth-040610-133425.

Ring, U., Glodny, J., Will, T. & Thomson, S., 2010. The Hellenic subduction System: High-Pressure Metamorphism, Exhumation, Normal Faulting, and Large-Scale Extension, *Ann. Rev. Earth planet Sci.,* **38,** 45-76, doi:10.1146/annurev.earth.050708.170910.

Ring, U. & Reischmann, T., 2002. The weak and superfast Cretan detachment, Greece: exhumation at subduction rates in extruding wedges, *J. geol. Soc. London,* **159,** 225-228, doi:10.1144/0016-764901-150.

Royden, L.H. & Papanikolaou, D.J., 2011. Slab segmentation and late Cenozoic disruption of the Hellenic arc, *Geochem. Geophys. Geosyst.,* **12,** Q03010, doi:10.1029/2010gc003280.

Ryan, W.B.F., Kastens, K.A. & Cita, M.B., 1982. Geological evidence concerning compressional tectonics in the eastern Mediterranean, *Tectonophysics,* **86,** 213-242.

Ryan, W.B.F., Hsü, K.J., Cita, M.B., Dumitrica, P., Lort, J., Maync, W., Nesteroff, W.D., Pautot, G., Stradner, H. & Wezel, F.C., 1973. Initial reports of the Deep Sea Drilling Project, pp. 1-514 Government Printing Office, Washington, D.C.

Schlische, R.W., Young, S.S., Ackermann, R.V. & Gupta, A., 1996. Geometry and scaling relations of a population of very small rift-related normal faults, *Geology,* **24,** 683-686, doi:10.1130/0091-7613(1996)024<0683:gasroa>2.3.co;2.

Scholz, C.H. & Contreras, J.C., 1998. Mechanics of continental rift architecture, *Geology,* **26,** 967-970, doi:10.1130/0091-7613(1998)026<0967:mocra>2.3.co;2.

Schultz, R.A. & Fossen, H., 2002. Displacement-length scaling in three dimensions: the importance of aspect ratio and application to deformation bands, *J. Struct. Geol.,* **24,** 1389-1411.

Schwartz, D.P. & Coppersmith, K.J., 1984. Fault behavior and characteristic earthquakes: examples from the Wasatch and San Andreas Fault Zones, *J. Geophys. Res.,* **89,** 5681-5698, doi:10.1029/JB089iB07p05681.

Seidel, E., Okrusch, M., Kreuzer, H., Raschka, H. & Harre, W., 1981. Eo-alpine metamorphism in the uppermost unit of the Cretan nappe system — Petrology and geochronology, *Contributions to Mineralogy and Petrology,* **76,** 351-361, doi:10.1007/bf00375462.

Seidel, E., Kreuzer, H. & Harre, W., 1982. A Late Oligocane/early Miocene pressure belt in the External Hellenides, *Geologisches Jahruch. Reihe E: Geophyik,* **23**, 165-206.

Shaw, B., Ambraseys, N.N., England, P.C., Floyd, M.A., Gorman, G.J., Higham, T.F.G., Jackson, J.A., Nocquet, J.M., Pain, C.C. & Piggott, M.D., 2008. Eastern Mediterranean tectonics and tsunami hazard inferred from the AD 365 earthquake, *Nature Geosci.,* **1,** 268-276.

Shaw, B. & Jackson, J., 2010. Earthquake mechanisms and active tectonics of the Hellenic subduction zone, *Geophys. J. Int.,* **181,** 966-984.

Snopek, K., Meier, T., Endrun, B., Bohnhoff, M. & Casten, U., 2007. Comparison of gravimetric and seismic constraints on the structure of the Aegean lithosphere in the forearc of the Hellenic subduction zone in the area of Crete, *J. Geodyn.,* **44,** 173-185.

Soliva, R. & Benedicto, A., 2005. Geometry, scaling relations and spacing of vertically restricted normal faults, *J. Struct. Geol.,* **27,** 317-325.

Soliva, R., Benedicto, A. & Maerten, L., 2006. Spacing and linkage of confined normal faults: Importance of mechanical thickness, *J. Geophys. Res.,* **111,** B01402, doi:10.1029/2004jb003507.

Stein, R.S., King, G.C.P. & Rundle, J.B., 1988. The Growth of Geological Structures by Repeated Earthquakes 2. Field Examples of Continental Dip-Slip Faults, *J. Geophys. Res.,* **93,** 13319-13331, doi:10.1029/JB093iB11p13319.

Stewart, I.S., 1993. Sensitivity of Fault-generated Scarps as Indicators of Active Tectonism: Some Constraints from the Aegean Region. *in Landscape Sensitivity*, pp. 129-147, eds. Thomas, D. S. G. & Allison, R. J. John Wiley & Sons, Chichester.

Stewart, I.S. & Hancock, P.L., 1991. Scales of structural heterogeneity within neotectonic normal fault zones in the Aegean region, *J. Struct. Geol.,* **13,** 191-204.

Stiros, S.C., 2001. The AD 365 Crete earthquake and possible seismic clustering during the fourth to sixth centuries AD in the Eastern Mediterranean: a review of historical and archaeological data, *J. Struct. Geol.,* **23,** 545-562.

Stiros, S.C., 2010. The 8.5+ magnitude, AD365 earthquake in Crete: Coastal uplift, topography changes, archaeological and historical signature, *Quatern. Int.,* **216,** 54-63.

Stöckhert, B., Wachmann, M., Küster, M. & Bimmermann, S., 1999. Low effective viscosity during high pressure metamorphism due to dissolution precipitation creep: the record of HP-LT metamorphic carbonates and siliciclastic rocks from Crete, *Tectonophysics,* **303,** 299-319.

Strasser, T.F., Runnels, C., Wegmann, K., Panagopoulou, E., McCoy, F., Digregorio, C., Karkanas, P. & Thompson, N., 2011. Dating Palaeolithic sites in southwestern Crete, Greece, *J. Quat. Sci.,* **26,** 553-560, doi:10.1002/jqs.1482.

Suckale, J., Rondenay, S., Sachpazi, M., Charalampakis, M., Hosa, A. & Royden, L.H., 2009. High-resolution seismic imaging of the western Hellenic subduction zone using teleseismic scattered waves, *Geophys. J. Int.,* **178,** 775-791, doi:10.1111/j.1365-246X.2009.04170.x.

Taymaz, T., Jackson, J.A. & Westaway, R., 1990. Earthquake mechanisms in the Hellenic trench near Crete, *Geophys. J. Int.,* **102,** 695-731.

ten Veen, J.H. & Kleinspehn, K.L., 2003. Incipient continental collision and plate-boundary curvature: Late Pliocene-Holocene transtensional Hellenic forearc, Crete, Greece, *J. geol. Soc. London,* **160,** 161-181, doi:10.1144/0016-764902-067.

Thomson, S.N., Brandon, M.T., Reiners, P.W., Zattin, M., Isaacson, P.J. & Balestrieri, M.L., 2010. Thermochronologic evidence for orogen-parallel variability in wedge kinematics during extending convergent orogenesis of the northern Apennines, Italy, *Geol. Soc. Am. Bull.,* **122,** 1160-1179, doi:10.1130/b26573.1.

Thomson, S.N., Stöckhert, B. & Brix, M.R., 1998. Thermochronology of the high-pressure metamorphic rocks of Crete, Greece: Implications for the speed of tectonic processes, *Geology,* **26,** 259-262, doi:10.1130/0091-7613(1998)026<0259:tothpm>2.3.co;2.

van Hinsbergen, D.J.J., Hafkenscheid, E., Spakman, W., Meulenkamp, J.E. & Wortel, R., 2005. Nappe stacking resulting from subduction of oceanic and continental lithosphere below Greece, *Geology,* **33,** 325-328, doi:10.1130/g20878.1.

van Hinsbergen, D.J.J. & Meulenkamp, J.E., 2006. Neogene supradetachment basin development on Crete (Greece) during exhumation of the South Aegean core complex, *Basin Res.,* **18,** 103-124.

van Hinsbergen, D.J.J. & Schmid, S.M., 2012. Map view restoration of Aegean–West Anatolian accretion and extension since the Eocene, *Tectonics,* **31,** doi. 10.1029/2012tc003132.

Vassilakis, E., Royden, L. & Papanikolaou, D., 2011. Kinematic links between subduction along the Hellenic trench and extension in the Gulf of Corinth, Greece: A multidisciplinary analysis, *Earth planet. Sci. Lett.,* **303,** 108-120.

Waelbroeck, C., Labeyrie, L., Michel, E., Duplessy, J.C., McManus, J., Lambeck, K., Balbon, E. & Labracherie, M., 2002. Sea-level and deep water temperature changes derived from benthic foraminifera isotopic records, *Quatern. Sci. Rev.,* **21,** 295-305.

Walsh, J.J., Bailey, W.R., Childs, C., Nicol, A. & Bonson, C.G., 2003. Formation of segmented normal faults: a 3-D perspective, *J. Struct. Geol.,* **2,** 1251-1262.

Walsh, J.J., Nicol, A. & Childs, C., 2002. An alternative model for the growth of faults, *J. Struct. Geol.,* **24,** 1669-1675.

Walsh, J.J. & Watterson, J., 1988. Analysis of the relationship between displacements and dimensions of faults, *J. Struct. Geol.,* **10,** 239-247.

Wells, D.L. & Coppersmith, K.J., 1994. New empirical relationships among magnitude, rupture length, rupture width, rupture area, and surface displacement, *B. Seismol. Soc. Am.,* **84,** 974-1002.

Wells, R.E., Blakely, R.J., Sugiyama, Y., Scholl, D.W. & Dinterman, P.A., 2003. Basin-centered asperities in great subduction zone earthquakes: A link between slip, subsidence, and subduction erosion?, *J. Geophys. Res.,* **108**, doi. 10.1029/2002jb002072.

Wegmann, K.W., 2008. Tectonic geomorphology above Mediterranean subduction zones; northern Apennines of Italy and Crete, Greece, Doctoral Dissertation, Lehigh University, Bethlehem, PA.

Wegmann, K.W., Brandon, M.T., Pazzaglia, F.J. & Fassoulas, C., 2010. Reassessment of the origin of the AD 365 Earthquake from geologic and geochronogic relationships, Crete, Greece [abstract], *Tectonic Crossroads: Evolving Orogens of Eurasia-Africa-Arabia***,** 61.

Wegmann, K.W., Brandon, M.T., Pazzaglia, F.J. & Fassoulas, C., *in review*. Seismic hazard of coastal escarpments: Reassessment of the AD 365 Earthquake from geologic and geochronologic relationships, Crete, Greece, *submitted to Earth planet. Sci. Lett*.

Willemse, E.J.M., 1997. Segmented normal faults: Correspondence between three-dimensional mechanical models and field data, *J. Geophys. Res.,* **102,** 675-692, doi:10.1029/96jb01651.

Willemse, E.J.M., Pollard, D.D. & Aydin, A., 1996. Three-dimensional analyses of slip distributions on normal fault arrays with consequences for fault scaling, *J. Struct. Geol.,* **18,** 295-309.

Willett, S.D., Beaumont, C. & Fullsack, P., 1993. Mechanical models for the tectonics of doubly vergent compressional orogens, *Geology,* **21,** 371-374.

Wortel, M.J.R. & Spakman, W., 2000. Subduction and Slab Detachment in the Mediterranean-Carpathian Region, *Science,* **290,** 1910-1917, doi:10.1126/science.290.5498.1910.

Yem, L.M., Camera, L., Mascle, J. & Ribodetti, A., 2011. Seismic stratigraphy and deformational styles of the offshore Cyrenaica (Libya) and bordering Mediterranean Ridge, *Geophys. J. Int.,* **185,** 65-77, doi:10.1111/j.1365-246X.2011.04928.x.

Zachariasse, W.J., van Hinsbergen, D.J.J. & Fortuin, A.R., 2008. Mass wasting and uplift on Crete and Karpathos during the early Pliocene related to initiation of south Aegean left-lateral, strike-slip tectonics, *Geol. Soc. Am. Bull.,* **120,** 976-993, doi. 10.1130/b26175.1.

APPENDICES

Appendix 2.1: Locations of measured Pleistocene terrace elevations, eustatic correlations, and sedimentary facies deposits

Location	Site (Fig. 3)	Lat (°N)	Lon (°E)	Terrace elevation (m asl)[1]	± σ (m)	dated age (kyrs)[2]	± σ (kyrs)	Assigned MIS[3]	Facies[4]	Notes
Cape Lithano	1	34.928	24.732	no terraces					-	Coast is highly indented (rias).
Kali Limenes	2	34.926	24.791	8	1			5c	C	Pebbly Beach lag cut on small bench. Buried by limestone breccia. Contains well preserved *Hippopotamus creutzburgi* and *Magaceros cetensis* (?) fossils
				19	0.3			5c	C	Small wave cut bench with beach lag of carbonate and phyllite pebbles
				45	0.6			5e	E	Broad wave cut bench covered by highly weathered cobble size beach lag.
				62	0.3			7	E	Broad wave cut bench covered by highly weathered cobble size beach lag.
Dytikos	3	34.933	24.885	10	4			4/5	F	Wave cut bench with thick beach fossiliferous (marine) lag buried by alluvial fan.
Lentas	4	34.932	24.931	19	0.6			4/5	F	Wave cut bench with thick beach fossiliferous (marine) lag buried by alluvial fan.
				42	4			5c	C	Wave cut notches. Beach lag of carbonate and phyllite pebbles.
				63	5			5c	C	Wave cut notches. Beach lag of carbonate pebbles and marine fossils.
				93	1			5e	B	Prominent coastal erosional features including sea arches and caves.
Cape Trekalo	5	34.927	24.959	4.5	0.5			4/5	E	Broad wave cut bench covered by pebble to cobble size beach lab in many locations.
				24	1			5c	B	Wave cut notch with beach lag
				40	1			5c	E	Broad wave cut bench covered by pebble to cobble size beach lag in many locations.
				68	0.5			5e	E	Broad wave cut bench covered by pebble to cobble size beach lag in some locations, highly eroded surface.
				93	2			7	E	Broad wave cut bench, highly eroded, minor coverage of pebble to cobble size beach lag.
				124	1			9	F	Wave cut bench with beach lag, buried by alluvial fan.

[1] Inner shoreline angle elevation of terrace in meters above sea level (m asl).

[2] Optically stimulated luminance (OSL) burial age. See table 2 for data.

[3] MIS: Marine isotope stage.

[4] Facies descriptions are as follows: A- bioerosional notch. B – bioerosional notch and fringing algal reef. C – bioerosional notch and pebbly beach-lag couplet. D – Beach rock and abrasion platform. E – transgressive algal reef on beach rock overlain by an alluvial fan. Facies F – Beach rock and abrasion platform buried by an alluvial fan.

Appendix 2.1: Locations of measured Pleistocene terrace elevations, eustatic correlations, and sedimentary facies deposits continued

Location	Site (Fig. 3)	Lat (°N)	Lon (°E)	Terrace elevation (m asl)[1]	± σ (m)	dated age (kyrs)[2]	± σ (kyrs)	Assigned MIS[3]	Facies[4]	Notes
Trypiti	6	34.934	24.98	5	1			4/5	E	Broad wave cut bench covered by pebble to cobble size beach lab in many locations.
				22	0.1			5c	F	Wave cut bench with beach lag of carbonate and phyllite pebble and cobble and marine fossils, buried by alluvial fan.
				38	1.4			5c	F	Wave cut bench with beach lag of carbonate and phyllite pebble and cobble and marine fossils, buried by alluvial fan.
Agios Ioannis	7	34.942	25.067	13	1			4/5	D	Small wave cut bench with beach lag of carbonate and phyllite pebbles capped by calcareous algae and buried by alluvial fan
Tris Ekklisies	8	34.955	25.149	25	0.3	72	8	4/5	F	Wave cut bench with beach lag of carbonate and phyllite pebble and cobble and marine fossils, buried by alluvial fan.
				43	2			5c	C	Small wave cut bench with beach lag
				60	3			5c	C	Small wave cut bench with beach lag
				96	0.4			5e	F	Wave cut bench with beach lag of carbonate and phyllite pebble and cobble and marine fossils, buried by alluvial fan.
Agios Nikita	9	34.967	25.263	30	0.4			4/5	F	Wave cut bench with beach lag of carbonate and phyllite pebble and cobble and marine fossils, buried by alluvial fan.
				47	1			5c	A	Wave cut notches and sea caves. Calcareous algae at base of erosional features.
				65	0.2			5c	B	Prominent coastal erosional features including sea stacks, notches and caves.
				103	0.1			5e	F	Wave cut bench with beach lag of carbonate and phyllite pebble and cobble, buried by alluvial fan.
Tsourtsouros	10	34.983	25.278	27	0.5	78	8	4/5	F	Wave cut bench with beach lag of carbonate and phyllite pebble and cobble and marine fossils, buried by alluvial fan.
				47	0.5			5c	C	Wave cut notch accompanied by beach lag of mainly carbonate pebbles.
				65	2			5c	C	Wave cut notch accompanied by beach lag of mainly carbonate pebbles.
				97	1			5e	F	Wave cut bench with beach lag of carbonate and phyllite pebble and cobble and marine fossils, buried by alluvial fan.
				139	2			7	E	Wave cut bench locally covered by beach lag of carbonate and phyllite pebbles and cobbles

[1] Inner shoreline angle elevation of terrace in meters above sea level (m asl).

[2] Optically stimulated luminance (OSL) burial age. See table 2 for data.

[3] MIS: Marine isotope stage.

[4] Facies descriptions are as follows: A- bioerosional notch. B – bioerosional notch and fringing algal reef. C – bioerosional notch and pebbly beach-lag couplet. D – Beach rock and abrasion platform. E – transgressive algal reef on beach rock overlain by an alluvial fan. Facies F – Beach rock and abrasion platform buried by an alluvial fan.

Appendix 2.1: Locations of measured Pleistocene terrace elevations, eustatic correlations, and sedimentary facies deposits continued

Location	Site (Fig. 3)	Lat (°N)	Lon (°E)	Terrace elevation (m asl)[1]	± σ (m)	dated age (kyrs)[2]	± σ (kyrs)	Assigned MIS[3]	Facies[4]	Notes
Tsourtsouros	10	34.983	25.278	166	3			8	E	Wave cut bench, highly eroded and locally covered by highly degraded and sparse beach lag of carbonate and phyllite pebbles and cobbles
				210	1.5			9	E	Wave cut bench, highly eroded and locally covered by highly degraded and sparse beach lag of carbonate and phyllite pebbles and cobbles
				251	1			11	E	Wave cut bench, highly eroded and locally covered by highly degraded and sparse beach lag of carbonate and phyllite pebbles and cobbles
Sarakinos	11	34.986	25.306	50	3			5e	F	Broad wave cut bench, thick (> 1m) beach cobble deposit with marine fossils. Buried by thick (> 1m) alluvial fan.
				65	3			7	F	Broad wave cut bench, thick (> 1m) beach cobble deposit with marine fossils. Buried by thick (> 1m) alluvial fan.
				103	5			9	F	Broad wave cut bench, thick (> 1m) beach cobble deposit with marine fossils. Buried by thick (> 1m) alluvial fan.
Dermatos	12	34.99	25.324	50	3	127	13	5e	F	Broad wave cut bench, thick (> 1m) beach cobble deposit with marine fossils. Buried by thick (> 1m) alluvial fan.
				70	2			7	F	Broad wave cut bench, thick (> 1m) beach cobble deposit with marine fossils. Buried by thick (> 1m) alluvial fan.
				105	4			9	F	Broad wave cut bench, thick (> 1m) beach cobble deposit with marine fossils. Buried by thick (> 1m) alluvial fan.
Keratokampos	13	35.001	25.39	42	0.5			5e	F	Broad wave cut bench, thick (> 1m) beach cobble deposit with marine fossils. Buried by thick (> 1m) alluvial fan.
				55	1.3			7	F	Broad wave cut bench, thick (> 1m) beach cobble deposit with marine fossils. Buried by thick (> 1m) alluvial fan.
				92	1.3			9	F	Broad wave cut bench, thick (> 1m) beach cobble deposit with marine fossils. Buried by thick (> 1m) alluvial fan.

[1] Inner shoreline angle elevation of terrace in meters above sea level (m asl).

[2] Optically stimulated luminance (OSL) burial age. See table 2 for data.

[3] MIS: Marine isotope stage.

[4] Facies descriptions are as follows: A- bioerosional notch. B – bioerosional notch and fringing algal reef. C – bioerosional notch and pebbly beach-lag couplet. D – Beach rock and abrasion platform. E – transgressive algal reef on beach rock overlain by an alluvial fan. Facies F – Beach rock and abrasion platform buried by an alluvial fan.

Appendix 2.1: Locations of measured Pleistocene terrace elevations, eustatic correlations, and sedimentary facies deposits continued

Location	Site (Fig. 3)	Lat (°N)	Lon (°E)	Terrace elevation (m asl)[1]	± σ (m)	dated age (kyrs)[2]	± σ (kyrs)	Assigned MIS[3]	Facies[4]	Notes
Xerokampos	14	34.993	25.217	45	0.1			5e	F	Broad wave cut bench, thick (> 1m) beach cobble deposit with marine fossils. Buried by thick (> 1m) alluvial fan.
				61	0.1			7	F	Broad wave cut bench, thick (> 1m) beach cobble deposit with marine fossils. Buried by thick (> 1m) alluvial fan.
				114	0.5			9	F	Broad wave cut bench, thick (> 1m) beach cobble deposit with marine fossils. Buried by thick (> 1m) alluvial fan.
Arvi	15	34.993	25.248	1	0.1			5e	E	Broad wave cut bench, thick (> 1m) beach cobble deposit with marine fossils.
				39	2			7	F	Broad wave cut bench, thick (> 1m) beach cobble deposit with marine fossils. Buried by thick (> 1m) alluvial fan.
				50	2			9	F	Broad wave cut bench, thick (> 1m) beach cobble deposit with marine fossils. Buried by thick (> 1m) alluvial fan.
Neo Arvi/ Sidonia	16	34.986	25.287	2	0.1			5e	E	Broad wave cut bench, thick (> 1m) beach cobble deposit with marine fossils. Buried by thick (> 1m) alluvial fan.
				40	3			7	F	Broad wave cut bench, thick (> 1m) beach cobble deposit with marine fossils. Buried by thick (> 1m) alluvial fan.
				59	3			9	F	Broad wave cut bench, thick (> 1m) beach cobble deposit with marine fossils. Buried by thick (> 1m) alluvial fan.
Tertsa	17	34.993	25.537	56	0.1			7	F	Broad wave cut bench, thick (> 1m) beach cobble deposit with marine fossils. Buried by thick (> 1m) alluvial fan.
				117	0.1			9	F	Broad wave cut bench, thick (> 1m) beach cobble deposit with marine fossils. Buried by thick (> 1m) alluvial fan.
Ierapetra	18	35.016	25.734	31	3			5e	F	Broad wave cut bench, thick (> 1m) beach cobble deposit with marine fossils. Buried by thick (> 1m) alluvial fan.
				71	3			7	F	Broad wave cut bench, thick (> 1m) beach cobble deposit with marine fossils. Buried by thick (> 1m) alluvial fan.
				114	4			9	F	Broad wave cut bench, thick (> 1m) beach cobble deposit with marine fossils. Buried by thick (> 1m) alluvial fan.

[1] Inner shoreline angle elevation of terrace in meters above sea level (m asl).

[2] Optically stimulated luminance (OSL) burial age. See table 2 for data.

[3] MIS: Marine isotope stage.

[4] Facies descriptions are as follows: A- bioerosional notch. B – bioerosional notch and fringing algal reef. C – bioerosional notch and pebbly beach-lag couplet. D – Beach rock and abrasion platform. E – transgressive algal reef on beach rock overlain by an alluvial fan. Facies F – Beach rock and abrasion platform buried by an alluvial fan.

Appendix 2.2: Soil profile descriptions

All soil types are keyed to text and figures 6 and 7.

Type 1

Location: Site 4, East of Lentas. N: 34.93381, E: 024.95317

Soil has developed on alluvial/colluvial fan material. It is clast supported. Clasts are many and predominantly angular, medium to large, limestone. The slope is south facing and 6 – 15% grade. Well drained. Xeric moisture regime.

A (0 – 10 cm): 7.5YR 5/6 strong brown, loam. Moderate, medium, granular structure. Friable, nonsticky, nonplastic consistence. Clear smooth boundary.

Bt (10 – 30cm): 5YR 4/4 reddish brown, clay loam. Moderate, medium, subangular blocky structure. Friable, slightly sticky, non-plastic consistence. Peds have clay films. Clear smooth boundary.

Bk_w (30 – 85cm): 7.5YR 7/6 reddish yellow, loamy sand. Strong, fine to medium subangular blocky structure. Firm, nonsticky, nonplastic consistence. Calcic films on peds, thin calcic rine on clasts. Gradual smooth boundary.

BC (>85cm): 7.5YR 6/6 reddish yellow, loamy sand. Strong medium to large subangular blocky structure. Firm, nonsticky, nonplastic consistence. Calcic films on peds, thin calcic rines on clasts . Gradual smooth boundary.

Type 1

Location: Site 7, East of Agio Ioannis. N: 34.94146, E: 025.06564

Soil has developed on alluvial/colluvial fan parent material. It is clast supported. Clasts are many and predominantly angular, medium to large, limestone. Slope is south-facing and 6 – 15 % grade. Well drained. Xeric moisture regime

A (0 – 34 cm): 7.5YR 5/6 strong brown, sandy loam (or loamy sand). Moderate, medium, granular structure. Friable, slightly sticky, non-plastic consistence. Some very thin calcic rines on clasts. Clear smooth boundary.

Bk_w1 (34 – 58cm): 7.5YR 7/6 reddish yellow, loamy sand. Weak fine subangular blocky structure. Very friable, non sticky, non-plastic consistence. Some peds show calcic films, clasts have thin calcic rines. Clear smooth boundary.

Bk_w2 (>58 cm): 7.5YR 6/6 reddish yellow, loamy sand. Strong, medium subangular blocky structure. Slightly sticky, non-plastic. Calcic films on peds, thick calcic rines on clasts.

Type 1

Location: Site 10, West of Tsourtsouras. GPS → N: 34.98178, E: 025.27839

Soil has developed on alluvial/colluvial parent material. It is clast supported. Clasts are many and predominantly angular, medium to large, limestone. Slope is south-east facing and 6 to 15 % grade. Well drained. Xeric moisture regime.

A (0 – 29 cm): 7.5 YR 5/4 brown, clay loam. Moderate, medium, granular structure. Firm (?), non-sticky, non-plastic consistence. Surface texture feels silty. Gradual smooth boundary.

Bw (29 – 60 cm): 7.5 YR 4/4 brown, clay loam. Strong, medium, subangular blocky structure. Friable, slightly sticky, non-plastic consistence. Gradual smooth boundary.

Bw (60cm – 105cm): 7.5 4/6 strong brown, clay loam. Moderate, medium to fine, subangular blocky structure. Very friable, slightly sticky, non-plastic consistence.

Notes:

Could only dig to 105 cm depth.

Type 2A

Location: Site 7, East of Agio Ioannis. N: 34.94146, E: 025.06564

Soil has developed on alluvial/colluvial parent material. It is clast supported. Clasts are many and predominantly angular, medium to large, limestone. Slope is south-east facing and 6 to 15 % grade. Xeric moisture regime.

Bk (0 - > 2m): 10R 7/1 light gray.

Notes:

Cannot describe structure, wet or dry consistence, or other soild properties because this is a well developed petrocalcic horizon.

Type 2B

Location: Site 11, East of Tsourtsouras. N: 34.98428, E: 025.31847

Soil has developed on alluvial/colluvial parent material. It is matrix supported. Clasts are many and predominantly angular, medium, gravel. Slope is south facing and 5 – 10 % grade. Well drained. Xeric moisture regime.

Ap (0 – 10cm): 7.5YR 4/6 strong brown, loamy sand. Weak, fine, granular structure. Very friable, non-sticky, non-plastic structure. Clear smooth boundary.

Bt (10 – 42 cm): 2.5 YR 3/8 dark red, clay loam. Moderate, medium, subangular blocky structure. Friable, slightly sticky, non-plastic consistence. Clay films on peds. Clear smooth boundary.

Btk1 (42 – 130 cm): 2.5 YR ¾ dark reddish brown, sandy loam. Moderate, medium, subangular blocky structure. Friable, slightly sticky, non-plastic consistence. Clay and calcic films on peds. Clasts have thin calcic rines. Clear smooth boundary.

Btk2 (> 130 cm): 2.5 YR 5/6 red, sandy loam. Moderate, large, subangular blocky structure. Friable, slightly sticky, non-plastic. Clay and calcic films on peds. Clasts have thin calcic rines.

Appendix 2.3: Correlation of measured terrace inner shoreline angle elevations to the Late Quaternary Eustatic Curve.

Correlation of the terrace elevations from mapped localities in South-central Crete to Late Quaternary eustatic curve compiled from 0 to 125 kyrs from Lambeck and Chappell (2000) and from 125 to 450 kyrs from Waelbroek et al. (2002). Marine isotope stage (MIS) boundaries are from Lisiecki & Raymo (2005). Available optically stimulated luminance (OSL) burial age-dates, radiometric age-dates from marine bivalves and index fossil evidence anchors terrace sequences to the eustatic curve (Tables 1,2). Gray color for terrace sequences indicates mostly carbonate bedrock and the tan color indicates most Neogene turbidite bedrock. Right inset diagrams show the assigned terrace age versus total amount of uplift with associated errors (1-σ) in paleo-sea level and terrace elevations and assigned terrace ages at. The linear regressions represent site average uplift rates over the late Quaternary. Right inset diagram shows uplift rates for individual terraces versus assigned terrace age determined using equation (2). Associated errors are smaller than the symbols at the scale of these diagrams.

Kali Limemes (34.926°N, 24.791°E) – Fig. 3, site 2

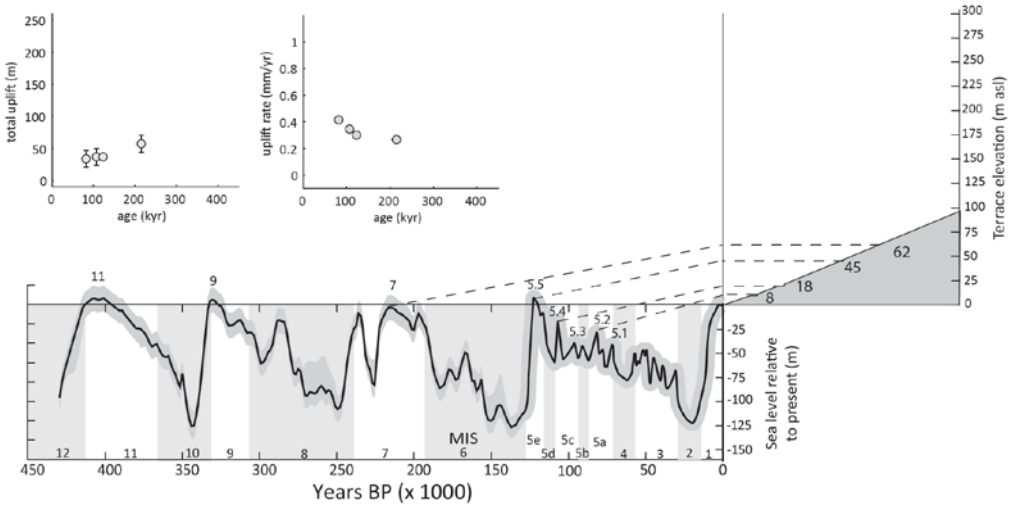

Dytikos (34.933°N, 24.885°E) – Fig. 3, site 3

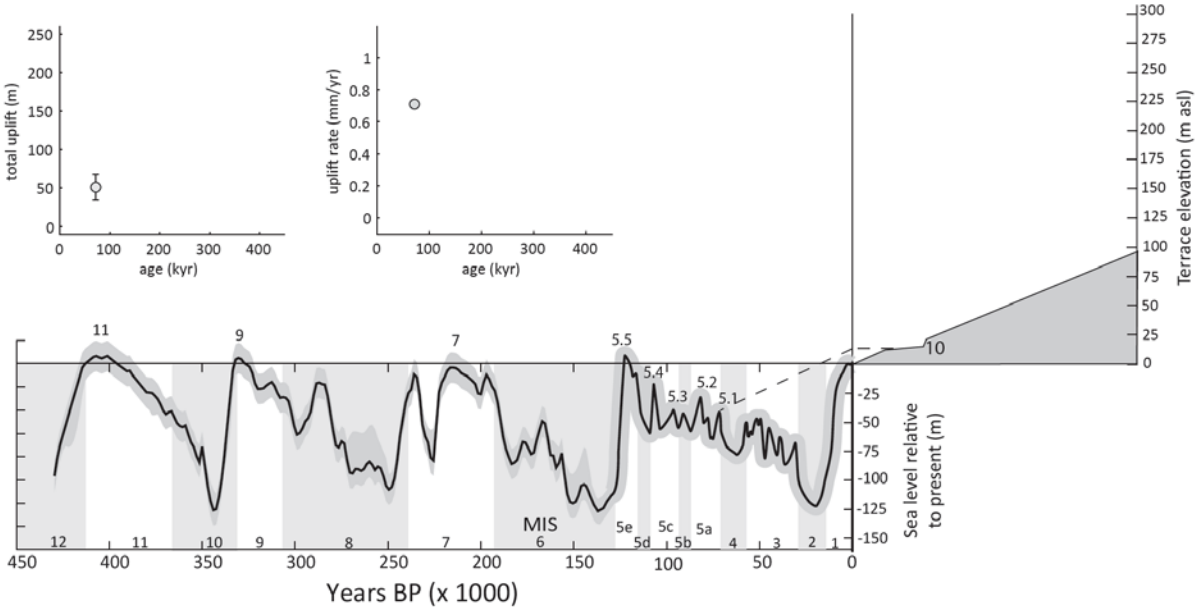

Lentas (34.932°N, 24.931°E) – Fig. 3, site 4

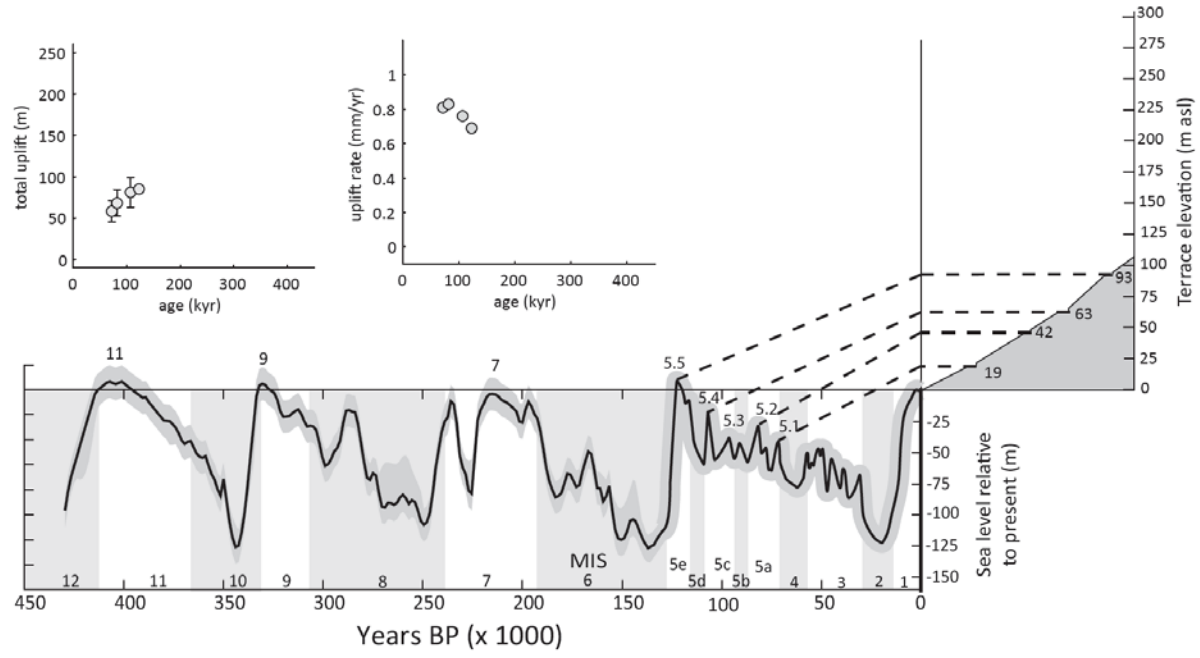

Cape Trekalo (34.927°N, 24.959°E) – Fig. 3, site 5

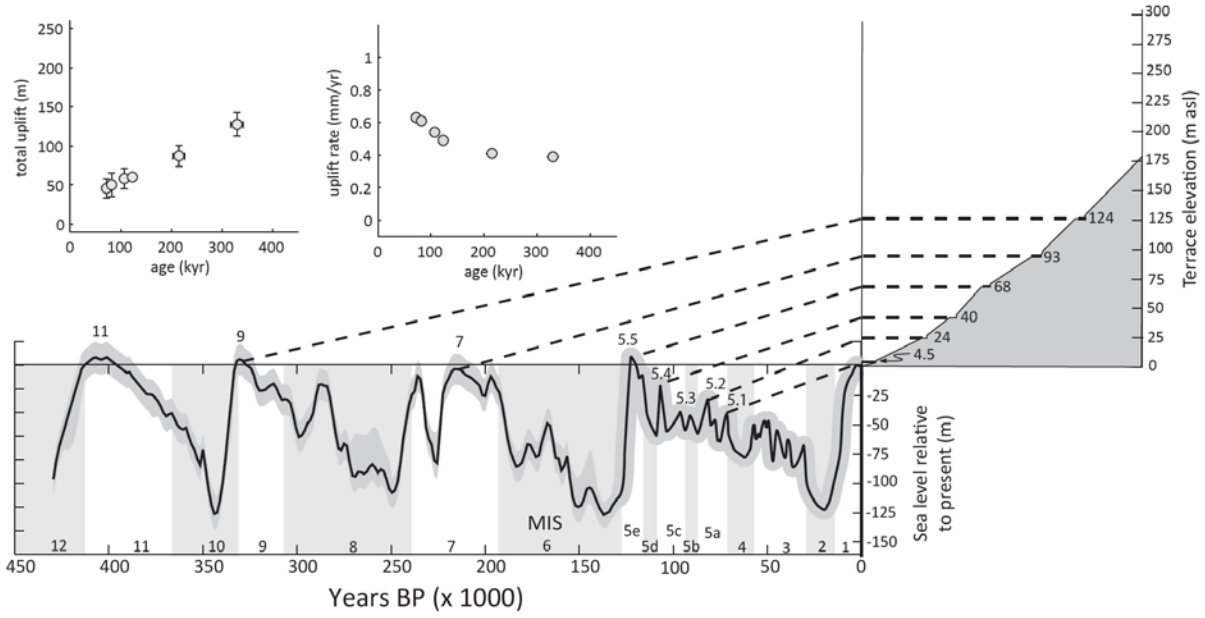

Trypiti (34.934°N, 24.980°E) – Fig. 3, site 6

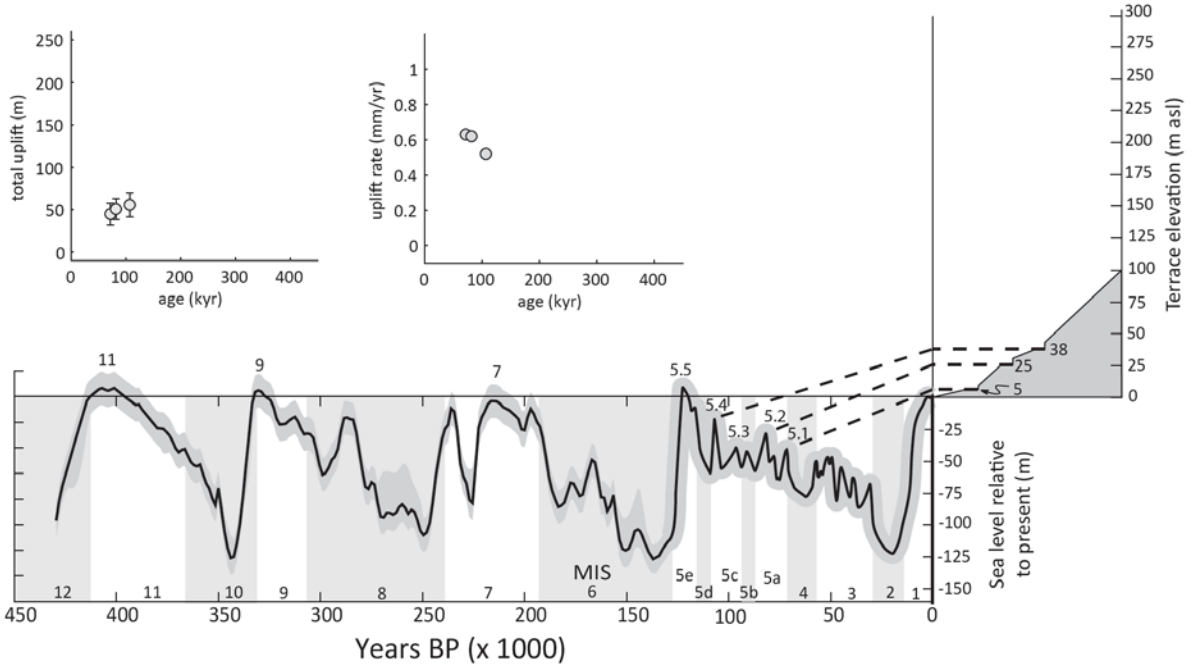

Agios Ioannis (34.942°N, 25.067°E) – Fig. 3, site 7

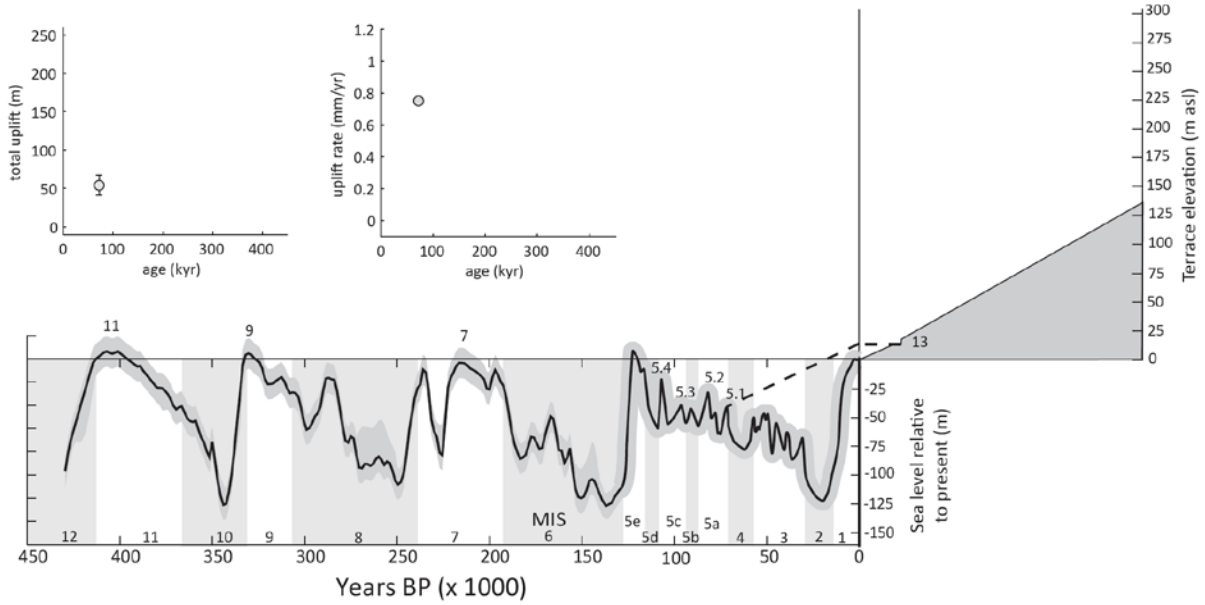

Tris Ekklisies (34.955°N, 25.149°E) – Fig. 3, site 8

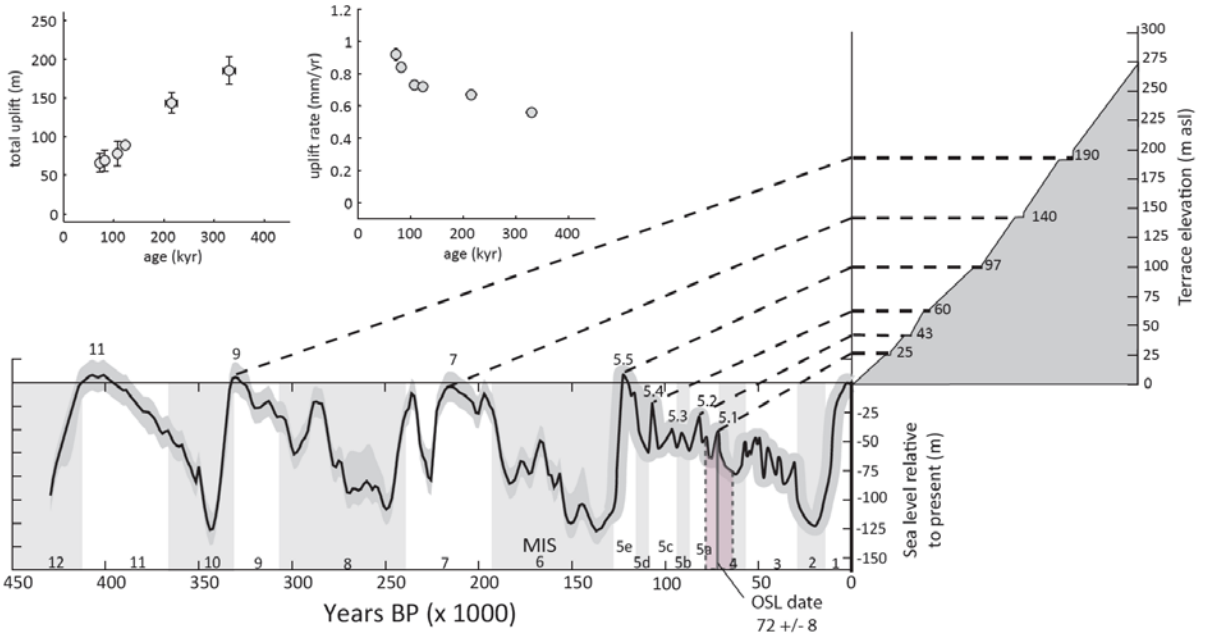

Agios Nikita (34.967°N, 25.263°E) – Fig. 3, site 9

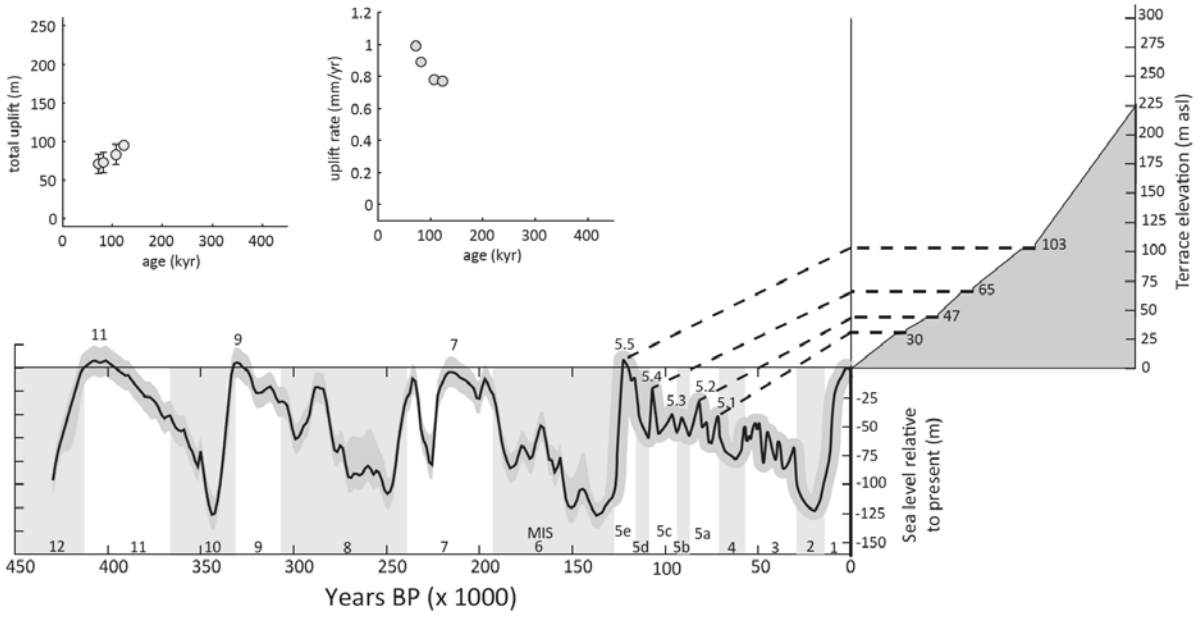

Tsourtsouros (34.983°N, 25.278°E) – Fig. 3, site 10

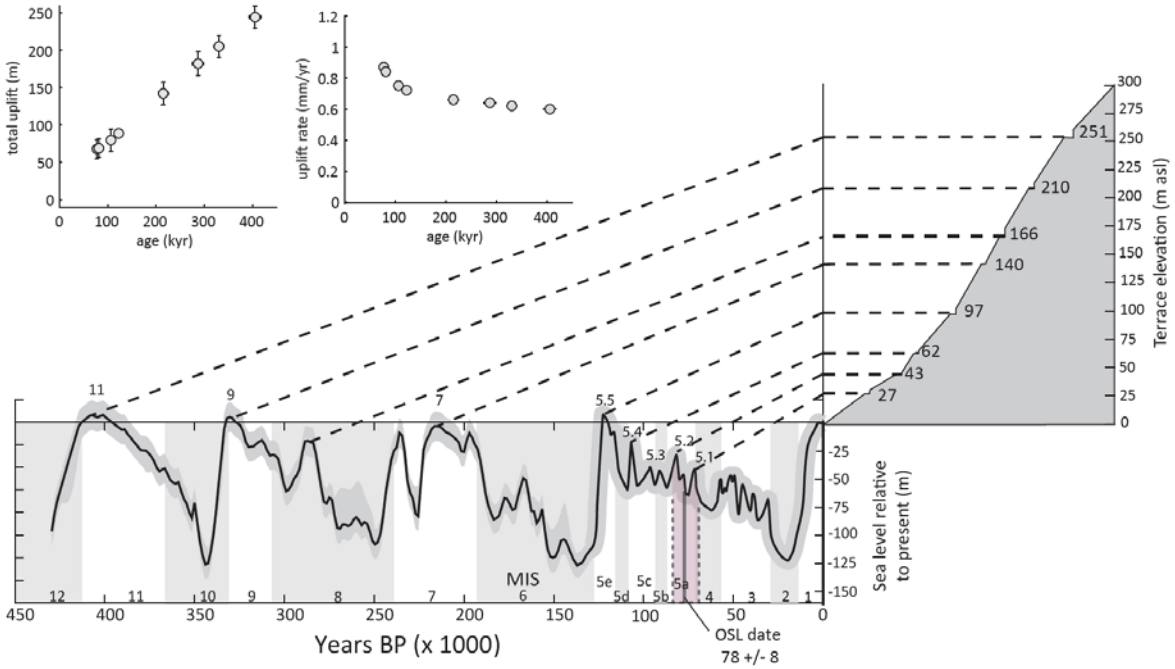

Sarakinos (34.986°N, 25.324°E) – Fig. 3, site 11

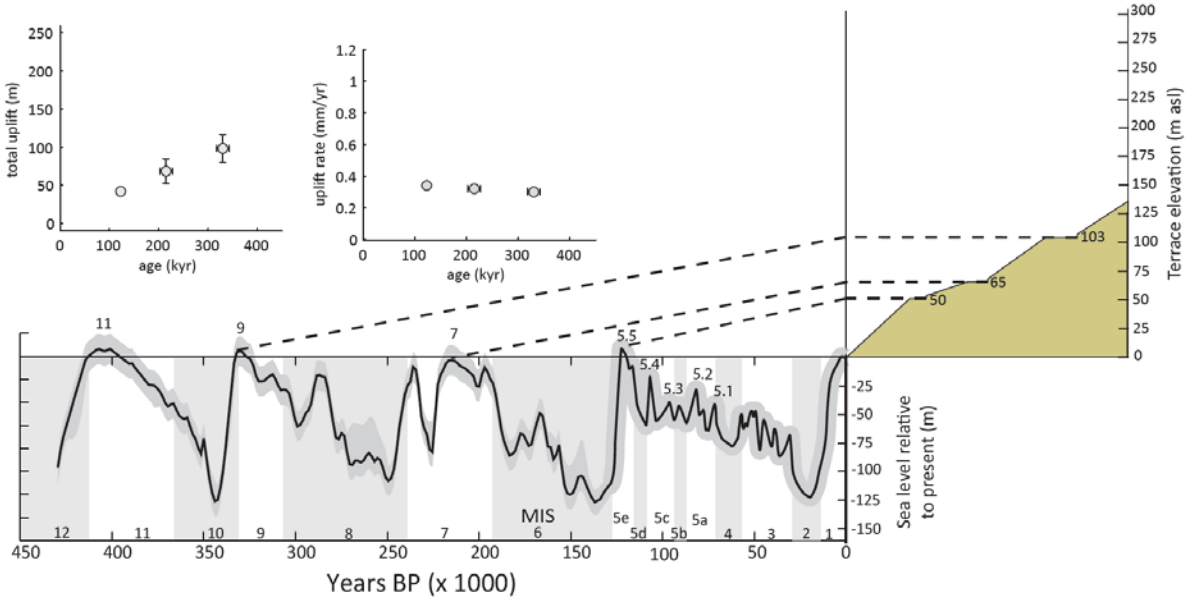

Dermatos (34.990°N, 25.324°E) – Fig. 3, site 12

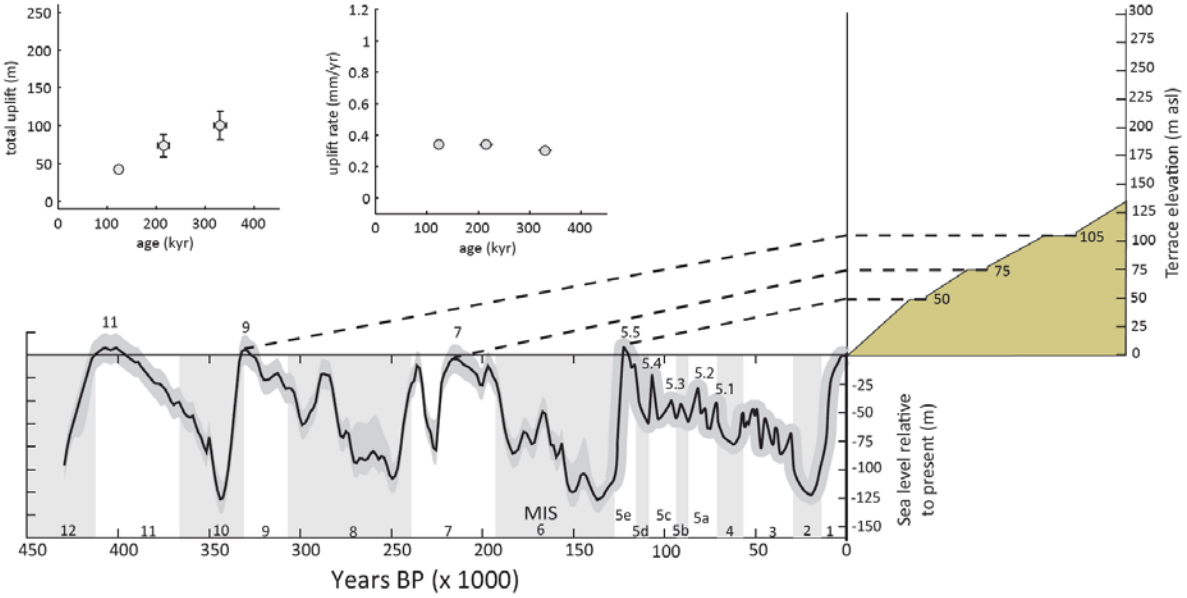

Keratokampos (35.001°N, 25.390°E) – Fig. 3, site 13

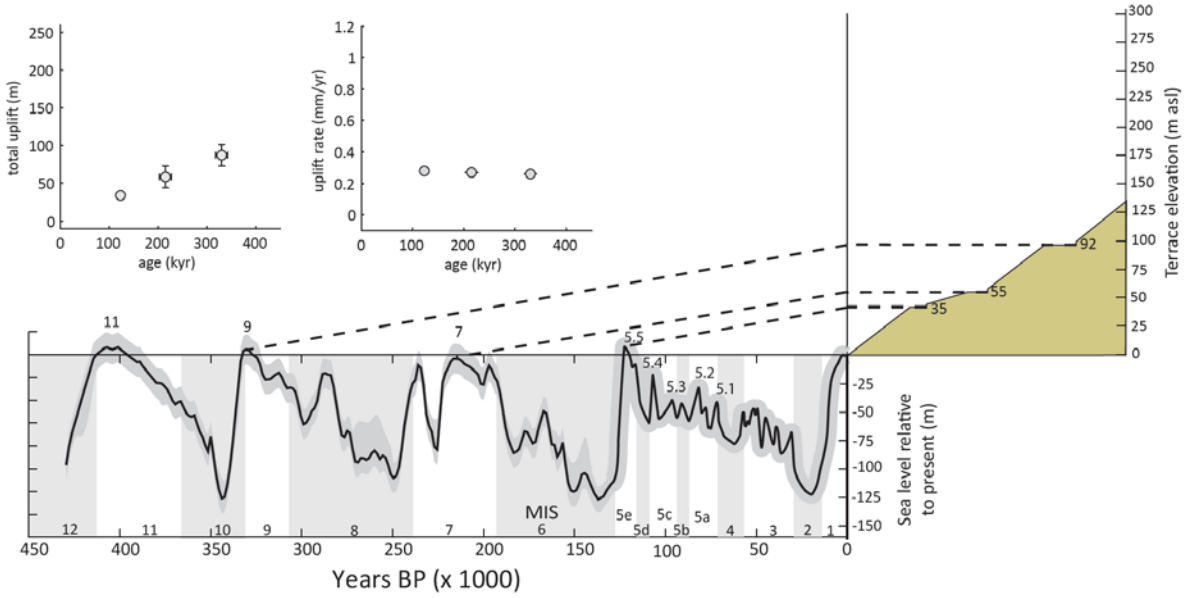

Xerokampos (34.993°N, 25.217°E) – Fig. 3, site 14

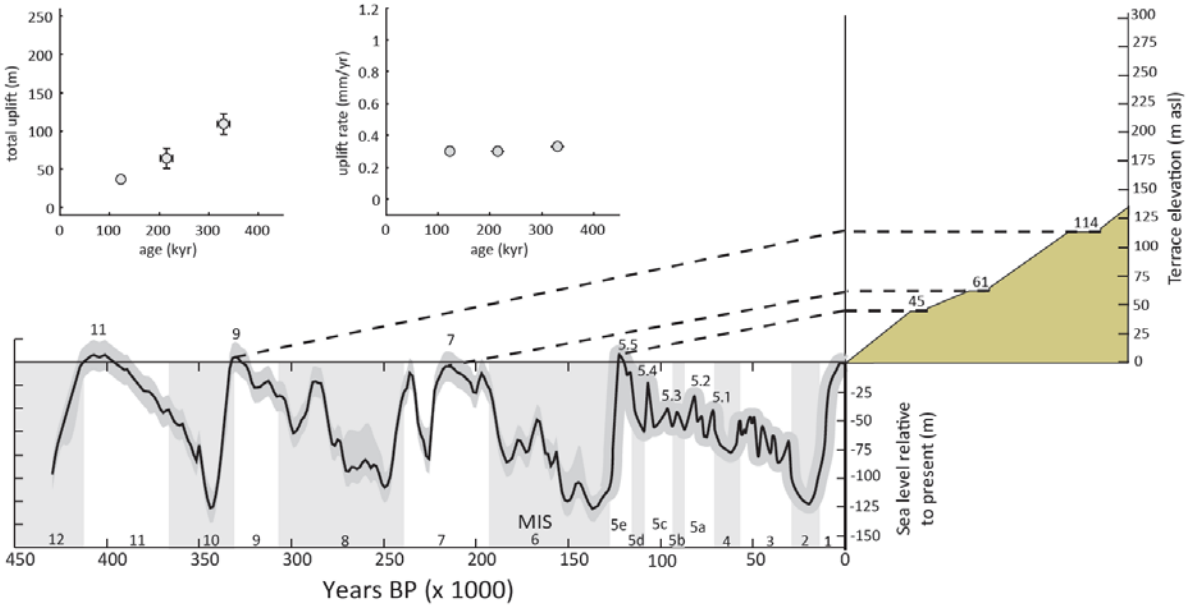

Arvi (34.993°N, 25.248°E) – Fig. 3, site 15

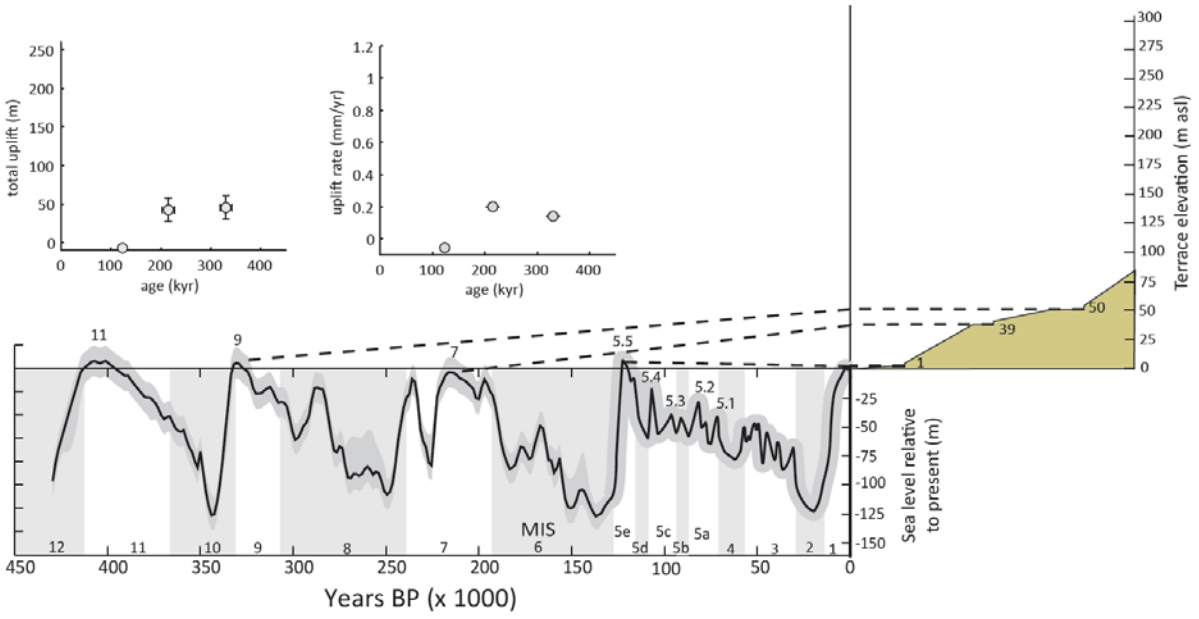

Neo Arvi/Sidonia (34.986°N, 25.287°E) – Fig. 3, site 16

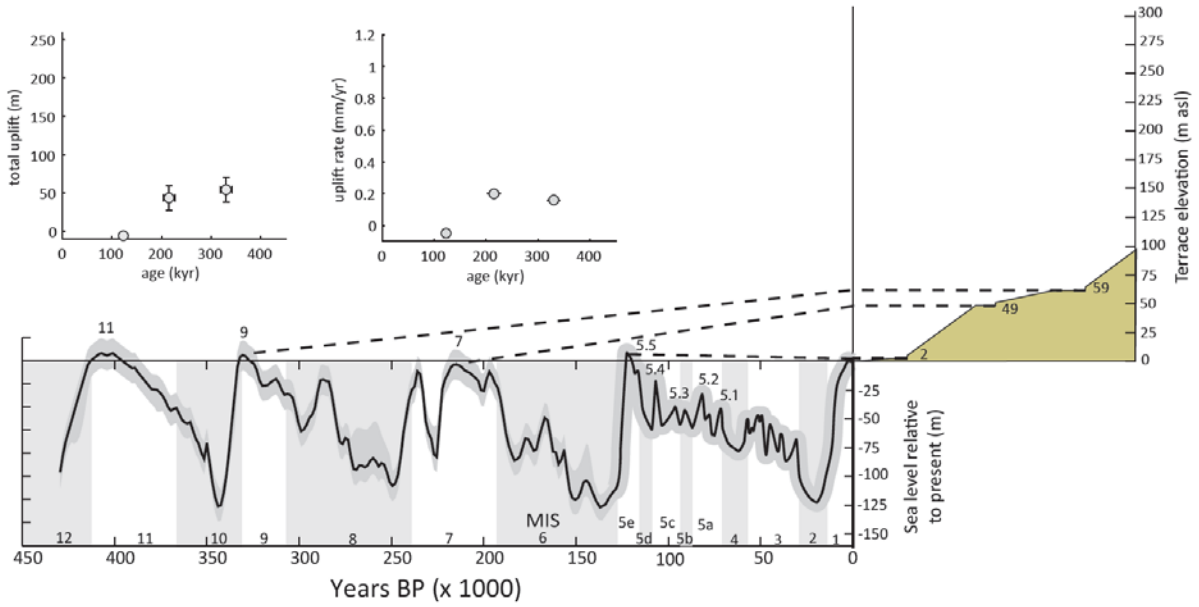

Tertsa (34.993°N, 25.537°E) – Fig. 3, site 17

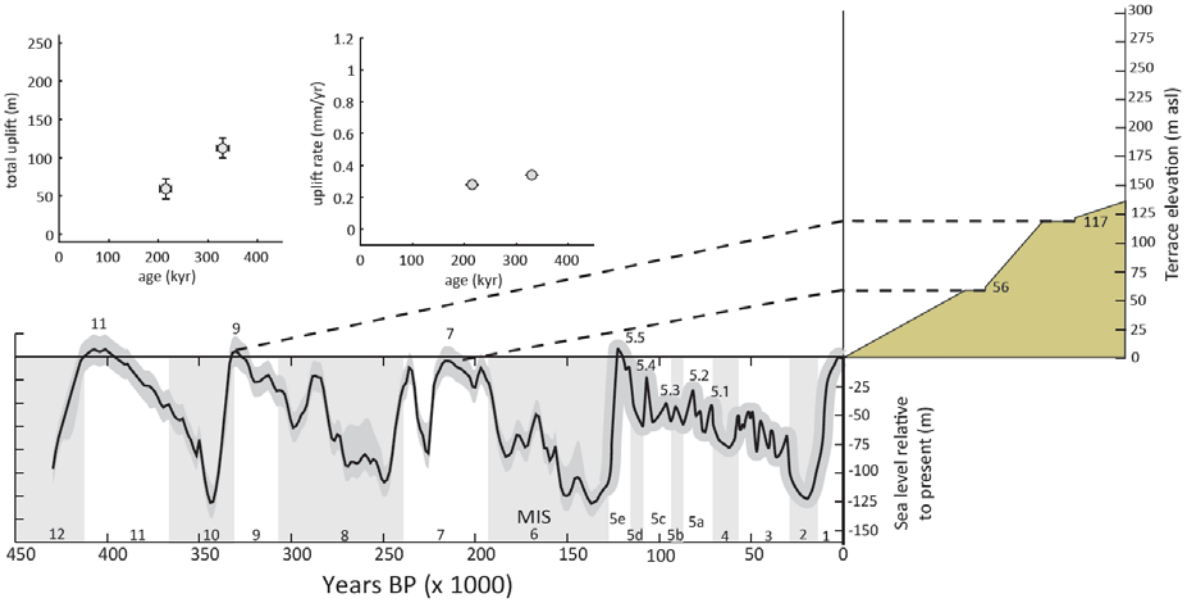

Ierapetra (35.016°N, 25.734°E) – Fig. 3, site 18

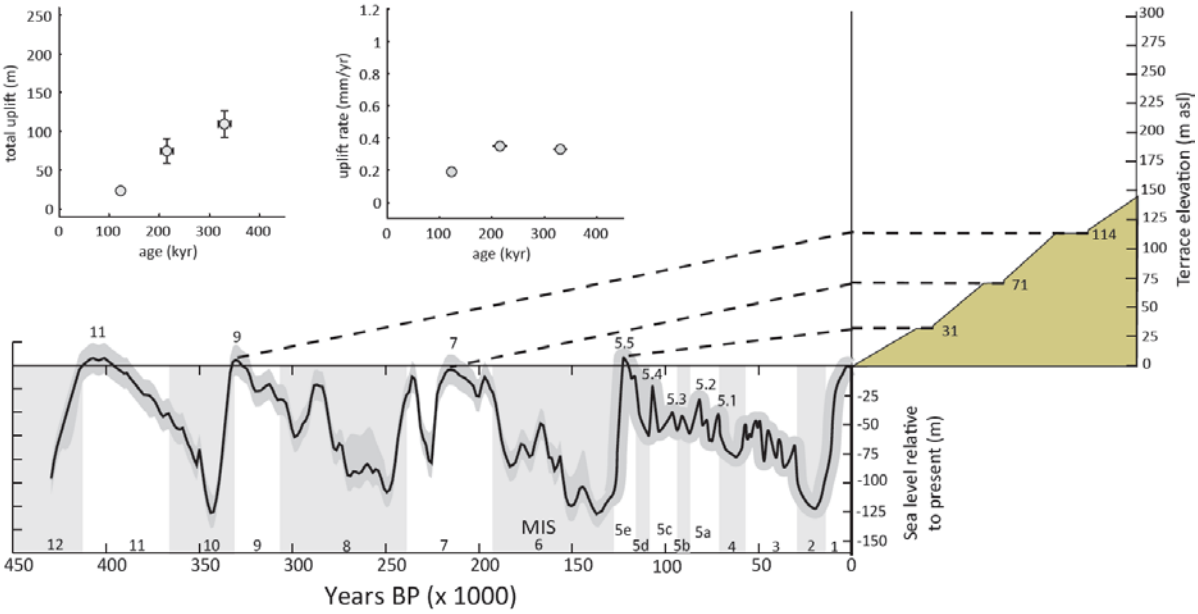

Chapter 3

Evaluating Landscape Response Times and Sensitivity to Temporal Gradients in Rock Uplift and Lithology in the Hellenic Forearc, Crete, Greece

In preparation for submission to *Geomorphology* with the following coauthor:

Wegmann, K.W.[1]

[1] Department of Marine, Earth and Atmospheric Sciences, North Carolina State University, Raleigh, NC, USA.

Abstract

Previously published late Quaternary uplift rates derived from Pleistocene marine terraces are used in conjunction with a suite of landscape metrics derived from a ~30 m horizontal pixel resolution DEM and 1:50,000-scale geologic maps to explore geomorphic response and sensitivity to well-documented rates of vertical tectonics and changes in bedrock geology in South-central Crete, Greece. A suite of drainage basin metrics previously shown to be sensitive to gradients in the rate of rock uplift were extracted from 24 drainage basins in the Asterousia and Dikti Mountains. Their spatial distributions follow a pattern consistent with tectonic displacement along three fault segments at various stages of linkage. In the Asterousia, these metrics are strongly tied to topography, but are only weakly associated with the pattern of late Quaternary rock uplift. The patterns exhibited by the suite of metrics cannot be explained by changes in rock-type alone. These finding suggests that the landscape records a signal of uplift integrated over 10^6 - 10^7 yrs and the geomorphic system has yet to fully adjust or equilibrate to changes in rates of rock uplift that initiated > 400 kyr ago at the eastern end of the Asterousia. Comparison of drainage basin metrics, topography and geology of the Asterousia and Dikti reveals differences in the landscape response to long-term uplift between the two ranges that are best explained by lithologic and hydraulic differences. Flysch-dominated bedrock in the Asterousia promotes hillslope erosion and river incision via fluvial and debris flow processes. Carbonates that underlie the Dikti result in hillslope denudation primarily by dissolution and rock falls and promote the development of karst where river incision occurs predominantly by dissolution. The karstic fluvial system in the Dikti appears to reduce landscape sensitivity to rock uplift in comparison to the Asterousia, possibly dampening, or delaying geomorphic response times to tectonic and climatic forcing.

This study highlights important shortcomings and considerations for extracting tectonic signals from topography. Geomorphic response times in some settings are long (> 10^6 yr) and thus topography may not be representative of the active tectonic regime. Such long estimates of geomorphic response times (> 4 x 10^5 yr) are in line with estimates of analytical and numerical experiments and investigations of landscape evolution at fault tips in natural settings. While not surprising, yet often overlooked, resistant rock-types and karstic fluvial systems apparently reduce the sensitivity of landscapes to tectonic forcing. Thus, caution is required when extracting tectonic signals from topography where large variations in rock type exist, particularly when carbonates are present in semi-arid to arid climate zones, like across the Mediterranean basin. These findings are particularly relevant to tectonic geomorphologists, given the increasingly widespread use of digital elevation models (DEMs) to infer tectonics from topographic proxies.

Introduction

The topography of tectonically active landscapes is the sum of surficial processes and time-integrated tectonic displacements. Geoscientists have focused much effort into extracting tectonic signals from topography (e.g., Bull and McFadden, 1977; Merritts and Vincent, 1989; Snyder et al., 2000; Kirby and Whipple, 2001; Wobus et al., 2006). These studies are often confounded by non-linearity between rock uplift and erosion particularly in high relief settings, variations in rates of deformation, and changes in climate and the physical and chemical properties of bedrock (e.g. Tucker and Slingerland, 1997; Heimsath et al., 1997; Montgomery and Brandon, 2002; Wobus et al., 2010; Dibiase et al., 2012; Dixon et al., 2012). Even in the face of such challenges, detailed field investigations coupled with quantitative analyses of digital elevation models (DEMs) illustrate that non-random relationships exist between the rates of tectonic uplift versus topographic and fluvial drainage basin metrics, suggesting that specific landscape processes (e.g. erosion, channel incision) scale with uplift rates (Merritts and Vincent, 1989; Snyder et al., 2000; Frankel and Pazzaglia, 2005; Wobus et al., 2006; Kirby and Whipple, 2012; *and references therein*). For example, researchers have shown that basin metrics including mean slope, relief, mean elevation, basin area and volume, basin outlet spacing, first order stream gradient, and normalized channel steepness (k_{sn}) often exhibit predictable spatial patterns consistent with relative variations in rates of uplift over what are thought to be 10^5 to 10^7 yr time-scales (e.g., Kirby et al., 2003; Densmore et al. 2004; 2007a; Frankel and Pazzaglia, 2006; Whipple and Meade, 2006; Hilley and Arrowsmith, 2008). Few natural laboratories have been identified, however, where necessary geologic and geomorphic information is preserved in order to accurately determine the landscape response times resulting from changes in tectonic, climatic, or lithologic conditions (e.g. Densmore et al., 2005; Hilley and Arrowsmith,

2008; Palumbo et al., 2010). Due to these limitations, most of our current understanding of landscape response times to spatial and temporal gradients in uplift combined with climate and bedrock controls on topographic sensitivity to tectonics has been gleaned from landscape evolution simulations (e.g. Kooi and Beaumont, 1996; Tucker and Slingerland, 1997; Fernandes and Dietrich, 1997; Densmore et al., 1998; Ellis et al., 1999). At the same time, the widespread availability of high resolution DEMs has made extraction of topographic datasets easy. Thus, despite inherent complexities in interpreting tectonic signals from topography (e.g. Wobus et al., 2006), it is becoming increasingly common to interpret various landscape metrics through the lens of active tectonics, often based on either weakly-tested or untested assumptions.

Range fronts bounded by active extensional faults have been used to interpret both processes and rates of tectonic deformation as well as the influence of rock uplift rates on the geomorphic evolution of landscapes (*reviews in* Keller and Pinter, 2001; Bull, 2007; Burbank and Anderson, 2011). For the purposes of isolating tectonic signals from topography, these settings have become particularly attractive owning to the recognition of proportionality between fault length and displacement (e.g. Cowie and Scholz, 1992, Drawers et al., 1993; Schlische et al., 1996). Furthermore, these and other studies have established simple and predicable patterns for the growth and evolution of extensional fault systems, which are often recognizable by the unique imprint left on topography (Anders and Schlische, 1994; Dawers and Anders, 1995; Gupta and Scholz, 2000; Manighetti et al., 2001, 2005; Gallen et al., *in review*). It is the predictable fault-scaling relationships and patterns of displacement of active extensional faults in particular that provides the necessary framework from which to exploit these settings as windows of understanding into landscape and topographic response to variation in the rates of rock uplift (e.g. Densmore et al., 2004, 2005, 2007a, b; Whitaker and Boulton, 2012).

In this study, we report results from the Asterousia and Dikti Mountains South-central Crete, Greece, where three actively uplifting footwalls are bound by a ~100 km long extensional fault array in (Fig. 1; Gallen et al., *in review*). South-central Crete exhibits unique geologic and geomorphic conditions, allowing us to explore landscape response to temporal gradients in uplift, paired with the importance of contrasting lithologies to a landscape's sensitivity to tectonic forcing. We show that long-term uplift rates are approximately an order of magnitude higher than estimated erosion rates from these mountains, implying that topography represents the long-term (> 10^6 yr) integrated history of uplift and fault displacement. This interpretation is supported by topography that is consistent with expectations for displacement-scaling patterns along three largely independent extensional fault arrays (Gallen et al., *in review*). Pleistocene marine terraces preserved along the two footwalls comprising the Asterousia Mountain front allow for the synthesis of late Quaternary (10^4 to 10^5 yr) rates and patterns of rock uplift with respect to the geoid approximated by eustatic sea level. Along the Asterousia Mountain front, discrepancies exist between the long-term pattern of uplift estimated from topography versus intermediate time-scale uplift determine from marine terraces. The best explanation for this mismatch in uplift rates across different time spans results from the linkage of two fault segments > 400 ky BP, culminating in a rapid increase in the rate of uplift at the eastern end of the range (Gallen et al., *in review*). We utilize this unique circumstance to assess landscape response to changes in the rates of rock uplift. The bedrock geology of the Asterousia and Dikti contrast; the Asterousia are mostly underlain by relatively weak and easily eroded flysch, whereas large portions of the Dikti are composed of resistant carbonates (Fig. 1). We exploit adjacent footwall blocks with distinct rock types to investigate the role lithology plays in the sensitivity of a landscape as a reliable recorder of tectonic signals.

Figure 1: Tectonic and geologic setting of South-central Crete. Inset maps show the location of the study area in South-central Crete and generalized tectonic setting. **a.** Shaded relief map of South-central Crete with active faults shown in black (After Fassoulas, 1994; Peterek and Schwarze, 2004; Gaki-Papanastssiou et al., 2009; Gallen et al., *in review*). Lower-hemisphere equal area projections of fault plane measurements as great circles. Gray dots denote the trend and plunge of slicken-lines. **b.** Hillshade with the 24 drainage basins used in this study (white polygons), the 18 study sites of Gallen et al., *in review* that are keyed to Figure 2, and the area bounding the two swath topographic profiles shown in Figure 2. **c.** digitized 1:50,000-scale geologic maps (Greek Institute of Geology and Mineral Exploration, 1972; 1974; 1977; 1987) with the 24 drainage basins shown in white outline.

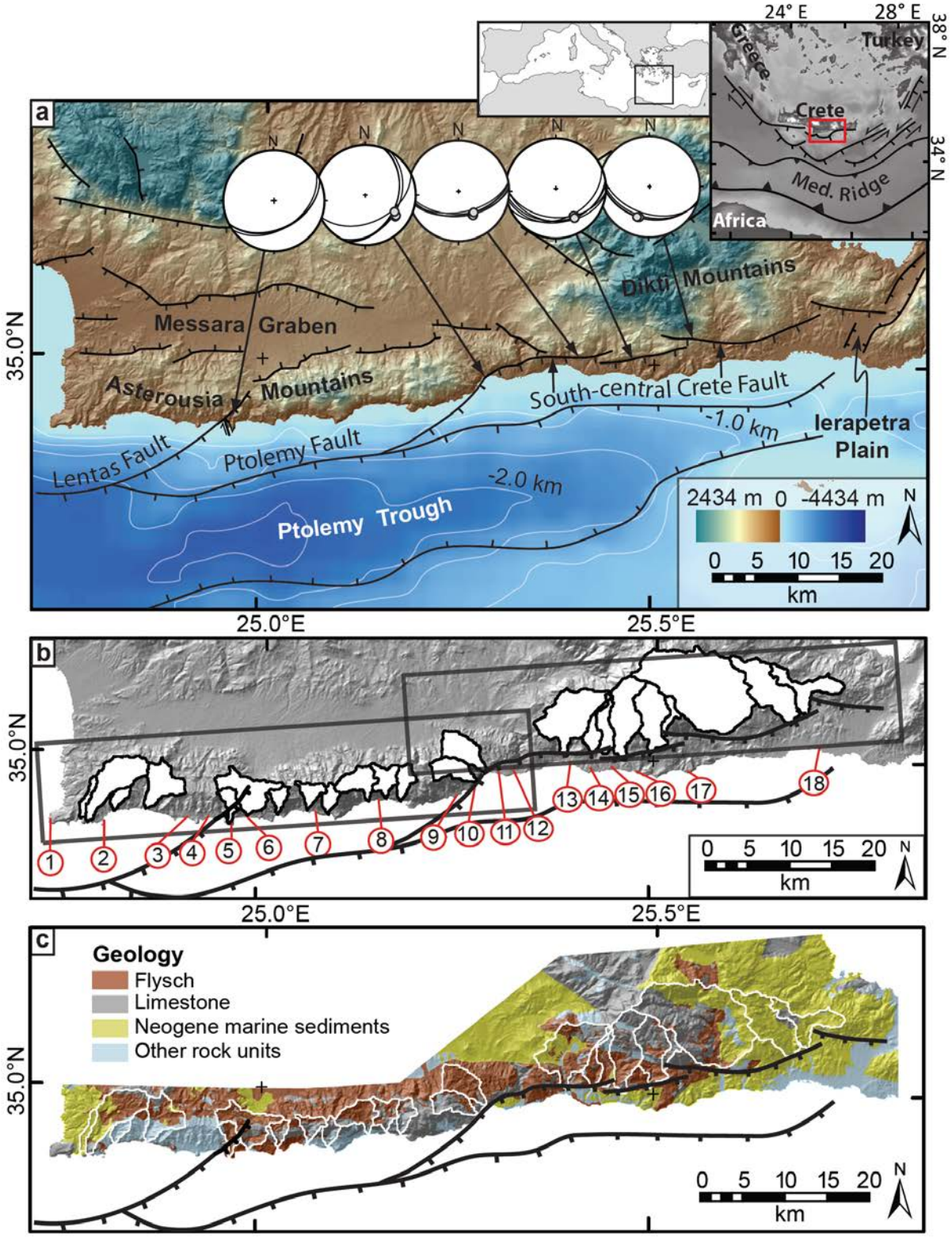
a
24° E
28° E
38° N
34° N
Greece
Turkey
Crete
Med. Ridge
Africa
Dikti Mountains
Messara Graben
Asterousia Mountains
South-central Crete Fault
-1.0 km
Ierapetra Plain
Lentas Fault
Ptolemy Fault
-2.0 km
Ptolemy Trough
2434 m 0 -4434 m
0 5 10 15 20
km
35.0°N
25.0°E
25.5°E
b
1 2 3 4 5 6 7 8 9 10 11 12 13 14 15 16 17 18
c
Geology
Flysch
Limestone
Neogene marine sediments
Other rock units

Background

Tectonic and geologic setting

Studies of arc volcanism (Pe-Piper and Piper, 2002) and seismic tomography (Wortel and Spakman, 2000) from the Aegean and eastern Mediterranean demonstrate that the Hellenic subduction zone has been active since at least 100 Ma in response to the continuous subduction of the Nubian (African) plate (Faccenna et al., 2003; van Hinsbergen et al., 2005). A well-defined Benioff seismic zone is observed to depths of 150 to 180 km below the central Aegean (e.g. Papazachos, 1971; Knapmeyer, 1999; Papazachoset al., 2000). Geodetic studies indicate that the subduction of the African Plate beneath the Eurasian plate continues today and can be resolved into a convergence vector with a velocity of ~ 36 mm yr^{-1} with respect to a fixed European reference frame (McClusky et al., 2000; Reilinger et al., 2006). Long lived convergence has resulted in the growth of a large south-facing accretionary subduction wedge extending from the north coast of Crete to the southern boundary of the aseismic Mediterranean Ridge accretionary complex (Fig. 1; Le Pichon et al., 1979, 1982; Kastens et al., 1992).

Crete is often considered a “rigid backstop” to the Mediterranean Ridge accretionary complex (Le Pinchon et al., 1982; 2002; Kastens, 1992; Huguen et al., 2001; Kopf et al., 2003; Chamot-Rooke et al., 2005). This interpretation, however, fails to account for the observed widespread and active deformation and uplift of this “backstop” since its formation ~ 30 Ma (e.g. Angelier 1978, 1979; Fassoulas et al., 1994; Jolivet et al., 1996). We favor a more encompassing view of the forearc that places Crete and adjacent forearc highs (e.g. the Peloponnese and island of Rhodes) within a larger subduction wedge (Willett et al., 1993; Pazzaglia and Brandon, 2001; Rahl et al., 2005; Fuller et al., 2006; Wegmann, 2008). Continued growth of the orogen north of the

accretionary complex is largely drivien by the basal accretion of material into the wedge by deep underplating along the subduction interface (Anglier et al., 1982; Platt, 1986; Gallen et al., *in review*). Presently, the Hellenic forearc hosts both arc-parallel and arc-normal extensional deformation resulting from widespread crustal tension (i.e. Angelier et al., 1982) that has dominated since the mid Miocene (Joliet et al., 1996; van Hinsbergen and Schmid, 2012). Extension is driven by gravitation instability of the upper crust due to a super critical coulomb wedge (Anglier et al., 1982; Platt, 1986; Gallen et al., *in review*) and lithospheric processes related to the southerly rollback of the African slab that initiated in the Eocene and continues today (Thompson et al., 1998; Faccenna et al., 2003; Jolviet and Brun, 2010).

The island of Crete consists of a sequence of sedimentary nappes imbricated and accreted between ~40 and 30 Ma (Bonneau, 1984; Hall et al., 1984; Meulenkamp et al., 1988). Some of these units were subducted, underplated and rapidly exhumed during the Miocene (~24 to 20 Ma) and are now preserved as high pressure-low temperature phyllite-quartzite nappes on Crete (Seidel et al., 1981; Fassoulas et al., 1994; Jolivet et al., 1996; Ring and Reischmann, 2002; Rahl et al., 2005). Other dominant units found on Crete include Late Miocene to Pliocene marine and terrestrial basin fills (Meulenkamp et al., 1994; Fassoulas, 2001; ten Veen and Kleinspehn, 2003; Peterek and Schwarze, 2004; Zachiasse et al., 2008) and lesser amounts of Quaternary alluvial fans and marine terraces (Angelier, 1979; Pope et al., 2008; Strasser et al., 2011; Gallen et al., *in review*).

Evidence for active deformation and sustained uplift within the forearc is observed on Crete as numerous active extensional faults, deeply incised gorges, steep erosional coastlines, and Quaternary marine terraces now tens of meters above sea level (Angelier, 1979; Pirazzoli et al., 1982; Meulenkamp et al., 1994; Wegmann, 2008; Strasser et al., 2011; Gallen et al., *in review*).

Contemporary faults on Crete are generally high (Bohnhoff et al., 2005) and low-angle extensional faults (Fassoulas et al., 1994) with no active contractional faults exposed at the surface. Recent research has shown that the southern coastlines of Crete are bound by large south-dipping extensional-to-transtensional faults (Gallen et al., *in review*). Crete can thus be described as a horst embedded in an inflating forearc overlying the Hellenic subduction Zone (Anglier et al., 1982; Kreemer and Chamoot-Rooke, 2004; Chamoot-Rooke et al., 2005; Meier et al., 2007; Gallen et al., *in review*).

Climate

The island of Crete is in the Mediterranean climate zone, with cool moist winters and warm dry summers (Rackham and Moody, 1996). Almost all of the rivers draining the Asterousia and Dikti are ephemeral. Mean annual precipitation is ~ 650 mm yr^{-1}, locally increasing to > 1000 mm in the mountain ranges due to orographic lifting (Rackhan and Moody, 1996). Average temperatures are 27° C in summer and 12° C in winter, and winds prevail from the north to northwest year-round, but are strongest during the summer months. Geomorphic studies indicate that the climate on the island was relatively wetter during glacial intervals, evidenced by the deposition of large alluvial fans along the south coast that are temporally consistent with cooler periods in the late Quaternary (Pope et al., 2008; Wegmann, 2008; Gallen et al., *in review*). Interstadial intervals throughout the late Quaternary are thought to be analogous to today's climate.

Geology and Geomorphology of South-central Crete

South-central Crete is comprised of two mountain ranges, the Asterousia and Dikti, bound to the south by three large extensional fault systems (Fig. 1; Gallen et al., *in review*). The lithology of the two ranges contrasts. The Asterousia are mostly composed of pre-Neogene flysch with lesser

amounts of Mesozoic ophiolite and carbonate, and poorly lithified Neogene turbidites (Fig. 1c). The Dikti contain a larger percentage of carbonates and Neogene turbidites relative to the Asterousia, but pre-Neogene flysch units still cover a significant portion of the range (Fig. 1c). The cohesive strength of each rock-type varies greatly, acting as a strong control on local fluvial and hillslope processes. The flysch and ophiolite are strongly deformed and fractured and are thus prone to frequent shallow and sometime deep-seated mass-wasting. Neogene turbidites are generally poorly lithified, weak relative to other units in the study area, and have been tilted and faulted post-deposition. These units are often associated with large both shallow and deep-seated slope failures. Mesozoic carbonates are commonly massive and stand out in relief as the most resistant unit. Carbonates are less prone to mass-wasting than the other lithologies and observed slope failures are most often rock-falls.

The geomorphic system is presently transport-limited; most channel beds having a thin alluvial cover with local patches of exposed bedrock. In the pre-Neogene flysch, ophiolite, and Neogene turbidites the dominant mode of sediment transport is hillslope and fluvial advection. Valleys cut into these units are generally wide and V-shaped with most hillslopes at or near the angle of repose. By contrast, material transport in the Mesozoic carbonated units appears to occur chiefly by chemical dissolution, evidenced by the development of narrow slot canyons and karst drainage. Hillslopes in these units largely denude by dissolution and rock falls.

Previous studies of South-central Crete

A recent synthesis of structural mapping, coastal surveys of Pleistocene marine terraces, new optically stimulated luminescence (OSL) burial dating, previously published U-series dating of marine bivalve shells and the reported occurrence of the warm-water index fossil *Strombus*

bubonius (Angelier, 1979), and correlations to the late Quaternary global sea level curve are used to support a late Quaternary history of rock and surface uplift along the coastline of South-central Crete (Gallen et al., *in review*). This study takes the active formal faults identified by Gallen et al. (*in review*) and divides the coast into three fault-bounded blocks (Fig. 1, 2). The footwalls of two of these faults comprise the Asterousia Mountains with the Lentas and Ptolemy faults forming the subaqueous range front (Fig. 1). These faults are linked and each is > 40 km in length (Fig. 1). The third fault block, the Dikti Mountains, is bound to the south by the ~ 55 km long segmented South-central Crete fault (Figs. 1, 2).

Marine terrace sequences preserved on each fault block are distinct in both number and form, yielding independent uplift histories. Because marine terraces are cut into the footwall of faults in the Asterousia Mountains, direct comparisons can be made between the late Quaternary pattern of uplift, topography and drainage basin metrics. The terraces from both Asterousia fault blocks, the Lentas and Ptolemy blocks, are tilted westward (Fig. 2). Average uplift rates for the footwall of the Lentas fault, derived from marine terrace sequences, vary between 0.3 and 0.7 mm yr^{-1}. The Lentas block uplift rate is highest in the east, at the onshore exposure of the Lentas fault, and decline steadily to zero at the western end of the range (Figs. 2b, c). Average late Quaternary slip rates on the Lentas fault are ~ 0.2 mm yr^{-1} (Gallen et al., *in review*). The Ptolemy fault footwall is rising above sea level at an average rate of 0.65 mm/yr and rates generally increase eastward, from 0.4 to 0.8 mm yr^{-1} before the terraces are truncated by the South-central Crete fault (Fig. 2b). Late Quaternary slip rates at the site of linkage between the South-central Crete and Ptolemy faults are ~ 0.35 mm yr^{-1} (Gallen et al., *in review*). Marine terraces are preserved in the hanging wall, but not

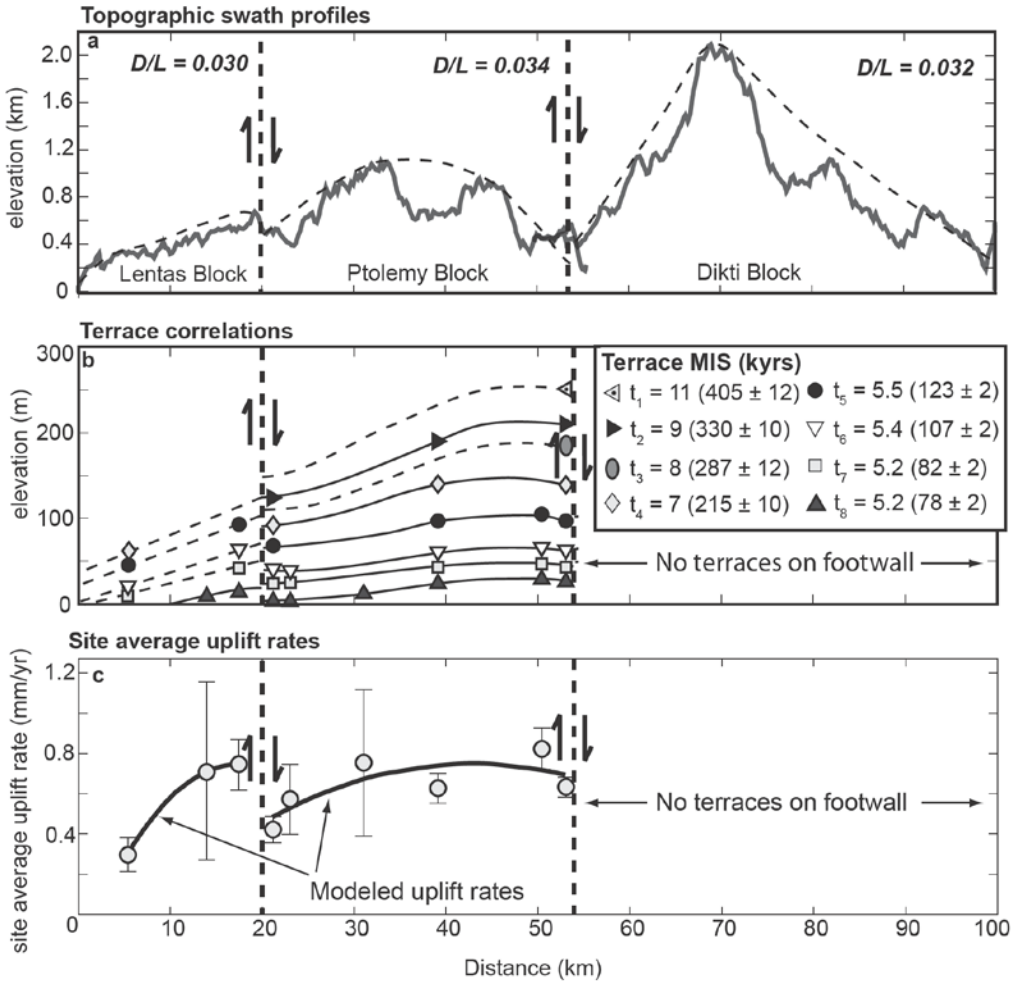

Figure 2: a. Maximum topography of South-central Crete as determined by swath profiles taken along the Asterousia and Dikti Mountains (see figure 1b for location). Dashed lines indicate the profile of maximum displacement as determined by correlation of the highest peaks in the respective fault blocks. Vertical dashed lines mark the location and sense of motion of two large active extensional faults that extend offshore into the Ptolemy trough (see figure 1 for locations)**. b.** Correlation of Pleistocene marine terraces of the same age along the Asterousia coastline (Gallen et al., *in review*). **c.** Site average late Quaternary uplift rate versus mountain range distance for the Asterousia footwall. The site average uplift rates were determined using a Monte Carlo simulation to incorporate all errors associated with elevation measurements and geochronology. Bold black lines are best fit second-order polynomial regressions through the data in each footwall.

the footwall of the South-central Crete fault. Average rock uplift rates in the hanging wall are 0.1 to 0.4 mm yr^{-1} (Angelier, 1979; Gallen et al., *in review*).

There is no definitive evidence of active contractional faults inboard of the Mediterranean Ridge accretionary complex (cf. Meulenkamp et al. 1994; Shaw et al., 2008; Shaw & Jackson, 2010). Regional uplift on the order of 0.55 to 0.8 mm yr^{-1} is thought to be driven by underplating at the base of the subduction wedge. This process apparently outpaces stretching in the upper crust (Angelier et al., 1982; Gallen et al., *in review*), such that even the hanging walls of extensional faults exhibit net vertical uplift. Motion on the three large fault arrays that bound the Asterousia and Dikti Mountains overprints the regional secular uplift signal, giving rise to the patterns of uplift preserved in the topography and quantifiable from late Quaternary marine terrace sequences along the south-central coast of Crete.

Fault growth and linkage

The history of fault-growth and linkage is often recorded in displacement profiles along active faults (Anders and Schlische, 1994; Dawers and Anders, 1995; Gupta and Scholz, 2000; Manighetti et al., 2001, 2005). Faults grow through repeated earthquakes in a self-similar fashion; propagating laterally at their tips while accumulating displacement maxima near their centers (Fig. 3; Drawers et al., 1993). Displacement profiles measured along isolated faults show a large degree of variability (Drawers et al., 1993; Drawers and Anders, 1995; Manighetti et al., 2001, 2005); however, general characteristics emerge such as a maximum in fault displacement observed near fault center that tapers to minima at the fault tips. When adjacent faults begin to overlap their stress fields interact and fault displacement profiles temporarily deviate from typical shapes (Fig. 3).

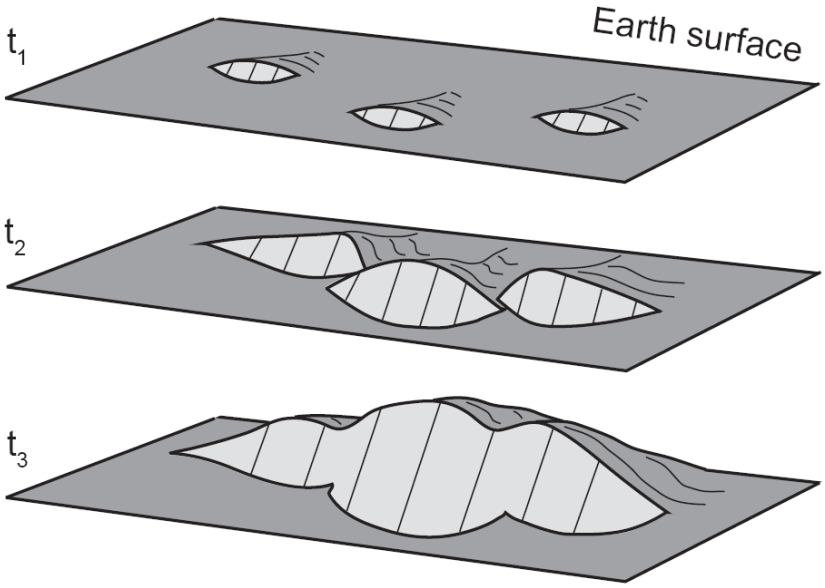

Figure 3: Cartoon showing the growth and linkage of normal faults at three time steps. Initially, faults grown in isolation (t1) and have smooth displacement profiles with maxima near the fault centers that taper to minima at the fault tips. Faults begin to overlap (t2) and their stress fields interact, skewing their displacement profiles. After hard linkage occurs (t3), the now composite fault will recover slip deficits at sites of overlap and linkage, while fault growth continues in a fashion similar to that for single isolated faults (after Anders and Schlische, 1994).

Once overlapping faults mechianically link the displacement profile will rapidly evolve towards a pattern similar to what is observed for a single isolated fault (Fig. 3; Cartwright et al., 1995). Further, field-based and theoretical studies suggest that the maximum vertical displacement, *D*, is linearly related to fault length, *L*, through a scaling constant, *c* (Cowie and Scholz, 1992; Drawers et al., 1993; Schlishe et al., 1996). Based on a global data set of natural fault populations spanning eight-orders of magnitude the value of *c* will vary depending on rock properties and the stress field around the growing fault, with the total range of values being between 0.3 and 0.003, (Schlische et al., 1996).

The fundamental geometric and scaling properties of faults suggest that a systematic relationship exists between the maximum elevations of a fault-bounded mountain range and slip on the controlling fault (Cowie and Scholz, 1992; Dawers et al., 1993; Drawers and Anders, 1995; Cowie and Roberts, 2001). Indeed, active faults have long been observed to leave a unique imprint on topography, while the record of fault slip preserved in topography will become less apparent with time as erosion erases the relationship between fault displacement and maximum range elevation (e.g. Densmore et al., 2004, 2005). Along active faults where uplift far outpaces erosion, however, mountain range topography has been shown to serve as an adequate proxy for long-term vertical fault displacements (e.g. Ander and Schlishe, 1994; Hetzel et al., 2004).

Methods

We used an ASTER-derived 30 m DEM to analyze the topography of South-central Crete. Two 12-km wide swath topographic profiles were extracted from the Asterousia and Dikti Mountains in order to characterize maximum range elevations along fault strike (Fig. 1a, b). Using a topographic envelope approach, we estimated the volume of material eroded from the Asterousia

and Dikti Mountains as a long-term proxy for range-specific erosion rates by fitting a spline interpolation with tension over drainage divides and interfluves that was then smoothed with a 100m focal maximum moving window. The resulting "topographic surface" was differenced from the original 30-m DEM to obtain minimum estimates of the magnitude of mountain scale erosion (Fig. 4). Erosion rates were determined by normalizing the total volume of eroded material as a function of area and dividing it by the approximate time since the mountain range became subaerial, which was determined by dividing the maximum range altitude by the long-term uplift rate (Angelier, 1979; Meulenkamp et al., 1994; Zachiasse et al., 2008; Wegmann, 2008; Gallen et al., *in review*).

Twenty-four drainage basin were delineated, 15 in the Asterousia and 9 in the Dikti, using the flow direction and flow accumulation algorithms from the Hydrologic modeling toolbar in ArcGIS 9.3. Only basins draining ≥ 3 km^2 were analyzed because it has been shown that ephemeral streams, such as those on Crete, have difficulty responding to tectonic forcing at small drainage areas (e.g. Frankel and Pazzaglia, 2005). We defined the initiation points of the fluvial network in each basin at ~1 km^2, where we observed a break in local channel slope versus contributing drainage area. This scaling break is often interpreted as the along-channel transition from hillslope and landslide dominated erosional processes to the portion of the channel where erosion occurs primarily by fluvial processes (e.g. Montgomery and Foufoula-Georgiou, 1993; Wobus et al., 2006).

We extracted a suite of commonly used topographic and drainage basin metrics shown to have sensitivity to spatial gradients of uplift from the DEM. These metrics were plotted as a function of basin outlet distance from the western end of the Asterousia (Fig. 5). Topographic

metrics include total basin relief, mean basin slope and hypsometric integral (HI), which is approximated by the equation:

$$HI = E_{mean} - E_{min}/(E_{max} - E_{min}) \quad (1)$$

where E_{max}, E_{mean}, and E_{min} are the maximum, mean, and minimum elevations for the basin, respectively (Pike and Wilson, 1971).

For fluvial metrics we utilize the gradient of first-order channels (Strahler, 1957), and the normalized steepness index (k_{sn}). Both first-order channel gradient and k_{sn} have been shown to be sensitive indicators of the relative rates of uplift (e.g., Merritts and Vincent, 1989; Snyder et al., 2000; Kirby and Whipple, 2003). The normalized steepness index, in particular, is becoming a common and widely used metric to evaluate relative tectonic activity in erosional landscapes (Kirby and Whipple, 2012). The k_{sn} approach normalizes stream channel gradient to contributing drainage area so that the steepness of rivers draining drastically different areas can be directly compared (e.g. Snyder et al., 2000; Kirby et al., 2003). Stream steepness (k_s) is defined by the empirically derived equation that describes the shape of a stream's longitudinal profile as a power-law function relating drainage area (A) and slope (S) such that,

$$S = k_s A^{-\theta} \quad (2),$$

where θ is channel concavity (e.g., Flint, 1974). Using a reference stream concavity (θ_{ref}) of 0.45, we calculated k_{sn} for each 30 m^2 pixel along channels draining areas ≥ 1 km^2 after averaging channel slope in 250 m increments (e.g. Wobus et al., 2006; Kirby and Whipple, 2012), where

$$k_{sn} = SA^{\theta ref} \quad (3).$$

We used 1:50,000-scale geologic maps to evaluate the role of lithology on topography and drainage basin metrics (Fig. 1c; Greek Institute of Geology and Mineral Exploration, 1972; 1974; 1977; 1987). The geologic maps were digitized and rock types classified as pre-Neogene flysch and carbonate, Neogene turbidites, or other, which comprises ophiolite, phyillite-quartzite nappes, and Quaternary deposits that collectively comprise < 10 % of the study area (Figs. 1c, 5). The percent area underlain by the different lithologies in each drainage basin was calculated in a geographic information system (GIS) and plotted as a function of distance from the western end of the Asterousia (Fig. 5).

Late Quaternary uplift rates derived from dated marine terrace sequences were used to model uplift rate as a function of distance along the coast (Fig. 2c). Site-specific average uplift rates were determined using all terraces, geochronologic age constraints, and assigned ages for a given terrace flight from Gallen et al. (*in review*). A Monte Carlo sampling approach was adopted based upon the assumption of normally-distributed sources of error because it allowed for the appropriation of all uncertainties resulting from the present elevation of a terrace, its geochronologic age, and eustatic elevation and age uncertainties at the time of terrace formation. For each study site random samples from each theoretical measurement were used to calculate the total change in the elevation of each individual terrace in a given flight since formation and a linear regression through the data was preformed. For each of the 18 study sites five-thousand of Monte Carlo-regression simulations were carried out to determine site average uplift rates and assign 1-σ uncertainties to the derived uplift rates. Second-order polynomial regressions were used to model average late Quaternary uplift at the drainage basin outlet locations along the coast (Fig. 2c).

Application of the Pearson's correlation coefficient quantifies the relationship between topographic and fluvial drainage basin metrics, maximum range altitude, and lithology for both the Asterousia and Dikti Mountains. Additionally, modeled late Quaternary uplift rates from the Asterousia were compared to all other metrics of that range. Those that had p-values ≤ 0.05 were considered significant. Correlation matrices provide the basis from which to discriminate the relative importance between gradients in long-term uplift versus the relative contribution of lithology to the modern topography of the Asterousia and Dikti Mountains.

Results

We estimate that the Asterousia and Dikti Mountains emerged above sea level between 1.2 to 4.6 and 2.2 to 7.3 Ma, respectively. The rock mass eroded since that time is ca. 29 km^3 in the Asterousia and 43 km^3 in the Dikti (Fig. 4), indicating that the time-averaged rate of erosion varies between 17 to 59 m my^{-1} and 13 to 45 m my^{-1} for the two ranges, respectively. These erosion rate estimates are an approximate order of magnitude lower than the slowest rates of uplift determined for Crete during the late Cenozoic (e.g. Angelier, 1979; Meulenkamp et al., 1994; Zachiasse et al., 2008; Gallen et al., *in review*). The length of the three range-front faults versus the maximum range elevations is ~ 0.03 for each footwall, consistent with expectations for fault displacement based on fault-scaling properties (Fig. 2a; Cowie and Scholz, 1992; Drawers et al., 1993; Schlishe et al., 1996).

The topographic and fluvial drainage basin metrics show distinct patterns associated with the three fault-bounded blocks. To a first-order, metric values reach maximums near the fault centers, tapering to lower values closer to the fault tips (Fig. 5). This pattern is not as clear in the western Lentas block, where most metric values increase steadily until reaching the on-shore

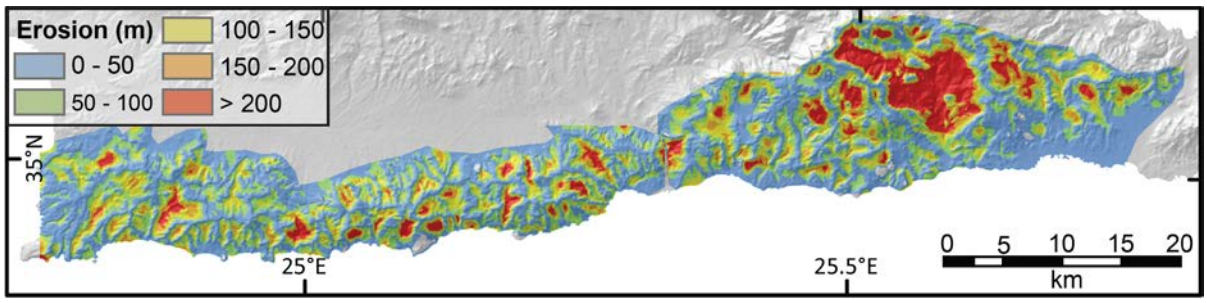

Figure 4: Estimates of vertical bedrock erosion from the Asterousia and Dikti ranges. Calculations are based on a smoothed spline fit with tension (value of 10) applied across drainage divides and interfluves in each range. The volume of "missing bedrock" is 29 and 43 km^3 for the Asterousia and Dikti, respectively, and represents a minimum of eroded bedrock in each range.

exposure of the Lentas fault (Fig. 5). In the Ptolemy and Dikti Mountains blocks, this pattern is clear in all metrics except for the hypsometric integral, which is more variable (Fig. 5).

All Asterousia basin metrics are significantly and strongly correlated to the maximum elevations of the range at 95 percent. Mean slope, basin relief, and normalized steepness index correlate to modeled late Quaternary uplift rates at significant levels, while first order channel gradient and hypsometric integral do not. These correlations, however, are not as strong as with topography (Fig 5; Table 1). In the Dikti Mountains, only basin relief shows significant positive correlations to topography. The other basin metrics positively correlate with topography, but not significantly, following similar albeit lower-amplitude trends (Fig. 5; Table 2). No significant correlation is noted between the basin metrics and range lithologies, with the exception of first-order stream gradient and carbonates in the Dikti Mountains. In both ranges, most all basin metrics are positively correlated at 95 percent confidence with one another, with the exception of the hypsometric integral.

In the Asterousia, only pre-Neogene flysch and Neogene turbidites show significant, albeit weak, correlations to topography (Fig. 5; Table 1). In the Dikti, flysch and carbonates are significantly correlated to maximum range elevations, while Neogene sediments exhibit a significant negative correlation to topography (Fig. 2, 5; Table 2).

Discussion

Landscape metrics and uplift over long and intermediate time-scales

In South-central Crete, estimated erosion rates are approximately an order of magnitude lower than long-term uplift rates, suggesting that the maximum altitude of the Asterousia and Dikti

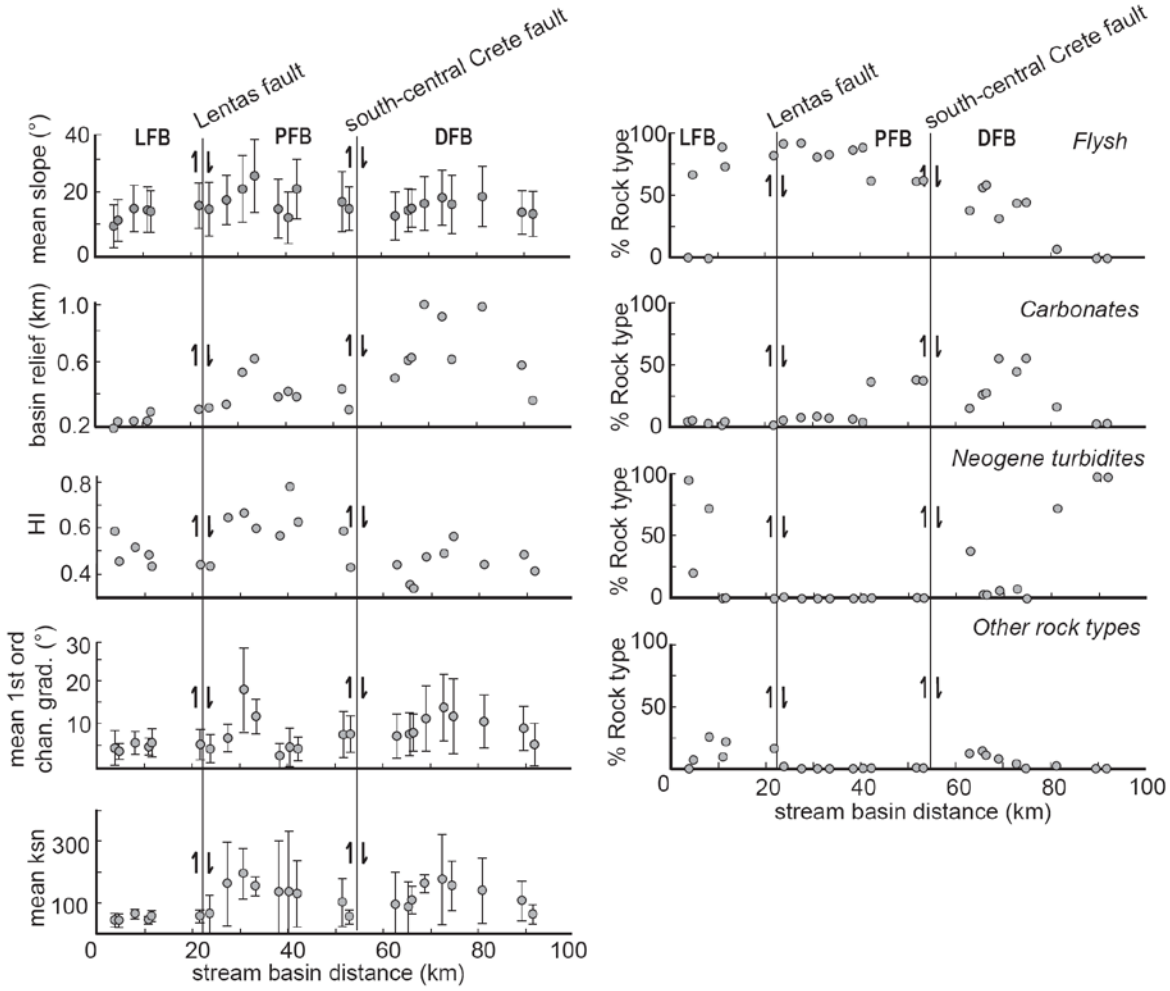

Figure 5: Topographic and fluvial drainage basin metrics and rock-type percentages for each of the 24 catchments plotted as a function of distance along the south-central Cretan coast from west-to-east (see Figure 1 for reference). The location and sense of motion of the two major active faults are shown as thin vertical lines and the Lentas (LFB), Ptolemy (PFB), and Dikti (DFB) fault blocks are labeled. Reported 1-σ errors are shown for the plots of mean slope, first-order channel gradient, and normalized channel steepness indices (k_{sn}). Note that all basin metrics show distinct patterns associated with each fault bounded block, where as rock-type percentages do not. See tables 1 and 2 for correlation matrices.

Mountains is a suitable proxy for the long-term integrated uplift history along their fault-bounded segments (Fig. 2a; cf. Hetzel et al., 2004). This assertion is supported by the pattern of topography and fault length-to-displacement ratios that are consistent with global expectations of fault displacements (Cowie and Scholz, 1992; Drawers et al., 1993; Anders and Schlische 1994; Dawers and Anders 1995; Schlishe et al., 1996; Gupta and Scholz 2000; Manighetti et al., 2001, 2005).

Surprisingly, all of the landscape metrics in the Asterousia are more strongly correlated to the long-term integrated history of uplift expressed in topography than to the intermediate record of rock uplift derived from the marine terraces (Table 1). We interpret observation this as the result of linkage of the Ptolemy and South-central Crete faults at the eastern end of the Asterousia. It is likely that the increase in uplift rate associated with fault linkage occurred rapidly, in a geological sense, affecting drainage basins across the linkage zone similarly (e.g. Gupta et al., 1998). The geomorphic system in the footwall of the Ptolemy fault has not fully responded to the change in the rate of uplift that initiated ≥ 400 kyBP, suggesting that this landscape preserves a record of long-term vertical displacement in the footwalls of the active fault segments.

Interestingly, the patterns exhibited by the topography, basin metrics and marine terraces of the Lentas footwall differ from that of the Ptolemy (Figs. 2, 5). In the Lentas footwall, the patterns of topography and late Quaternary uplift rates are similar; both exhibit a skewed pattern with highest values east of fault center, indicative of linkage between the Ptolemy and Lentas faults (Fig. 2; cf. Cartwright et al., 1995). All of the basin metrics extracted from the six catchments draining this footwall, with the exception of hypsometric integral, mimic this skewed pattern of displacement (Fig. 5). The consistency between topography, marine terraces and basin metrics indicates that fault linkage and its concomitant change in the rate of rock uplift occurred at time in the past that is greater than, or equal to the time required for river system and hillslope

Table 1: Asterousia Mountain basin metrics and topography correlation coefficients

	Maximum elevation	Mean slope	Relief	HI[1]	1st ord.[2]	ksn	flysch	carbonate	Neogene	other units	LQ up[3]
Maximum elevation	1										
mean slope	0.84*	1									
relief	0.86*	0.83*	1								
HI[1]	0.58*	0.27	0.51	1							
1st ord[2]	0.61*	0.65*	0.70*	0.30	1						
ksn	0.90*	0.69*	0.82*	0.77*	0.60*	1					
flysch	0.54*	0.33	0.45	0.08	0.13	0.40	1				
carbonate	0.12	0.29	0.21	0.04	0.09	0.10	-0.07	1			
Neogene	-0.56*	-0.47	-0.52	-0.03	-0.20	-0.40	-0.92*	-0.25	1		
other units	-0.47	-0.23	-0.46	-0.51*	-0.21	-0.51	-0.32	-0.39	0.26	1	
LQ up[3]	0.68*	0.59*	0.65*	0.34	0.27	0.60*	0.57*	0.30	-0.74*	-0.17	1

Notes: * denotes significant correlation at 95% confidence

[1] Hypsometric integral (HI)

[2] First order stream gradient (1st ord.)

[3] Modeled late Quaternary uplift rate from marine terraces (LQ up)

Table 2: Dikti Mountain basin metrics and topography correlation coefficients

	Maximum elevation	Mean slope	Relief	Hyps. Int.	1st ord.	ksn	flysch	Carbonate	Neogene	other units
Maximum elevation	1									
mean slope	0.50	1								
Relief	0.67*	0.88*	1							
HI	-0.03	0.33	0.24	1						
1st ord.	0.54	0.84*	0.79*	0.64*	1					
ksn	0.29	0.73*	0.56*	0.52	0.79*	1				
flysch	0.67*	0.09	0.11	-0.25	0.22	0.28	1			
Carbonate	0.81*	0.56	0.56	0.43	0.74*	0.57	0.61	1		
Neogene	-0.84*	-0.31	-0.35	0.02	-0.46	-0.43	-0.94*	-0.84*	1	
other units	0.53	-0.27	-0.01	-0.65	-0.26	-0.19	0.71*	0.11	-0.56	1

Notes: * denotes significant correlation at 95% confidence

[1] Hypsometric integral (HI)

[2] First order stream gradient (1st ord.)

equilibration. Based on this evidence, we suggest that the fault arrays bounding the south-central coastline of Crete have a long history of fault growth and linkage. The Lentas and Ptolemy faults were the first to link, and the landscape has had enough time to equilibrate to local rates of uplift. More recently, the Ptolemy and South-central Crete faults linked, yet the landscape is still in disequilibrium with the newly imposed rates of tectonic uplift following linkage.

The strong correlation between landscape metrics and topography in the Asterousia, relative to the record of late Quaternary uplift, is likely a result of long geomorphic lag times. The semi-arid and slowly eroding Cretan environment leads to a decoupling of tectonic and geomorphic systems because river incision is insufficient in keeping pace with uplift, due to low and ephemeral stream discharge (e.g. Frankel and Pazzaglia, 2005). This finding is important for researchers seeking to extract tectonics from topography, because signals encoded in the landscape may not reflect the active rock displacement field. Based on the results of this study, for example, we suggest that at sites of fault linkage the landscape is insensitive to rate changes in vertical tectonics over at least 10^5 yrs. It may take $\geq 10^6$ yrs for the landscape to fully equilibrate to new tectonic conditions. Importantly, this estimate is in line with many studies using quasi-physically based numerical models to simulate landscape response to tectonic forcing (e.g. Densmore et al., 2007a; Allen, 2008).

The role of lithology on landscape sensitivity

Carbonates in the Dikti exhibit significant positive correlations to topography (Table 2), but several observations imply that this relationship is coincidental rather than causal. First, highly erodible pre-Neogene flysch units are also significantly correlated with topography (Table 2). Second, while an inverse relationship is observed between Neogene turbidites and topography, the three easternmost basins have mean elevations between 0.5 to 1.2 km and are 75 to 100%

underlain by these weak sedimentary rocks (Figs. 1c, 5). These observations in concert with the consistency of topography with fault displacement and scaling patterns support our earlier assertion that the altitudes of the Dikti are predominantly the result of displacements along the South-central Crete fault rather than variable erodibility of different rock units.

We interpret the along strike basin-metric patterns of the Dikti as a reflection of long term uplift along the South-central Crete fault. This assertion is founded on the observations that all of the basin metrics, besides hypsometric integral, exhibit strong correlations to one another, do not exhibit clear relationships to different rock-types, and follow along-strike patterns consistent with displacement along an active extensional fault (Fig. 5; Table 2). These findings indicate that basin metrics here are responding to similar forcing. The simplest explanation for the apparent decoupling between the long-term records of uplift preserved in topography and the landscape metrics sensitive to local rates of uplift in the Dikti is the presence of carbonates and the development of karst hydrology.

The percentage of carbonates is significantly higher in the Dikti than in the Asterousia, which is predominantly underlain by flysch. These lithologies control the development of the fluvial system of each range. In the Asterousia, hillslopes denude largely by advection and most rivers flow over alluvium with locally-exposed bedrock patches, draining directly into the sea. The geomorphic system of the Asterousia is more similar to that assumed in typical landscape evolution models (e.g., Tucker and Slingerland, 1997; Fernandes and Dietrich, 1997; Densmore et al., 1998; Ellis et al., 1999). In contrast, the Dikti exhibit numerous features characteristic of karst such as internally drained basins, caves and springs, and deep slot canyons in carbonate. We speculate that the process of dissolution associated with karstic systems is a less effective mechanism of river incision

relative to other processes such as plucking, abrasion and cavitation (e.g. Whipple et al., 2000). Further, in karstic fluvial systems discharge may actually decease downstream as surface water is lost to the subsurface (Allan, 1995; O'Driscoll and DeWalle, 2006). If true, specific stream metrics such as k_{sn} should be avoided when carbonates are present because the assumption that upstream contributing drainage area scales with river discharge is violated. These findings imply that the development of karst reduces the ability of landscapes to response to rock uplift, and thus increase geomorphic response times that in turn decrease landscape sensitivity to tectonic signals. This finding highlights limitations in current knowledge of how karstic fluvial systems reflect tectonic signals.

Implications for landscape evolution and tectonics from topography

One of the unforeseen outcomes of this study is the observation of a decoupling of the geomorphic system and active tectonic displacement fields observed in South-central Crete versus what has been reported for other extensional fault arrays, such as the U.S. Basin and Range. In their Basin and Range-based research, Densmore et al (2004, 2005, 2007a) find that topography and cumulative displacement on active extensional faults become decoupled along fault strike. Topographic relief and normalized channel steepness (k_{sn}) are only sensitive to gradients in vertical displacement from the fault tip to ~ 15 km towards the center of the fault. The authors attribute this "fault tip scaling" to the geometry and spacing of faults that impose external boundary conditions on drainage basin development and the establishment of a flux steady state, *sensu lato* Willet and Brandon (2002), toward the core of the range.

There are several possible reasons why fault tip scaling is not observed in South-central Crete. First, the faults are not as "mature" as those studied by Densmore et al (2004, 2005, 2007a).

The fault array studied in this investigation is ~ 100 km in length and hard linkage of all segments is incomplete. The faults studied in the Basin and Range are all ~ 150 km in length and linkage of all segments is argued to be complete. Perhaps allowed enough time, fault tip scaling will apply once decoupling of the tectonic displacement field and topography occurs as relief increases and threshold hillslopes develop, allowing erosion then to keep pace with uplift rates (e.g. Montgomery and Brandon, 2002). Second, the depth of the seismogenic crust beneath Crete is ~ 20 km (Becker et al., 2006). Brittle crust of this thickness may result in a larger range half width than observed in the Basin and Range were crustal elastic thickness is as thin as ~ 10 km in places (Jackson and White, 1989). If correct, the tip scaling length in Crete would be greater than that in the Basin and Range, and the studied fault segments may simply be too short for tip-scaling relationships to apply. Finally, fault tip scaling is not only a function of tectonic and structural boundary conditions, but it is also dependent of erosional efficiency of the landscape (Densmore et al., 2004). In Crete, we argue erosional efficiency is particularly low, primarily due to the semi-arid climate and is further enhanced by the presence of climatically-resistant lithologies, like limestone. Landscapes will respond sluggishly to changes in the tectonic displacement field when rivers struggle to keep pace with uplift. While none of the above explanations are mutually exclusive, our favored interpretation for the absence of observed fault tip scaling in South-central Crete relies on reduced erosional efficiency due to climate and lithology. This is based on the findings that rates of long-term uplift outpace the estimated rate of erosion by a factor of 10 along with the reduction in topographic sensitivity to tectonic displacements in the carbonate-dominated Dikti Mountains (Fig. 5).

Interestingly, the landscape remains coupled with the long-term tectonic displacement field despite strong orographic gradients in precipitation along fault strike, particularly in the Dikti (e.g.

Rackham and Moody, 1996). As postulated by Densmore et al. (2004; 2007a), enhanced precipitation at higher altitudes near fault center should act to enhance erosional efficiency over time-scales relevant to the evolution of the fault systems and associated topography. Such precipitation gradients should act as a negative feedback, decreasing the time required to reach a flux steady state in the center of the mountain range. Herein, we argued that a flux steady-state has not been reached because relief, among other topographic and drainage basin metrics, show no evidence of obtaining uniform "threshold" values approaching the midpoint of any of the faults studied (Fig. 5). This evidence coupled with the finding that the landscape in the Asterousia has not yet responded to increased rates of uplift that initiated > 400 kyBP ago suggests that a substantial geomorphic lag time to tectonic and possibly climatic forcing exists on Crete. These findings emphasize that topography does not always represent the modern tectonic displacement field, especially in slowly-eroding landscapes, which may preserve tectonic signals from 10^6 to 10^7 yr BP.

The findings presented in this paper are important for those researchers looking to infer tectonic signals from topography. The recognition of long response times may be a disadvantage to those seeking to use topography to infer the active tectonics of a region; however, they can be advantageous when topography is used in conjunction with other approaches to look at erosion and displacement over different timescales. For example, the use of topography, drainage basin metrics, and marine terraces in this study allows for inferences to be made about the growth history of the fault array that bounds the south-central coast of Crete. Caution is required before making interpretations of tectonic signals, particularly in carbonate dominated regions, as the geomorphic system may operate under entirely different conditions from what is typically assumed. Based on our results, the efficiency of erosion will dictate how sensitive the landscape is to tectonic forcing. It

is hypothesized that higher erosional efficiency in a landscape will increase the coupling of active tectonics and topography, whereas lower erosional efficiency, as in the semi-arid Cretan landscape, will cause significant lag times.

Conclusions

The south-central coast of Crete is bound by three large-scale (10's of km's long) south-dipping predominantly extensional dip-slip faults (Gallen et al., *in review*). Topography along all three fault segments is consistent with patterns and scaling of vertical displacement across three fault segments that are at different stages of interaction and linkage (Fig. 2). Erosion rates from the ranges bounded by these three faults are approximately an order of magnitude lower than long-term regional uplift rates, supporting the assertion that topography serves as a proxy for the long-term (> 10^6 yr) record of relative uplift (Figs. 1, 2). The late Quaternary pattern of uplift along the footwalls of two fault segments, as recorded in uplifted late Pleistocene marine terraces, differs from the along-strike topography (Fig. 2). The best explanation for this mismatch is rapid accumulation of displacement at the site of fault linkage (cf. Cartwright et al., 1995; Gupta et al., 1998) between the Ptolemy and South-central Crete faults.

Drainage basin metrics that have previously been shown to be sensitive to relative gradients in vertical rock uplift show no significant correlations to changes in lithology, but most are strongly correlated to one another and follow patterns consistent with displacement along three fault segments. From these observations we conclude that basin metrics are a reflection of uplift over long timescales (>10^6 yr). Topography is strongly correlated with basin metrics in the Asterousia and less so in the Dikti. Lithology is not a first-order control on the topography of South-central Crete, but is an important player in determining landscape sensitivity to tectonic forcing. Fault-tip scaling

properties (cf. Densmore et al., 2004; 2005; 2007a) are not observed in South-central Crete. Explanations for the absence of fault-tip scaling include incomplete linkage of the fault array, thick (~20 km) seismogenic crust, and low landscape erosional efficiency resulting from a combination of lithology (carbonates) and regional climate.

Discrepancies between the long-term records of uplift observed in drainage basin metrics and topography versus the late Quaternary pattern of uplift in the Asterousia are best explained by long geomorphic response time to temporal gradients in rock uplift, at a minimum 4×10^5 and likely $> 10^6$ yr. It is argued that the development of karst hydrology will further enhance geomorphic lag time and dampen tectonic signals encoded in topography. These findings highlight the fact that topography and landscape do not necessarily represent the active tectonics of a given setting, as is sometimes assumed. Nonetheless, valuable information can be gleaned from an assessment of the tectonic signals encoded in topography when compared to geomorphic markers that integrate vertical motions over shorter time intervals.

Acknowledgements

Acknowledgment is made to the Donors of the American Chemical Society Petroleum Research Fund for primary support of this research under grant #50792-DNR8. Additional support was provided by the National Science Foundation Continental Dynamics program awards #0208652 and #0207980, and a 2010 Geological Society of America Graduate Student Research Grant to Gallen. We would also like to thank the Institute of Geology & Mineral Exploration in Greece for granting us permition to carry out field work on Crete. Nicholas Panzera is thanked for his hard work in digitizing the geologic map of South-central Crete.

References

Allan, J.D., 1995. Stream ecology: structure and function of running waters. Kluwer Academic Pub.

Allen, P.A., 2008. Time scales of tectonic landscapes and their sediment routing systems. Geological Society, London, Special Publications, 296(1): 7-28, doi: 10.1144/sp296.2.

Anders, M.H. and Schlische, R.W., 1994. Overlapping faults, intrabasin highs, and the growth of normal faults. Journal of Geology, 102(2): 165.

Angelier, J., 1978. Tectonic evolution of the Hellenic arc since the late Miocene. Tectonophysics, 49(1-2): 23-36.

Angelier, J., 1979. Recent quaternary tectonics in the Hellenic arc; examples of geological observations on land; recent crustal movements. Tectonophysics, 52(1-4): 267-275.

Angelier, J., Lybéris, N., Pichon, X.L., Barrier, E. and Huchon, P., 1982. The tectonic development of the Hellenic arc and the Sea of Crete: A synthesis Tectonophysics, 86(1-3): 159-196.

Becker, D., Meier, T., Rische, M., Bohnhoff, M. and Harjes, H.-P., 2006. Spatio-temporal microseismicity clustering in the Cretan region. Tectonophysics, 423(1-4): 3-16.

Bohnhoff, M., Harjes, H.-P. and Meier, T., 2005. Deformation and stress regimes in the Hellenic subduction zone from focal Mechanisms. Journal of Seismology, 9(3): 341-366.

Bonneau, M., 1984. Correlation of the Hellenide nappes in the south-east Aegean and their tectonic reconstruction. Geological Society, London, Special Publications, 17(1): 517-527, doi: 10.1144/gsl.sp.1984.017.01.38.

Bull, W.B., 2007. Tectonic Geomorphology of Mountains: A New Approach to Paleoseismology, 316. Blackwell Publishing, Malden, MA.

Bull, W.B. and McFadden, L.D., 1977. Tectonic geomorphology north and south of the Garlock fault, California, Geomorphology in Arid Regions. Proceedings of the Eighth Annual Geomorphology Symposium, State University of New York, Binghamton, NY, pp. 115-138.

Burbank, D.W. and Anderson, R.S., 2011. Tectonic Geomorphology. Wiley-Blackwell, 480 pp.

Cartwright, J.A., Trudgill, B.D. and Mansfield, C.S., 1995. Fault growth by segment linkage: an explanation for scatter in maximum displacement and trace length data from the Canyonlands Grabens of SE Utah. Journal of Structural Geology, 17(9): 1319-1326.

Chamot-Rooke, N., Rangin, C., Le Pichon, X. and the DOTMED working group, 2005. DOTMED: Deep Offshore Tectonics of the Mediterranean. Les Mémoires de la Société Géologique de France, 177: 64.

Cowie, P.A. and Roberts, G.P., 2001. Constraining slip rates and spacings for active normal faults. Journal of Structural Geology, 23(12): 1901-1915.

Cowie, P.A. and Scholz, C.H., 1992. Physical explanation for the displacement-length relationship of faults using a post-yield fracture mechanics model. Journal of Structural Geology, 14(10): 1133-1148.

Dawers, N.H. and Anders, M.H., 1995. Displacement-length scaling and fault linkage. Journal of Structural Geology, 17(5): 607-614.

Dawers, N.H., Anders, M.H. and Scholz, C.H., 1993. Growth of normal faults: Displacement-length scaling. Geology, 21(12): 1107-1110, doi: 10.1130/0091-7613(1993)021<1107:gonfdl>2.3.co;2.

Densmore, A.L., Gupta, S., Allen, P.A. and Dawers, N.H., 2007a. Transient landscapes at fault tips. Journal of Geophysical Research, 112(F3): F03S08, doi: 10.1029/2006jf000560.

Densmore, A.L., Allen, P.A. and Simpson, G., 2007b. Development and response of a coupled catchment fan system under changing tectonic and climatic forcing. Journal of Geophysical Research, 112(F1): F01002, doi: 10.1029/2006jf000474.

Densmore, A.L., Dawers, N.H., Gupta, S. and Guidon, R., 2005. What sets topographic relief in extensional footwalls? Geology, 33(6): 453-456, doi: 10.1130/g21440.1.

Densmore, A.L., Dawers, N.H., Gupta, S., Guidon, R. and Goldin, T., 2004. Footwall topographic development during continental extension. Journal of Geophysical Research, 109(F3): F03001, doi: 10.1029/2003jf000115.

Densmore, A.L., Ellis, M.A. and Anderson, R.S., 1998. Landsliding and the evolution of normal-fault-bounded mountains. Journal of Geophysical Research, 103(B7): 15203-15219, doi: 10.1029/98jb00510.

DiBiase, R.A., Heimsath, A.M. and Whipple, K.X., 2012. Hillslope response to tectonic forcing in threshold landscapes. Earth Surface Processes and Landforms, 37(8): 855-865, doi: 10.1002/esp.3205.

Dixon, J.L., Hartshorn, A.S., Heimsath, A.M., DiBiase, R.A. and Whipple, K.X., 2012. Chemical weathering response to tectonic forcing: A soils perspective from the San Gabriel Mountains, California. Earth and Planetary Science Letters, 323-324(0): 40-49, doi: http://dx.doi.org/10.1016/j.epsl.2012.01.010.

Ellis, Densmore and Anderson, 1999. Development of mountainous topography in the Basin Ranges, USA. Basin Research, 11(1): 21-41, doi: 10.1046/j.1365-2117.1999.00087.x.

Faccenna, C., Jolivet, L., Piromallo, C. and Morelli, A., 2003. Subduction and the depth of convection in the Mediterranean mantle. Journal of Geophysical Research, 108(B2): 2099, doi: 10.1029/2001jb001690.

Fassoulas, C., 2001. The tectonic development of a Neogene basin at the leading edge of the active European margin: the Heraklion basin, Crete, Greece. Journal of Geodynamics, 31(1): 49-70.

Fassoulas, C., Kilias, A. and Mountrakis, D., 1994. Postnappe stacking extension and exhumation of high-pressure/low-temperature rocks in the Island of Crete, Greece. Tectonics, 13(1): 125-138.

Fernandes, N.F. and Dietrich, W.E., 1997. Hillslope evolution by diffusive processes: The timescale for equilibrium adjustments. Water Resources Research, 33(6): 1307-1318, doi: 10.1029/97wr00534.

Flint, J.J., 1974. Stream gradient as a function of order, magnitude, and discharge. Water Resour. Res., 10(5): 969-973, doi: 10.1029/WR010i005p00969.

Frankel, K. and Pazzaglia, F.J., 2005. Tectonic geomorphology, drainage basin metrics, and active mountain fronts. Geografia Fisica e Dinamica Quaternaria, 28(1): 7-21.

Frankel, K. and Pazzaglia, F.J., 2006. Mountain fronts, base-level fall, and landscape evolution; insights from the Southern Rocky Mountains. In: S.D. Willett, N. Hovius, M.T. Brandon and D.M. Fisher (Editors), Tectonics, climate, and landscape evolution (Geological Society of America - Special Paper (398). Geological Boulder, pp. 419-434.

Fuller, C.W., Willett, S.D. and Brandon, M.T., 2006. Formation of forearc basins and their influence on subduction zone earthquakes. Geology, 34(2): 65-68, doi: 10.1130/G21828.1.

Gallen, S.F., Wegmann, K.W., Bohnenstiehl, D., Pazzaglia, F.J., Brandon, M.T., Fassoulas, C., *in review,* Coastal Uplift, Activity and the Kinematics of the Hellenic Trough Faults: Tectonic Geomorphology of an Extending Forearc above a Retreating Subduction Zone, Crete, Greece: Geophysical Journal International.

Greek Institute of Geology and Mineral Exploration, 1987. Geological Map of Greece, Ano Viannos Sheet: Athens, Institute of Geology and Mineral Exploration (IGME), scale 1: 50,000.

Greek Institute of Geology and Mineral Exploration, 1977. Geological Map of Greece, Ierapetra Sheet: Athens, Institute of Geology and Mineral Exploration (IGME), scale 1: 50,000.

Greek Institute of Geology and Mineral Exploration, 1974. Geological Map of Greece, Akhendhriar Sheet: Athens, Institute of Geology and Mineral Exploration (IGME), scale 1: 50,000.

Greek Institute of Geology and Mineral Exploration, 1972. Geological Map of Greece, Andiskarion Sheet: Athens, Institute of Geology and Mineral Exploration (IGME), scale 1: 50,000.

Gupta, A. and Scholz, C.H., 2000. A model of normal fault interaction based on observations and theory. Journal of Structural Geology, 22(7): 865-879.

Gupta, S., Cowie, P.A., Dawers, N.H. and Underhill, J.R., 1998. A mechanism to explain rift-basin subsidence and stratigraphic patterns through fault-array evolution. Geology, 26(7): 595-598, doi: 10.1130/0091-7613(1998)026<0595:amterb>2.3.co;2.

Hall, R., Audley-Charles, M.G. and Carter, D.L., 1984. The significance of Crete for the evolution of the eastern Mediterranean; Geological Society Special Publications, vol.17, pp.499-517, 1984. In: The geological evolution of the eastern Mediterranean. Geological Society of London. London, United Kingdom, pp. 499-517.

Heimsath, A.M., Dietrich, W.E., Nishiizumi, K. and Finkel, R.C., 1997. The soil production function and landscape equilibrium. Nature, 388(6640): 358-361.

Hetzel, R. et al., 2004. Implications of the fault scaling law for the growth of topography: mountain ranges in the broken foreland of north-east Tibet. Terra Nova, 16(3): 157-162, doi: 10.1111/j.1365-3121.2004.00549.x.

Hilley, G.E. and Arrowsmith, J.R.n., 2008. Geomorphic response to uplift along the Dragon's Back pressure ridge, Carrizo Plain, California. Geology, 36(5): 367-370, doi: 10.1130/g24517a.1.

Huguen, C. et al., 2001. Deformational styles of the eastern Mediterranean Ridge and surroundings from combined swath mapping and seismic reflection profiling. Tectonophysics, 343(1-2): 21-47.

Jackson, J.A. and White, N.J., 1989. Normal faulting in the upper continental crust: observations from regions of active extension. Journal of Structural Geology, 11(1-2): 15-36, doi: http://dx.doi.org/10.1016/0191-8141(89)90033-3.

Jolivet, L. and Brun, J.-P., 2010. Cenozoic geodynamic evolution of the Aegean. International Journal of Earth Sciences, 99(1): 109-138, doi: 10.1007/s00531-008-0366-4.

Jolivet, L.G., B; Monie, P; Truffert-Luxey, C; Patriat, M; Bonneau, M, 1996. Miocene detachment in Crete and exhumation P-T-t paths of high-pressure metamorphic rocks. Tectonics, 15(6): 1129-1153.

Kastens, K.A., Breen, N.A. and Cita, M.B., 1992. Progressive deformation of an evaporite-bearing accretionary complex: SeaMARC I, SeaBeam and piston-core observations from the Mediterranean Ridge. Marine Geophysical Research, 14(4): 249-298, doi: 10.1007/bf01203620.

Keller, E.A. and Pinter, N., 2001. Active Tectonics: Earthquakes, uplift, and landscape. Upper Saddle River, Prentice Hall, 362 pp.

Kirby, E. and Whipple, K., 2001. Quantifying differential rock-uplift rates via stream profile analysis. Geology, 29(5): 415-418, doi: 10.1130/0091-7613(2001)029<0415:qdrurv>2.0.co;2.

Kirby, E. and Whipple, K.X., 2012. Expression of active tectonics in erosional landscapes. Journal of Structural Geology, 44(0): 54-75, doi: http://dx.doi.org/10.1016/j.jsg.2012.07.009.

Kirby, E., Whipple, K.X., Tang, W. and Chen, Z., 2003. Distribution of active rock uplift along the eastern margin of the Tibetan Plateau: Inferences from bedrock channel longitudinal profiles. Journal of Geophysical Research: Solid Earth, 108(B4): doi: 10.1029/2001jb000861.

Knapmeyer, M., 1999. Geometry of the Aegean Benioff Zone. Annali di Geofisica, 42(1): 27-38.

Kooi, H. and Beaumont, C., 1996. Large-scale geomorphology: Classical concepts reconciled and integrated with contemporary ideas via a surface processes model. Journal of Geophysical Research: Solid Earth, 101(B2): 3361-3386, doi: 10.1029/95jb01861.

Kopf, A., Mascle, J. and Klaeschen, D., 2003. The Mediterranean Ridge: A mass balance across the fastest growing accretionary complex on Earth. Journal of Geophysical Research, 108(B8): 2372, doi: 10.1029/2001jb000473.

Kreemer, C. and Chamot-Rooke, N., 2004. Contemporary kinematics of the southern Aegean and the Mediterranean Ridge. Geophysical Journal International, 157(3): 1377-1392, doi: 10.1111/j.1365-246X.2004.02270.x.

Le Pichon, X., Lallemant, S.J., Chamot-Rooke, N., Lemeur, D. and Pascal, G., 2002. The Mediterranean Ridge backstop and the Hellenic nappes. Marine Geology, 186(1-2): 111-125.

Le Pichon, X., Lybéris, N., Angelier, J. and Renard, V., 1982. Strain distribution over the east Mediterranean ridge: A synthesis incorporating new Sea-Beam data. Tectonophysics, 86(1-3): 243-255, 259-274.

Le Pichon, X., Angelier, J., Aubouin, J., Lyberis, N., Monti, S., Renard, V., Got, H., Hsu¨, K., Mart, Y., Mascle, J., Matthews, D., Mitropoulos, D., Tsoflias, P., and Chronis, G., 1979. From subduction to transform motion: a seabeam survey of the Hellenic trench system. Earth and Planetary Science Letters, 44(3): 441-450.

Manighetti, I., Campillo, M., Sammis, C., Mai, P.M. and King, G., 2005. Evidence for self-similar, triangular slip distributions on earthquakes: Implications for earthquake and fault mechanics. Journal of Geophysical Research, 110(B5): B05302, doi: 10.1029/2004jb003174.

Manighetti, I., King, G.C.P., Gaudemer, Y., Scholz, C.H. and Doubre, C., 2001. Slip accumulation and lateral propagation of active normal faults in Afar. Journal of Geophysical Research, 106(B7): 13667-13696, doi: 10.1029/2000jb900471.

McClusky, S., Balassanian, S., Barka, A., Demir, C., Ergintav, S., Georgiev, I., Gurkan, O., Hamburger, M., Hurst, K., Kahle, H., Kastens, K., Kekelidze, G., King, R., Kotzev, V., Lenk, O., Mahmoud, S., Mishin, A., Nadariya, M., Ouzounis, A., Paradissis, D., Peter, Y., Prilepin, M., Reilinger, R., Sanli, I., Seeger, H., Tealeb, A., Toksoz, M.N., and Veis, G., 2000. Global positioning system constraints on plate kinematics and dynamics in the eastern Mediterranean and Caucasus. Journal of Geophysical Research, 105(B3): 5695-5719.

Meier, T., Becker, D., Endrun, B., Rische, M., Bohnhoff, M., Stockhert, B., and Harjes, H.-P., 2007. A model for the Hellenic subduction zone in the area of Crete based on seismological investigations. Geological Society, London, Special Publications, 291(1): 183-199, doi: 10.1144/sp291.9.

Merritts, D. and Vincent, K.R., 1989. Geomorphic response of coastal streams to low, intermediate, and high rates of uplift, Mendocino triple junction region, northern California. Geological Society of America Bulletin, 101(11): 1373-1388, doi: 10.1130/0016-7606(1989)101<1373:grocst>2.3.co;2.

Meulenkamp, J.E., van der Zwaan, G.J. and van Wamel, W.A., 1994. On late miocene to recent vertical motions in the Cretan segment of the Hellenic arc Tectonophysics, 234(1-2): 53-72.

Meulenkamp, J.E., Wortel, M.J.R., van Wamel, W.A., Spakman, W. and Hoogerduyn Strating, E., 1988. On the Hellenic subduction zone and the geodynamic evolution of Crete since the late Middle Miocene. Tectonophysics, 146(1-4): 203-215.

Montgomery, D.R. and Brandon, M.T., 2002. Topographic controls on erosion rates in tectonically active mountain ranges. Earth and Planetary Science Letters, 201(3-4): 481-489.

Montgomery, D.R. and Foufoula-Georgiou, E., 1993. Channel network source representation using digital elevation models. Water Resources Research, 29(12): 3925-3934.

O'Driscoll, M.A., DeWalle, D.R., 2006. Stream–air temperature relations to classify stream–ground water interactions in a karst setting, central Pennsylvania, USA. Journal of Hydrology, 329(1), 140-153.

Palumbo, L., Hetzel, R., Tao, M. and Li, X., 2010. Topographic and lithologic control on catchment-wide denudation rates derived from cosmogenic 10Be in two mountain ranges at the margin of NE Tibet. Geomorphology, 117(1-2): 130-142, doi: 10.1016/j.geomorph.2009.11.019.

Papazachos, B.C. and Comninakis, P.E., 1971. Geophysical and Tectonic Features of the Aegean Arc. Journal of Geophysical Research, 76(35): 8517-8533.

Papazachos, B.C., Karakostas, V.G., Papazachos, C.B. and Scordilis, E.M., 2000. The geometry of the Wadati-Benioff zone and lithospheric kinematics in the Hellenic arc. Tectonophysics, 319(4): 275-300.

Pazzaglia, F.J. and Brandon, M.T., 2001. A Fluvial Record of Long-term Steady-state Uplift and Erosion Across the Cascadia Forearc High, Western Washington State. American Journal of Science, 301(4-5): 385-431, doi: 10.2475/ajs.301.4-5.385.

Pe-Piper, G. and Piper, D.J.W., 2002. The igneous rocks of Greece: the anatomy of an orogen. Beitrăge zur regionalen Geologie der Erde ; Bd. 30. Gebr. Borntraeger, Berlin, xv, 573 p.

Peterek, A. and Schwarze, J., 2004. Architecture and Late Pliocene to recent evolution of outer-arc basins of the Hellenic subduction zone (South-central Crete, Greece). Journal of Geodynamics, 38(1): 19-55.

Pike, R.J. and Wilson, S.E., 1971. Elevation-Relief Ratio, Hypsometric Integral, and Geomorphic Area-Altitude Analysis. Geological Society of America Bulletin, 82(4): 1079-1084, doi: 10.1130/0016-7606(1971)82[1079:erhiag]2.0.co;2.

Pirazzoli, P.A., Thommeret, J., Thommeret, Y., Laborel, J. and Montag-Gioni, L.F., 1982. Crustal block movements from Holocene shorelines: Crete and antikythira (Greece). Tectonophysics, 86(1-3): 27-43.

Platt, J.P., 1986. Dynamics of orogenic wedges and the uplift of high-pressure metamorphic rocks. Geological Society of America Bulletin, 97(9): 1037-1053, doi: 10.1130/0016-7606(1986)97<1037:doowat>2.0.co;2.

Pope, R., Wilkinson, K., Skourtsos, E., Triantaphyllou, M. and Ferrier, G., 2008. Clarifying stages of alluvial fan evolution along the Sfakian piedmont, southern Crete: New evidence from analysis of post-incisive soils and OSL dating. Geomorphology, 94(1-2): 206-225.

Rackham, O. and Moody, J., 1996. The making of the Cretan landscape. Manchester University Press, Manchester, UK, 237 pp.

Rahl, J.M., Anderson, K.M., Brandon, M.T. and Fassoulas, C., 2005. Raman spectroscopic carbonaceous material thermometry of low-grade metamorphic rocks: Calibration and application to tectonic exhumation in Crete, Greece. Earth and Planetary Science Letters, 240(2): 339-354.

Reilinger, R., McClusky, S., Vernant, P., Lawrence, S., Ergintav, S., Cakmak, R., Ozener, H., Kadirov, F., Guliev, I., Stepanyan, R., Nadariya, M., Hahubia, G., Mahmoud, S., Sakr, K., ArRajehi, A.,

Paradissis, D., Al-Aydrus, A., Prilepin, M., Guseva, T., Evren, E., Dmitrotsa, A., Filikov, S.V., Gomez, F., Al-Ghazzi, R., and Karam, G., 2006. GPS constraints on continental deformation in the Africa-Arabia-Eurasia continental collision zone and implications for the dynamics of plate interactions. Journal of Geophysical Research, 111(B5): 26, doi: 10.1029/2005JB004051

Ring, U. and Reischmann, T., 2002. The weak and superfast Cretan detachment, Greece: exhumation at subduction rates in extruding wedges. Journal of the Geological Society, 159(3): 225-228, doi: 10.1144/0016-764901-150.

Schlische, R.W., Young, S.S., Ackermann, R.V. and Gupta, A., 1996. Geometry and scaling relations of a population of very small rift-related normal faults. Geology, 24(8): 683-686, doi: 10.1130/0091-7613(1996)024<0683:gasroa>2.3.co;2.

Seidel, E., Okrusch, M., Kreuzer, H., Raschka, H. and Harre, W., 1981. Eo-alpine metamorphism in the uppermost unit of the Cretan nappe system — Petrology and geochronology. Contributions to Mineralogy and Petrology, 76(3): 351-361, doi: 10.1007/bf00375462.

Snyder, N.P., Whipple, K.X., Tucker, G.E. and Merritts, D.J., 2000. Landscape response to tectonic forcing: Digital elevation model analysis of stream profiles in the Mendocino triple junction region, northern California. Geological Society of America Bulletin, 112(8): 1250-1263, doi: 10.1130/0016-7606(2000)112<1250:lrttfd>2.0.co;2.

Strahler, A.N., 1957. Quantitative analysis of watershed geomorphology. Transactions of the American Geophysical Union, 38(6): 913-920.

Strasser, T.F., Runnels, C., Wegmann, K., Panagopoulou, E., McCoy, F., Digregorio, C., Karkanas, P. and Thompson, N., 2011. Dating Palaeolithic sites in southwestern Crete, Greece, Journal of Quaternary Science, 26, 553-560, doi: 10.1002/jqs.1482.

ten Veen, J.H. and Kleinspehn, K.L., 2003. Incipient continental collision and plate-boundary curvature: Late Pliocene-Holocene transtensional Hellenic forearc, Crete, Greece. Journal of the Geological Society, 160(2): 161-181, doi: 10.1144/0016-764902-067.

Thomson, S.N., Stöckhert, B. and Brix, M.R., 1998. Thermochronology of the high-pressure metamorphic rocks of Crete, Greece: Implications for the speed of tectonic processes. Geology, 26(3): 259-262, doi: 10.1130/0091-7613(1998)026<0259:tothpm>2.3.co;2.

Tucker, G.E. and Slingerland, R., 1997. Drainage basin responses to climate change. Water Resources Research, 33(8): 2031-2047, doi: 10.1029/97wr00409.

van Hinsbergen, D.J.J., Hafkenscheid, E., Spakman, W., Meulenkamp, J.E. and Wortel, R., 2005. Nappe stacking resulting from subduction of oceanic and continental lithosphere below Greece. Geology, 33(4): 325-328, doi: 10.1130/g20878.1.

van Hinsbergen, D.J.J. and Schmid, S.M., 2012. Map view restoration of Aegean–West Anatolian accretion and extension since the Eocene. Tectonics, 31(5): doi: 10.1029/2012tc003132.

Wegmann, K.W., 2008. Tectonic geomorphology above Mediterranean subduction zones; northern Apennines of Italy and Crete, Greece, Lehigh University, Bethlehem, PA, 169 pp.

Whipple, K.X. and Meade, B.J., 2006. Orogen response to changes in climatic and tectonic forcing. Earth and Planetary Science Letters, 243(1-2): 218-228, doi: 10.1016/j.epsl.2005.12.022.

Whittaker, A.C. and Boulton, S.J., 2012. Tectonic and climatic controls on knickpoint retreat rates and landscape response times. Journal of Geophysical Research: Earth Surface, 117(F2): doi: 10.1029/2011jf002157.

Willett, S.D., Beaumont, C. and Fullsack, P., 1993. Mechanical models for the tectonics of doubly vergent compressional orogens. Geology, 21: 371-374.

Willett, S.D. and Brandon, M.T., 2002. On steady states in mountain belts. Geology, 30(2): 175-178, doi: 10.1130/0091-7613(2002)030<0175:ossimb>2.0.co;2.

Wobus, C., Whipple, K.X., Kirby, E., Snyder, N., Johnson, J., Spyropolou, K., Crosby, B., and Sheehan, D., 2006. Tectonics from topography: Procedures, promise, and pitfalls. Geological Society of America Special Papers, 398: 55-74, doi: 10.1130/2006.2398(04).

Wobus, C.W., Tucker, G.E. and Anderson, R.S., 2010. Does climate change create distinctive patterns of landscape incision? Journal of Geophysical Research, 115(F4): F04008, doi: 10.1029/2009jf001562.

Wortel, M.J.R. and Spakman, W., 2000. Subduction and Slab Detachment in the Mediterranean-Carpathian Region. Science, 290(5498): 1910-1917, doi: 10.1126/science.290.5498.1910.

Zachariasse, W.J., van Hinsbergen, D.J.J. and Fortuin, A.R., 2008. Mass wasting and uplift on Crete and Karpathos during the early Pliocene related to initiation of south Aegean left-lateral, strike-slip tectonics. Geological Society of America Bulletin, 120(7-8): 976-993, doi: 10.1130/b26175.1.